NEW MATERIALS FOR SMART STRUCTURES: A US: JAPAN GLOBAL INITIATIVE

Period June 1, 2001 to March 31, 2004

Final Report

Office of Naval Research
Contract Grant Number N000 14-99-1-1011

L. Eric Cross

Materials Research Laboratory
University Park, PA 16802 USA

REPORT DOCUMENTATION PAGE

Form Approved
OMB No. 0704-0188

1. REPORT DATE *(DD-MM-YYYY)*	2. REPORT TYPE	3. DATES COVERED *(From - To)*
Dec 9, 2005	Written/final	30 Sep 1999 Through 31 Mar 2004

4. TITLE AND SUBTITLE
New Materials for Smart Structures: US Japan Global Initiative

5a. CONTRACT NUMBER
Nooo14-99-1-1011

5b. GRANT NUMBER

5c. PROGRAM ELEMENT NUMBER

6. AUTHOR(S)
L. Eric Cross
187 Materials Research Laboratory
University Park, PA 16802

5d. PROJECT NUMBER

5e. TASK NUMBER

5f. WORK UNIT NUMBER

7. PERFORMING ORGANIZATION NAME(S) AND ADDRESS(ES)
Pennsylvania State University
187 Materials Research Laboratory
University Park PA 16802

8. PERFORMING ORGANIZATION REPORT NUMBER

9. SPONSORING/MONITORING AGENCY NAME(S) AND ADDRESS(ES)
Office of Naval Research
South Dearborn Room380
Chicago, IL 60604-1595

Office of Naval Research
Materials Division ONR 332
Room 648
Arlington, VA 22217-5660

10. SPONSOR/MONITOR'S ACRONYM(S)

11. SPONSOR/MONITOR'S REPORT NUMBER(S)

12. DISTRIBUTION/AVAILABILITY STATEMENT
Approved for Public Release; distribution is Unlimited

13. SUPPLEMENTARY NOTES

14. ABSTRACT
This reports supplements the extensive earlier report of 2002 and covers work carried forward on supplementary funding for the period Jan 1, 2003 to Dec 31, 2003 and is now the final report on ONR Grant Number N000. 14. 99. 1. 1011.
The extended program continued to focus upon electro-active materials for actuating and transducing functions. The two most important technical areas are: 1. The study of bismuth based solid solutions with morphotropic phase boundaries (MPBs). Current work has generated new clues as to the origin of the large electric polarization in epitaxial thin film systems. 2. Examination of possible use of induced gradient effects (Flexoelectricity) to engineer completely new piezoelectric composites with properties impossible to engineer by other materials.

15. SUBJECT TERMS

16. SECURITY CLASSIFICATION OF:			17. LIMITATION OF ABSTRACT	18. NUMBER OF PAGES	19a. NAME OF RESPONSIBLE PERSON
a. REPORT	b. ABSTRACT	c. THIS PAGE			L. Eric Cross
UU	UU	UU			19b. TELEPHONE NUMBER *(Include area code)* 814-865-1181

New Materials for Smart Structures: A US:Japan Global Initiative

L. Eric Cross
The Pennsylvania State University
Materials Research Institute
187 Materials Research Laboratory
University Park, PA 16802 USA
Phone: 814.865.1181
Fax: 814.863.7846
E-Mail: lec3@psu.edu

Grant Number N000 14-99-1-1011

ONR Program officer R.C. Pohanka

TABLE OF CONTENTS

Abstract

This reports supplements the extensive earlier report of 2002 and covers work carried forward on supplementary funding for the period Jan 1, 2003 to Dec 31, 2003 and is now the final report on ONR Grant Number N000. 14. 99. 1. 1011. The extended program continued to focus upon electro-active materials for actuating and transducing functions. The two most important technical areas are:

1. The study of bismuth based solid solutions with morphotropic phase boundaries (MPBs). Current work has generated new clues as to the origin of the large electric polarization in epitaxial thin film systems.
2. Examination of possible use of induced gradient effects (Flexoelectricity) to engineer completely new piezoelectric composites with properties impossible to engineer by other materials.

I. INTRODUCTION

Based on long established precedent this report will be based on the published results from the program which are assembled as technical appendices.

For the exploration of new solid solutions with ferroelectric morphotropic phase boundaries (MPBs) the initial decision to focus on bismuth based compositions has now been amply justified. Initial disappointment at being unable to achieve an MPB in the bismuth gallate:lead titanate system has been relieved by the control of electrical conductivity which are achieved by even small additions (5 mole % Ga raises resistivity p> 10^{13} ohm.cm at room temperature) and the realization of the MPB in the Gallate:Scandate system and in the modified bismuth lanthanum ferrate lead titanate systems.

A major puzzle in $BiFeO_3$ which has a ferroelectric Curie temperature at 850° and an antiferromagnetic Néel Temperature at 350° C single crystals only exhibit polarization 6μ/um^2 at room temperature. (1) A breakthrough by R. Ramesh (2) showed Ps ~ 90 μc/cm^2 in thin films epitaxed on 001 strontium ruthenate on strontium titanate. Initially it was believed that epitaxial strain forced a new tetragonal structure, but subsequent work (3) has shown that 110 and 111 oriented films also show Ps along 111 of 100 μc/cm^2. Obviously also in the thin films the antiferromagnetic coupling is broken and the films show switchable magnetization. A new major clue as to the origin of the high switchable polarization is provided by our most recent work on the modified bismuth lanthanum ferrate: gallate solid solutions with MPBs. In suitable composition switchability is only possible with limited electrode in a larger disk, and the fully electroded disk will not switch. In the

homogeneous ceramic no macro-stress is generated on cooling so it is most likely that constraint is the requirement as is obviously supplied by the substrate in all of the thin film studies. In the ceramic however, now by changing the electrode diameter to control the constraining annulus it should be possible to explore the level of constraint which is necessary for switching.

In the gradient studies, the focus continued on the flexoelectric behavior and we are now much closer to being able to answer the two questions posed in the previous report. Firstly it does appear to be the chemical make up that is more important in determining the γ constant which relates flexoelectric μ and dielectric susceptibility in that γ in barium strontium titanate is order of magnitude larger than γ in PMN and the same is true in ferroelectric $BaTiO_3$ compared to PZT for both intrinsic and domain contributions to response.

The next phase of work is now to measure the longitudinal μ_{11}, the converse effect, i.e. electric strain generated by an electric field gradient, and to construct a demonstration piezoelectric composite which will contain no piezoelectric phase.

2. TECHNICAL PROGRESS REPORT

2.1 Bismuth based solid solutions with MPBs

Studies of the (1-x) (BiLa) $(Ga_{0.05}Fe_{0.96})\ O_3 - x\ PbTiO_3$ solid solution systems are summarized in Appendix 1. As expected the dielectric and piezoelectric properties peak at the MPB composition. The lanthanum modification enhances the electrical resistivity, strongly reduces the electrical coercivity and significantly improves d_{33} however, at the expense of reduced Curie Temperature. The small addition of gallium also improves resistivity and also piezoelectric d_{33}. These ceramics also have excellent dielectric strength withstanding electric field up to 150 kV/cm.

A more detailed study of the same solid solution system at the $(Bi_{0.9}La_{0.1})$ composition with a modified $(Pb_{0.9}Ba_{0.1})TiO_3$ end member is discussed in Appendix 2. The advantage of the barium content in this system is in broadening the composition range of strong piezoelectric response and simplifying the ceramic processing. The most recent work on the bismuth gallate ferrate: lead titanate solid solution is discussed in Appendix 3. At the $0.4Bi(Ga_{0.4}Fe_{0.6})O_3$-$0.6PbTiO_3$

composition the Curie temperature is 540° C. the most intriguing feature of its behavior is the high field hysteretic dielectric response. (fig 6). Able to withstand 300 kV/cm field a fully electroded disk would not switch however with a partial electrode strong hysteresis with remanent polarization of 30μc/cm^2 occurs under a driving field of 250 kV/cm. It would appear that transverse constrain may be critical to permit switching and this would agree with earlier thin film studies.

Work is now in progress at the University in Shanghai to ascertain the level of constraint needed by varying the unelectroded annulus.

Initial studies of thin films in the $BiFeO_3$:$PbTiO_3$ family produced by sol-gel processing are summarized in Appendix 4. A very thin PZT layer was used to promote adhesion of the BLF:PT film. Insulating films with permittivity $\epsilon \sim 800$ and $\tan \delta \sim 0.04$ were obtained.

A summary of much of the work on bismuth based perovskite ferroelectric solid solution with MPBs is given in Appendix 5. The discussion also covers some of the earlier work on this program on the bismuth scandate: lead titanate solid solutions.

2.2 Gradient related studies

The flexoelectric effects in a soft unpoled lead zirconate titanate ceramic are further explored in Appendix 6. We had already demonstrated the extrinsic contribution due to ferroelastic-ferroelectric domain wall motion by static measurements. These dynamics measurements give convincing evidence for a domain wall contribution to the dielectric response at higher E fields in these soft piezoelectrics.

2.3 Additional Studies

Interest in the single phase bismuth ferrate which has magneto-electric properties in the thin film and the composition modified forms catalyzed a renewed interest in the simpler magneto-electric composites embracing a piezoelectric elastically coupled to a magnetostrictor in a laminar structure. We have been working with Dr. Dwight Viehland's group at Virginia Polytechnic looking at the possibilities of high sensitivity magnetic sensors. This led to a consideration of a resonant structure and the realization (Appendix 7) that this could also provide a striking new type of transformer structure.

In a similar vein appendix 8 discusses some of the interesting unresolved problems in the behaviors of ferroelectric domain walls both in static and dynamic applications. This topic is further explored in appendix 9 which identifies a number of problem areas that do require continuing study.

3. REFERENCES

1. A. Kubel, H. Schmid, *Acta Cryst,* B 46, 689, 1990
2. J. Wang, J. B. Neaton, H. Zheng, V. Nagurajan, S. B. Ogale, B. Liu, D. Viehland, V. Vaithyunathan, D. G. Schlom, B. Waghmare, N.A. Spaldin, K. M. Rabe, M. Wutting, R. Ramesh, *Science* 299, 1719, 2003
3. G. Xu, H. Hirako, G. Shirane, J. Li, J. Wang, D. Viehland, *Appl Phys Letters*, 86, 182905, 2005

4. Graduate Student

None

5. HONORS AND AWARDS

None

6. PAPERS PUBLISHED IN REFEREED JOURNALS

1. L. Eric Cross, Wenyi Zhu, "Direct evidence of ferroelastic participation in 180° polarization switching and fatigue for 111 oriented rhombohedral ferroelectric 0.955 $Pb(Zn_{1/3}\ Nb_{2/3})O_3$:0.045 $PbTiO_3$ single crystals, Applied Physics Letters, **84**, No. 13, 29 March 2004.

2. J. Fousek, L. E. Cross, "Domain-related problems of ferroelectric ceramics", Ceramics International, **30, 7** (2004)1169-1173.

3. Jinrong Cheng, L. Eric Cross, "Bismuth-Based Perovskite Structure Solid Solutions with Ferroelectric Morphotropic Phase Boundaries for Piezoelectric Applications", Piezoelectric Single Crystals and their Application, 366-395, (2004)

4. Jinrong Cheng, L. Eric Cross, "Dielectric and Ferroelectric Properties of Modified $BiFeO_3$ (BLF-PT) Thin Films Derived from Sol-gel Processing", Maters Res Soc Symp. Porc Vol 784, c8.16.1

5. L. E. Cross, "Progress prospects and problems in advanced materials for dielectric piezoelectric and elctro-optic applications, Ceramics International **30** pg. 2045(2004)

6. Shuziang Dong, J. F. Li , D. Viehland, J. Cheng, and L. E. Cross, "A strong magnetoelectric voltage gain effect in magnetostrictive-piezoelectric composite" Applied Physics Letters, **85** Number 16, 18,3534-3536, October 18, 2004

7. A. Amin, L.E. Cross, "Intermediate states in $Pb(B'_{1/3}B''_{2/3})O_3$-$PbTiO_3$ ferroelectric single crystals" British Ceramic Transactions, **103** No. 2 , 89-91, 2004,

8. Jinrong Cheng, Zhong Meng, and L. E. Cross, "Piezoelectric performances of lead-reduced (1-x) $Bi_{0.9}Ba_{0.1})Ga_{0.05}Fe_{0.95})TiO_3$ crystalline solutions in the morphotropic phase boundary" Journal of Applied Physics, **96** , No. 11, 6611-6615, 1 Dec. 2004

9. Feiming Bai, Haimei Zheng, Hu Cao, L.E. Cross R. Ramesh, Jiefang Li and D. Viehland, "Epitaxially induced high temperature (>900K) cubic tetragonal structural phase transition in $BaTiO_3$ thin films", Applied Physics Letters, **85** No. 18, 4109-4111, 1 Nov 2004

7. PAPERS PUBLSIHED IN NON REFEREED JOURNAL

None

8. INVITED PAPERS

1. Jinrong Cheng, L. Eric Cross, "Bismuth Based Perovskite Structure Solid Solution with Morphotropic Phase Boundaries for Piezoelectric Applications", 106th Annual Mtg American Ceramic Society, Indianapolis, Indiana; 18-2 1, 2004

2. L. Eric Cross. "Ferroelectric Composites: The Flagship for many following Ferroelectric Device Structure" Franklin Institute Awards Week Program, Drexel University Philadelphia, April 28. 2004

3. A. Amin, L. Eric Cross, "Stress induced Orthorhombic Symmetry in High Coupling Crystals", 2004 US Navy Workshop on Acoustic transduction Materials and Devices, State College, PA May 11-13 2004

4. W. Zhu, L. Eric Cross, "Direct Evidence of Ferroelastic Participation in 180° Polarization and Fatigue for 111 Oriented Rhombohedral Ferroelectric 0.955 $Pb(Zn_1/_3Nb_2/_3)O_3$:0.045$PbTiO_3$ Single Crystals" 2004 Navy Workshop on Acoustic Transduction Materials and Devices State College PA, May 11-13, 2004

5. L. Eric Cross, "Progress in Studies of the Flexoelectric Effect", ONR Workshop on Future Directions in Materials for Electromechanical Transducers, Washington, D.C., July 12-13, 2004.

6. L. Eric Cross, Wenhui Ma, Wenyi Zhu, "Strain Gradient Induced Electric Polarization in Paraelectric Ferroelectric and Relaxor Ferroelectrics" 7th European Conference on Polar Dielectrics ECAP7, Sept 6-9, 2004 Liberec, Czech Republic.

7. L. Eric Cross, "Recent Progress in transducers Actuators and Sensors for Smart Systems" MRS Fall Meeting, Symposium D, Boston Nov 30, 2004

8. L. Eric Cross, "Recent Progress in transduction Materials for sensing and actuation" World Congress on Biomimetics Artificial muscles and nano-Bio 2004", Dec 6-8, 2004 Albuquerque, NM

9. CONTRIBUTED PAPERS
None

10. BOOKS IN CHAPTERS IN PRESS
None

11. PERSONNEL
1 Eric Cross, Evan Pugh Professor Emeritus of Electrical Engineering
2. Jinrong Cheng, Post Doctoral Research Fellow
3. Wenyi Zhu, Research Assistant
4. Nan Li, Research Assistant

12. TECHNICAL REPORTS AND NON-REFEREED PAPERS
None

13. INVENTION DISCLOSURES
None

14. PATENTS GRANTED
None

15. PATENTS PENDING
None

16. DEGREES GRANTED
None

APPENDIX 1

Effects of La substituent on ferroelectric rhombohedral/tetragonal morphotropic phase boundary in $(1-x)(Bi,La)(Ga_{0.05}Fe_{0.95})O_3-xPbTiO_3$ piezoelectric ceramics

Jin-Rong Cheng[a)]
Materials Research Institute, The Pennsylvania State University, University Park, Pennsylvania 16802 and School of Materials Science and Engineering, Shanghai University, Shanghai 201800, People's Republic of China

L. Eric Cross
Materials Research Institute, The Pennsylvania State University, University Park, Pennsylvania 16802

(Received 9 June 2003; accepted 28 July 2003)

Crystalline solutions of $(1-x)(Bi,La)(Fe_{0.95}Ga_{0.05})O_3-xPbTiO_3$ (BLGF–PT) have been fabricated with La concentrations of 0, 10, and 20 at.%. The BLGF–PT system has been found to have excellent insulation resistivity $\leq 10^{13}$ Ω cm. In addition, La substituent was found to decrease the coercive field, resulting in much improved dielectric and piezoelectric properties. A shift in the morphotropic phase boundary of BLGF–PT with increasing La content was identified for $x=0.3$, 0.4, and 0.43. We have achieved optimized dielectric constant, loss factor, Curie temperature, remnant polarization, and piezoelectric d_{33} properties of 881, 0.037, 386 °C, 30 $\mu C/cm^2$ and 163 pC/N, respectively, for 0.6BLGF–0.4PT with 10 at.% La. These results clearly demonstrate that BLGF–PT is a competitive alternative piezoelectric material to $Pb(Zr,Ti)O_3$ with reduced lead content. © *2003 American Institute of Physics.* [DOI: 10.1063/1.1610802]

I. INTRODUCTION

Perovskite $Pb(Zr,Ti)O_3$ PZT is a conventional piezoelectric material which is widely used in sensor and actuator applications.[1,2] Advantages of PZT based materials are a temperature insensitive near morphotropic phase boundary (MPB) composition between rhombohedral (FE_r) and tetragonal (FE_t) ferroelectric phases, and a coexistence of both phases near the MPB resulting in enhancements of the dielectric and piezoelectric properties. However, environmentally friendly alternatives to the toxic Pb-containing PZT are needed. To date, no MPB piezoelectrics have been developed that has the potential to replace PZT for acoustic materials applications. Bismuth-based materials are considered to be the most promising candidate.[3,4] $BiScO_3-PbTiO_3$ (BS–PT) and $Bi(Ga,Sc)O_3-PbTiO_3$ (BGS–PT) have been reported that have equivalent piezoelectric properties to PZT. However, Sc_2O_3 is expensive, limiting the potential applications of the BS–PT system; and in addition, this system contains relatively high PT content of ~60 at.% composition near the MPB.[5,6]

Bismuth ferrite based materials are also of great interest due to their simple perovskite structure and the simultaneous coexistence of ferroelectricity and antiferromagnetism.[7,8] $BiFeO_3$ has a ferroelectric Curie temperature T_C of 850 °C, and an antiferromagnet Néel temperature T_N of 310 °C.[9,10] However, one of major problems of earlier $BiFeO_3$ based materials is that a low electrical resistivity has prevented practical application of the material as either piezoelectric or magnetoelectric functional components. A further complication is that the coercive field E_c of $BiFeO_3$ is very high, making it an extremely difficulty to pole specimens into a piezoelectric state. Other perovskites [such as $PbTiO_3$, $BaTiO_3$, $SrTiO_3$, and $Pb(Fe_{0.5}Nb_{0.5})O_3$[11–14]] have been put into solid solution with $BiFeO_3$ in order to enhance the electrical insulation resistance. Although the perovskite structure of these crystalline solution materials has been shown to be stable, however, to date, the insulation resistance of $BiFeO_3$-based materials has not yet to be raised sufficiently, nor has E_c been lowered sufficiently.

The purpose of this investigation is to solve the main problems that have previously prevented application of $BiFeO_3$ based materials. We have focused efforts on increasing the electrical resistivity and reducing E_c by introduction of La^{3+} substituent in BF–PT ceramics for compositions close to the MPB. Our earlier work reported that a proper amount of Ga could reduce the conductivity of BF–PT solid solutions.[15] Therefore, Ga of 5 at.% was added into the compositions investigated. $(1-x)(Bi,La)(Fe_{0.95}Ga_{0.05})O_3-xPbTiO_3$ (BLGF–PT) ceramics with various La concentrations have been fabricated and their properties tested. We have achieved our goal of developing BF–PT based materials that are highly electrically insulating, and capable of being poled into a piezoelectric state.

II. EXPERIMENTAL PROCEDURE

Crystalline solutions of La-modified $(1-x)$BGF–xPT have been fabricated by conventional solid-state processing. Ceramics have been made with La concentrations of 0, 10, and 20 at.% for $0.2 \leq x \leq 0.65$. The starting materials used were Bi_2O_3, Fe_2O_3, La_2O_3, Ga_2O_3, $PbCO_3$, and TiO_2 which all were of purities greater than 99%. The oxide pow-

a)Electronic mail: jue12@psu.edu

ders were mixed by ball milling for 24 h, and subsequently calcined at 750 °C for 4 h. The powders were pressed and sintered at 1000–1100 °C for 0.8 h in a sealed crucible. The sintering weight loss and radial shrinkage were ~1% and ~18%, respectively. The structure and phase evolution of our specimens were characterized by x-ray diffraction (XRD) (Sintag-1). The microstructure of fresh fracture surfaces of sintered pellets was examined by scanning electron microscopy (SEM), (Hitachi S-3000H).

Specimens were electroded with a postfire silver paste (Dupont 6160). The electrical insulation resistance was measured using a Keithley 6517 meter. Temperature dependent dielectric measurements were made using a computer controlled HP4284 impedance analyzer. The ferroelectric hysteresis loops and induced strain were simultaneously measured using a modified Sawyer–Tower circuit with a linear variable differential transformer. Piezoelectric properties were characterized using a Berlincourt d_{33} meter, and by the IEEE resonance-antiresonance method using a HP4194A impedance analyzer.

III. RESULTS AND DISCUSSION

Figures 1(a)–1(c) show SEM images taken from fresh fracture surfaces for 0.7BGF–0.3PT (0 at. % La), 0.6BLGF–0.4PT with 10 at. % La, and 0.57BLGF–0.43PT with 20 at. % La. It can be seen that the ceramics were well densified, without significant residual porosity. The average grain size was ~1 μm, and was increased for specimens with higher La and PT contents. However, for systems 0.7BGF–0.3PT (0 at. % La) a much different microstructure was found, in which fracture was dominantly transgranular. This suggests that large internal stresses were introduced in the higher bismuth compositions, preventing fracture from beginning along grain boundaries. It was explainable combining the subsequent XRD results of the large c/a ratio and the coexistence of two phases near this composition, which caused the increased intrinsic crystalline stress. La modification released the stress obviously. The density of the ceramics was ~99% of the theoretical for BGF–PT (0 at. % La), and ~96% for La modified compositions. Relatively fine grain sizes result in higher densities.

The electrical resistivity of BLGF–PT as a function of PT and La concentration is shown in Fig. 2. For $0.25<x<0.5$, the resistivity was in the range of 10^{11}–10^{13} Ω cm. Specimens with higher La concentration (20 at. %) had higher resistivity. Our results clearly demonstrate that the BLGF–PT system is insulating. We conjecture that the crystal distortion introduced into BF–PT by La substitution suppress the reduction of $Fe^{3+}\rightarrow Fe^{2+}$, lowering the oxygen vacancy concentration and subsequently lowering the conductivity. Internal stresses originating from the crystalline distortion may prevent tilting of the oxygen octahedron, favoring stabilization of the Fe^{3+} species.

Analysis of XRD patterns revealed that BLGF–PT had a phase-pure perovskite structure. No secondary pyrochlore phases were observed, for PT contents of $x\geq 0.1$. The crystal structure was found change with composition from rhombohedral to tetragonal near a MPB. Figures 3(a)–3(c) show the

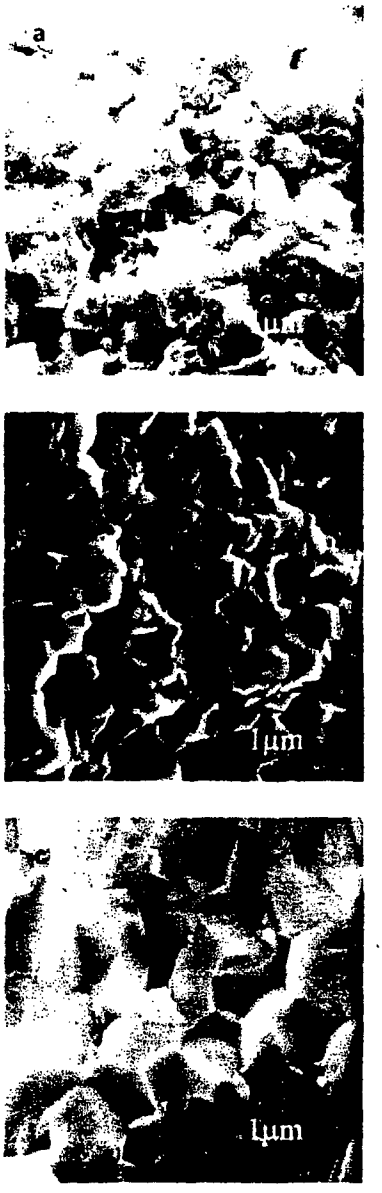

FIG. 1. SEM images of fresh fracture surfaces of $(1-x)$BLGF–xPT for (a) 0 at. % La and $x=0.3$; (b) 10 at. % La and $x=0.4$; and (c) 20 at. % La and $x=0.43$.

lattice parameters as a function of PT content for various La concentrations. In this figure, the MPB between FE_r and FE_t can be seen to shift to higher PT content with increasing La substituent concentration, with PT content of $x=0.3$, 0.4, and 0.43, respectively. In addition, the c/a ratio of the FE_t phase can be seen to decrease with increasing La concentration. For example, the c/a ratio decreased from 1.16 for 0.7BGF–0.3PT with 0 at. % La to 1.02 for 0.55BLGF–0.45PT with 20 at. % La. It is important to note that Fig. 3(a) shows a broadened region between $0.25<x<0.4$ over which the FE_r and FE_t phases coexist.

Figures 4(a)–4(c) show the room temperature dielectric constant K and tan δ of BLGF–PT as a function of PT content for La concentrations of 0, 10, and 20 at. %, respectively. Measurements were performed at frequencies of 10^3, 10^4,

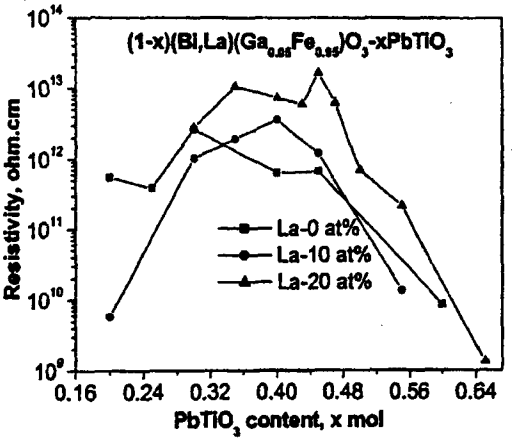

FIG. 2. Electrical resistivity of BLGF–PT as a function of PT content for various La concentrations at room temperature.

and 10^5 Hz. La modification of BGF–PT significantly enhanced the value of K, and also increased the frequency dispersion of K for higher Bi-content specimens. Maxima in the room temperature dielectric peaks were observed as a function of PT concentration, which shifted to higher PT content with increasing La concentration. The peak in K was found at PT content of $x=0.3$, 0.4, and 0.43 for La concentration of 0, 10, and 20 at. %, respectively. The maximum value of K at 10^3 Hz was 330 for 0.7BGF–0.3PT (0 at. % La), 881 and 1760 for 0.6BLGF–0.4PT and 0.57BLGF–0.43PT with 10 and 20 at. % La, respectively. The loss tangent of BLGF–PT was lower than 0.1, reflecting the good electrical insulation resistance of our specimens. The maximum in K with PT content coincided with the FE_r–FE_t transition at the MPB, as identified in Fig. 3. Near the MPB, the polarizability is enhanced due to the presence of many (i.e., 12) domain states. The enhancement of K by La substitution can be understood in a similar manner as a soft PZT, where random-fields disrupt the long-range polarization.[16] This will also result in a reduction in E_c and an improvement in the ease of achieving complete poling.

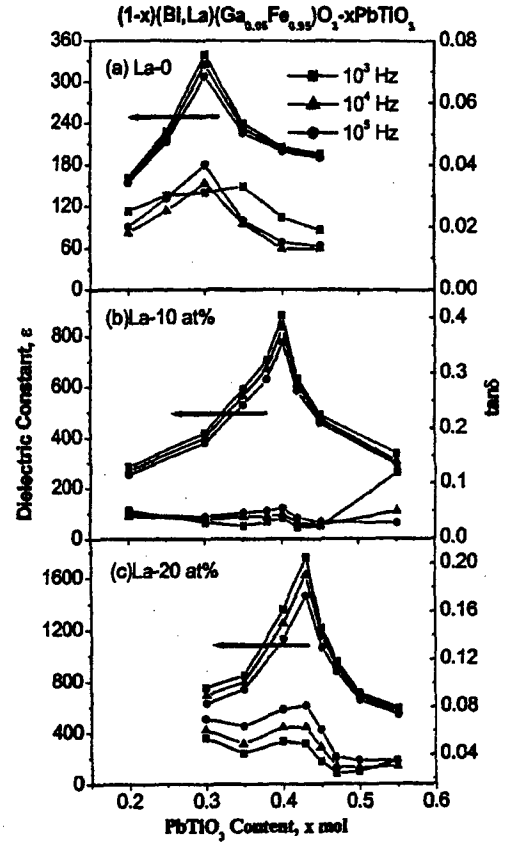

FIG. 4. Room temperature dielectric constant K and tan δ of BLGF–PT as a function of PT content for (a) 0; (b) 10; and (c) 20 at. % La.

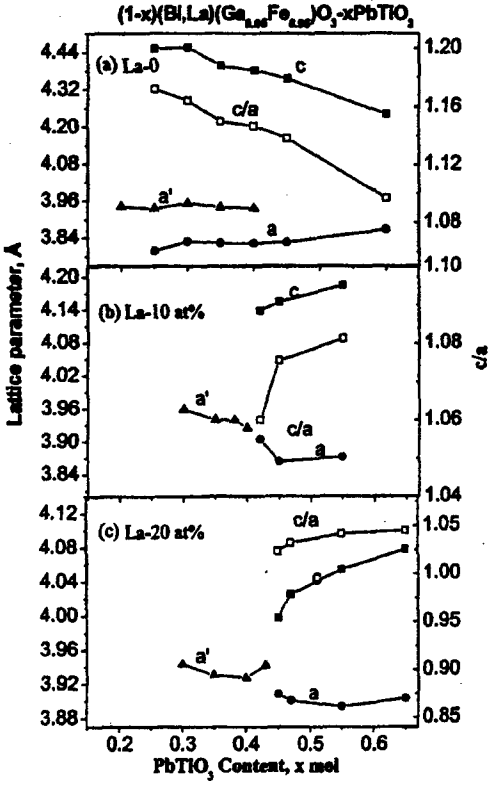

FIG. 3. Lattice parameters of BLGF–PT as a function of PT content for (a) 0; (b) 10; and (c) 20 at. % La.

Figure 5 shows K and tan δ as a function of temperature for 0.7BGF–0.3PT with 0 at. % La, 0.6BLGF–0.4PT with 10 at. % La, and 0.57BLGF–0.43PT with 20 at. % La, respectively. Measurements were taken using a frequency of 10^6 Hz. The maxima of K were shifted to the lower temperatures with increasing La concentration. The temperature dependent dielectric response can be seen to become increasingly broad with La modification. This demonstrates that La diffuses the ferroelectric phase transformation, in a manner similar to soft ferroelectrics[16] and to relaxors.[9] It is also important to note that La modification of BGF–PT decreased tan δ at elevated temperatures, until $T>500\,^{\circ}C$. This reflects that good insulation resistance was maintained in our specimens at high temperatures, which is important to high temperature piezoelectric applications.

Figure 6 summarizes the results for the compositional range of BLGF–PT that we have investigated in a phase

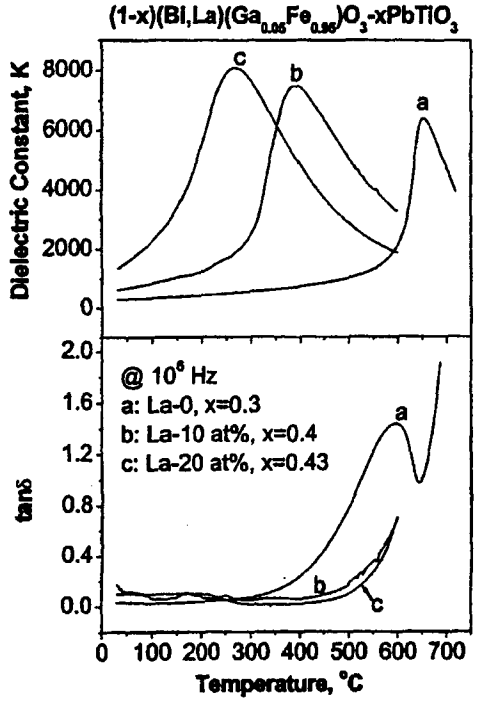

FIG. 5. Temperature dependent K and tan δ for various MPB compositions of BLGF–PT.

diagram. The temperature of the dielectric maximum determined the ferroelectric-paraelectric Curie temperature. The MPBs were identified by XRD analysis, and are shown in the phase diagram for $x=0.3$, 0.4, and 0.43. In this diagram, to the left of the MPB, the perovskite phase had rhombohedral symmetry; whereas to the right, it had tetragonal symmetry. For BGF–PT with 0 at. % La, the value of T_C was as high as 650 °C, which was only slightly changed with PT content. However, T_C was found to decrease noticeably with increasing La concentration. For example, in the vicinity of the MPB, T_C was 386 °C for the BGF–PT solution with 10 at. % La, and 264 °C for the one with 20 at. %. Interestingly, the BLGF–PT system did not have a monotonous relationship between T_C and composition, as found for PZT. Rather, a

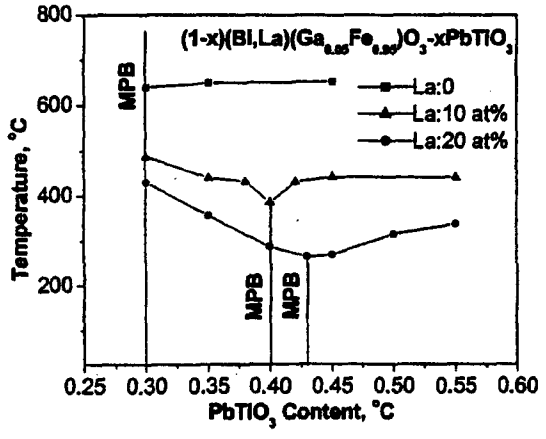

FIG. 6. Phase diagram of BLGF–PT as a function of PT content for La substituent concentrations of 0, 10, and 20 at. %.

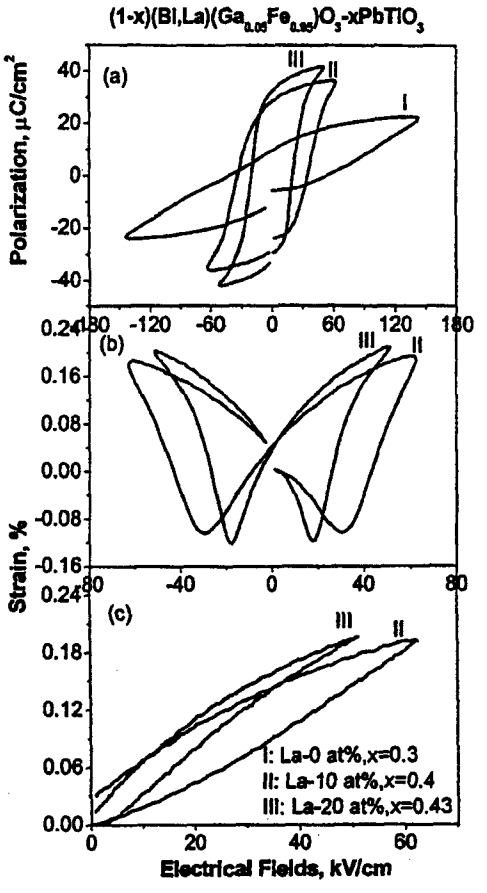

FIG. 7. Induced polarization and strain as a function of electric field for MPB compositions of BLGF–PT, (a) bipolar $P-E$ response; (b) bipolar $\varepsilon-E$ response; and (c) unipolar $\varepsilon-E$ response.

V-shaped boundary between the paraelectric and ferroelectric phases was obvious in the T_C-x boundary line. This suggests that the oxygen octahedron might be twisted near the MPB, and that the high temperature symmetry might not be the ideal prototypic cubic.

Figure 7(a) shows the induced polarization as a function of electric field (i.e., the P–E response) for MPB compositions of BGF–PT modified with 0, 10, and 20 at. % La. The measurement frequency was 10 Hz. For BGF–PT with 0 at. % La, polarization switching was observed until the applied electric fields up to 150 kV/cm. The remanent polarization P_r was about 10 μC/cm^2. In order to achieve a more switchable polarization within realistic fields, La modification was found to be essential. For MPB compositions of BGF–PT with either 10 or 20 at. % La, a P_r of around 30 μC/cm^2 was obtained. Clearly, the La substituent reduces E_c, and subsequently makes a dramatic change in the induced polarization realizable at a set field level. It is important that either BGF–PT or BLGF–PT specimens did not exhibit significant leakage currents in the $P-E$ response, even at fields up to 150 kV/cm. For BLGF–PT with 10 and 20 at. % La, the value of E_c was 35 and 20 kV/cm respectively, which are still $\sim 3-5x$ times larger than that of conventional PZT piezoelectric ceramics. This in conjunction with the high electrical strengths of BLGF–PT, demonstrates

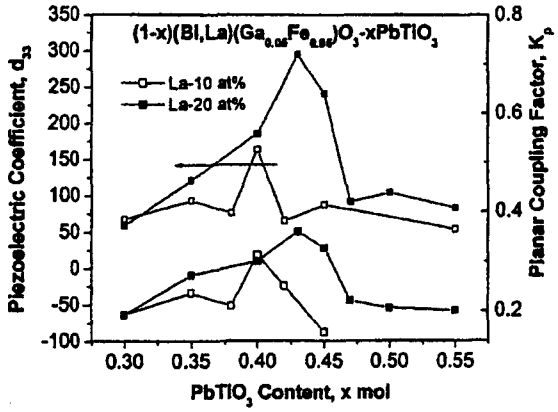

FIG. 8. Piezoelectric constant d_{33} and planar coupling factor K_p of BLGF–PT as a function of PT content with La concentrations of 10 and 20 at. %.

the potential of the material for high power electromechanical applications—as the $P-E$ product is enormous. Our results demonstrate that La modification in BGF–PT plays a critical dual role by (i) enhancing the electrical resistance and (ii) lowering the field required to pole the material.

The high field bipolar and unipolar strain $\varepsilon-E$ responses are shown in Figs. 7(b) and 7(c), respectively. MPB compositions of BLGF–PT with 10 and 20 at. % La had similar bipolar and unipolar strain levels of 0.35% and 0.2% under applied electric fields of 60 kV/cm, respectively. These induced strains are equivalent to that of PZT ceramics. We estimate a large amplitude d_{33} value from a linear approximation of the slope of the unipolar $\varepsilon-E$ responses as $d_{33}=\Delta\varepsilon/\Delta E$ up to ~380 pm/V. To confirm these high values of d_{33}, we next performed weak field d_{33} measurements by both Berlincourt meter and standard IEEE resonance-antiresonance methods. Figure 8 shows d_{33} as a function of PT content for BLGF–PT ceramics as a function of PT content with 10 and 20 at. % La. A maximum in d_{33} was found near the MPB. The piezoelectric d_{33} constant was found to be as large as 295 pC/N (20 at. % La) and 163 pC/N (10 at. % La), with planar coupling coefficients of k_p up to 0.36. These values of d_{33} are equivalent to those of PZT ceramics.

The effect of Ga was prominent in improving piezoelectric properties, rather than the high resistivity in the La and Ga comodified system. It was found that 0.55BLF–0.45PT without Ga still had the high resistivity of 1.88 $\times 10^{12}$ Ω cm. However, 0.55BLGF–0.45PT revealed higher P_r and d_{33} of 29 μC/cm^2 and 250 pC/N compared that of 21 μC/cm^2 and 162 pC/N for 0.55BLF–0.45PT. The only difference is that we had 5 at. % Ga in the former.

IV. CONCLUSIONS

Lanthanum and gallium comodified $BiFeO_3$–$PbTiO_3$ ceramics that are a competitive alternative to MPB compositions of PZT have been developed. La modification (i) enhances the electrical resistivity; (ii) reduces the coercive field E_c required for poling; and (iii) significantly enhanced d_{33}. In addition, BLGF–PT ceramics have enormously high dielectric strengths offering applications as a high power electromechanical material. Finally, BLGF–PT is also superior with regards to environmental friendliness, due to a significant reduction in Pb content relative to that of conventional piezoelectric materials.

ACKNOWLEDGMENTS

The authors are pleased to acknowledge support from the Office of Naval Research (ONR) under Contract No. N00014-99-1-1011. They thank Dr. Tom Shrout and Dr. Clive Randall for their suggestions and guidance in developing the ceramic systems and Nan Li for his great work on the ceramic processing.

[1] B. Jaffe, W. R. Cook, and H. Jaffe, *Piezoelectric Ceramics* (Academic, New York, 1971).
[2] S.-E. Park and T. R. Shrout, J. Appl. Phys. **82**, 1804 (1997).
[3] C. F. Buhrer, J. Chem. Phys. **36**, 798 (1962).
[4] A. Herabut and A. Safari, J. Am. Ceram. Soc. **80**, 2954 (1997).
[5] R. E. Eitel, C. A. Randall, T. R. Shrout, P. W. Rehrig, W. Hackenberger, and S.-E. Park, Jpn. J. Appl. Phys., Part 1 **40**, 5999 (2001).
[6] J. Cheng, R. E. Eitel, N. Li, and L. E. Cross, J. Appl. Phys. **94**, 605 (2003).
[7] M. M. Kumar and V. R. Palkar, Appl. Phys. Lett. **76**, 2764 (2000).
[8] T. Kanai, S. Ohkoshi, A. Nakajima, T. Watanabe, and K. Hashimoto, Adv. Mater. (Weinheim, Ger.) **7**, 487 (2001).
[9] G. Smolenskii, V. Isupov, A. Agranovskaya, and N. Krainik, Sov. Phys. Solid State **2**, 2651 (1961).
[10] P. Fischer, M. Polomskya, I. Sosnowska, and M. Szymanksi, J. Phys. C **13**, 1931 (1980).
[11] V. V. S. S. Sai Sunder, A. Halliyal, and A. M. Umarji, J. Mater. Res. **10**, 1301 (1995).
[12] R. Gerson, P. Chou, and W. J. James, J. Appl. Phys. **38**, 55 (1967).
[13] R. T. Smith, G. D. Achenbach, R. Gerson, and W. J. James, J. Appl. Phys. **39**, 70 (1968).
[14] M. M. Kumar, A. Srinivas, S. V. Suryanarayana, and T. Bhimasankaram, Phys. Status Solidi A **165**, 317 (1998).
[15] J. Cheng, N. Li, and L. E. Cross, J. Appl. Phys. **94**, 5153 (2003).
[16] D. Viehland and Y. Chen, J. Appl. Phys. **88**, 6696 (2000).

APPENDIX 2

JOURNAL OF APPLIED PHYSICS VOLUME 96, NUMBER 11 1 DECEMBER 2004

Piezoelectric performances of lead-reduced $(1-x)(Bi_{0.9}La_{0.1})(Ga_{0.05}Fe_{0.95})O_3$ -$x(Pb_{0.9}Ba_{0.1})TiO_3$ crystalline solutions in the morphotropic phase boundary

Jinrong Cheng[a] and Zhongyan Meng
School of Materials Science and Engineering, Shanghai University, Shanghai, 200072, People's Republic of China

L. Eric Cross
Materials Research Institute, The Pennsylvania State University, University Park, Pennsylvania 16802

(Received 21 April 2004; accepted 4 September 2004)

In this investigation, $(1-x)(Bi_{0.9}La_{0.1})(Ga_{0.05}Fe_{0.95})O_3$-$x(Pb_{0.9}Ba_{0.1})TiO_3$(BLGF-PBT) crystalline solutions have been fabricated by using the solid-state reaction method. A ferroelectric rhombohedral/tetragonal morphotropic phase boundary (MPB) of $(1-x)$BLGF-xPBT was observed for $x=0.4$. In the vicinity of MPB, 0.6BLGF-0.4PBT revealed the maximum dielectric constant K and piezoelectric d_{33} constant of 1168 and 186 pC/N, respectively. The substitution of 10 at. % Ba for Pb dramatically increased K and d_{33} of $(1-x)$BLGF-xPBT relative to $(1-x)$BLGF-xPT at the same x content. The Curie temperature T_c of $(1-x)$BLGF-xPBT was determined to be above 386 °C through the compositions investigated. The phase diagram of $(1-x)$BLGF-xPBT revealed a V-shaped relationship between T_c and x content. The planar coupling coefficient K_p was measured to be 0.37 for 0.6BLGF-0.4PBT, which was stable with increasing the measurement temperature until 170 °C. It is demonstrated that BLGF-PBT is a competitive alternative piezoelectric material, with the superior piezoelectricity and lead-reduced composition. © *2004 American Institute of Physics*. [DOI: 10.1063/1.1810633]

I. INTRODUCTION

Lead zirconium titanate (PZT) has been a strategically important material for many decades, on which rests sonar and medical ultrasonic imaging technologies.[1,2] However, the high lead content of PZT is one of the disadvantages due to the ecological restriction to the usage of lead. The lead content at the morphotropic phase boundary (MPB) has been known to be 50 at. % for conventional PZT ceramics. New piezoelectric compositions with reduced Pb content or lead-free ceramics are in increasing demand to meet this challenge. A lot of materials,[3–6] such as $(Bi_{0.5}Na_{0.5})TiO_3$, $(K_{0.5}Na_{0.5})NbO_3$ and their solid solutions with $BaTiO_3$ and $PbTiO_3$ have been investigated, focusing efforts on finding alternatives to the lead-rich ceramics. Messing and co-workers reported the lead-free piezoelectrics of Nb-modified $Bi_4Ti_3O_{12}$, and $(Na_{1/2}Bi_{1/2})TiO_3$-$BaTiO_3$ (<6.5% $BaTiO_3$)[7,8] giving the piezoelectric d_{33} constant up to 500 pC/N. However, layered $Bi_4Ti_3TO_{12}$ ceramics have the limitation of their lower piezoelectric constant, while the $(Na_{1/2}Bi_{1/2})TiO_3$ family ceramics are difficult to pole due to a large coercive field, and have a limited working temperature range resulting from a ferroelectric to antiferroelectric transition in the vicinity of ~100–200 °C.[9] The alternative lead-reduced $BiMeO_3$-$PbTiO_3$ MPB piezoelectric solid solutions have been recently developed to replace PZT for acoustic materials applications. Table I summarizes the lead content and properties of $BiMeO_3$-$PbTiO_3$ at the MPB.[10–13] It can be seen that Pb content can be reduced to 15 at. % for $BiFeO_3$-$PbTiO_3$ at the MPB, and the comparable piezoelectric properties have been obtained for these lead-reduced piezoelectric ceramics.

Perovskite $BiFeO_3$ has attracted many attentions for a long time due to its unique structure and properties[14,15]. $BiFeO_3$ is in the rhombohedral symmetry with a large rhombohedral angle of 89°24′, which implies a strong ferroelectric effect from cubic symmetry to rhombohedral distortion. T_c of $BiFeO_3$ is as high as 850 °C indicating promising applications for the high-temperature transducer. However, the development of previous $BiFeO_3$ family piezoelectric materials was hindered by two major problems. One was due to the conductivity caused by the valence variation of Fe^{3+} to Fe^{2+}, and another was the high switching field of $BiFeO_3$. Crystalline solutions of $BiFeO_3$ with $PbTiO_3$ and $BaTiO_3$ have also been investigated for many years to obtain the reliable piezoelectricity.[16,17] Up to date, the authors of this paper discovered that La substitute in Bi site of BF-PT could reduce the conductivity and coercive field simulta-

TABLE I. Lead content and electrical properties of lead-reduced $BiMeO_3$ -$PbTiO_3$ MPB piezoelectric ceramics.

Compositions	MPB	Pb content (at. %)	d_{33} (pC/N)	T_c (°C)
$(1-x)BiFeO_3$-$xPbTiO_3$	$x=0.3$	15	50	650
$(1-x)(Bi,La)FeO_3$-$xPbTiO_3$	$x=0.4$	20	163	386
$(1-x)Bi(Mg,Ti)O3$-$xPbTiO3$	$x=0.37$	18.5	225	478
$(1-x)BiScO_3$-$xPbTiO_3$	$x=0.64$	32	450	450

[a]Electronic mail: jrcheng@mail.shu.edu.cn

neously. The structure and piezoelectric properties of $BiFeO_3$-$PbTiO_3$ (BF-PT) could be flexibly tailored by using different substituents.

Our primary results indicated that modified BF-PT might be the new generation alternative MPB piezoelectric materials to conventional PZT. The objective of this work is to investigate the effect of Ba modification on La-modified BF-PT. Structural and electrical properties of Ba-modified BF-PT were summarized and compared with the compositions without Ba modification. We have achieved the goal of developing lead-reduced BF-PT-based piezoelectric materials.

II. EXPERIMENTAL PROCEDURE

Modified $(1-x)$BLGF-xPBT has been fabricated by the solid-state reaction methods, in which the content of La and Ga was chosen at 10 and 5 at. %, respectively, for $0.2 \leqslant x \leqslant 0.55$. We found that Ba of >20 at. % made BLGF-PT more relaxor rather than ferroelectrics. Therefore, Ba of 10 at. % was added to maintain the strong ferroelectricity of BF-PT. The starting materials used were Bi_2O_3, Fe_2O_3, La_2O_3, Ga_2O_3, $PbCO_3$, $BaCO_3$, and TiO_2, which all were of purities greater than 99%. The oxide powders were mixed by using the ball milling, and subsequently calcined at 750 °C for 4 h. Calcined powders were vibratory milled for an additional 24 h to make the powders fine and uniform. Powders were pressed and then sintered at 1000–1120 °C for 0.8 h in a crucible, which was sealed by high-temperature Al_2O_3 cement. Specimens of BLGF-PT without Ba were also prepared for the comparison purpose. The structure evolution of our specimens was confirmed by using x-ray diffraction (XRD) technique. Fresh fracture surfaces of sintered pellets were observed using scanning electron microscopy (SEM, Hitachi S-3000H). Specimens were electroded using a post-fired silver paste for electrical measurements. High-temperature dielectric measurements were carried out from room temperature to 600 °C using the measuring frequency of 10^3, 10^4, and 10^6 Hz, respectively. Field-induced polarization and strain were measured using a modified Sawyer-Tower circuit with a linear variable differential transducer at the frequency of 10 and 1 Hz, respectively. The poled specimen was characterized by using the Berlincourt d_{33} meter and HP4194A impedance analyzer. The IEEE resonance-antiresonance method was utilized to calculate the electromechanical coupling factor. Specimens for electrical measurements were of ~10.4 mm in diameter and <0.5 mm in thickness.

III. RESULTS AND DISCUSSIONS

Among $A^{3+}B^{3+}O_3$ family perovskite materials, only $BiFeO_3$ has the stable perovskite structure. The perovskite structure of $(1-x)BiFeO_3$-$xPbTiO_3$ remained stable when x was decreased to 0.2. However, $BiScO_3$ and $BiGaO_3$ required $PbTiO_3$ content of $x>0.5$ and $x>0.8$, respectively, to form the stable perovskite structure. Figure 1(a) shows XRD patterns of $(1-x)(Bi_{0.9}La_{0.1})(Ga_{0.05}Fe_{0.95})O_3$-$x(Pb_{0.9}Ba_{0.1})TiO_3$ for $0.38 \leqslant x \leqslant 0.45$. To the detection limits of our diffractometer, $(1-x)$BLGF-xPBT was detected as the single-phase perovskite structure. Both $(1-x)$BLGF-xPBT and $(1-x)$BLGF-xPT have the similar crystalline structure. Addition of Ba did not change the phase structure, but increased the intensity of corresponding diffraction peaks. According to Fig. 1(a), the crystalline symmetry of $(1-x)$BLGF-xPBT can be seen to shift from rhombohedral to tetragonal distortion with increasing x content. The phase transformation might start in the vicinity of $x=0.4$. The diffraction peak at 2θ of around 32° can be seen to split for $x=0.45$ indicating the formation of tetragonal phase. Figure 1(b) reveals the lattice parameters of $(1-x)$BLGF-xPBT as a function of x content. The tetragonal distortion c/a ratio was of 1.03 for 0.55BLGF-0.45PBT. However, 0.55BLGF-0.45PT (without Ba) has the c/a ratio of 1.08. XRD results indicated that Ba was dissolved into the lattice structure causing the tetragonal distortion to decrease dramatically.

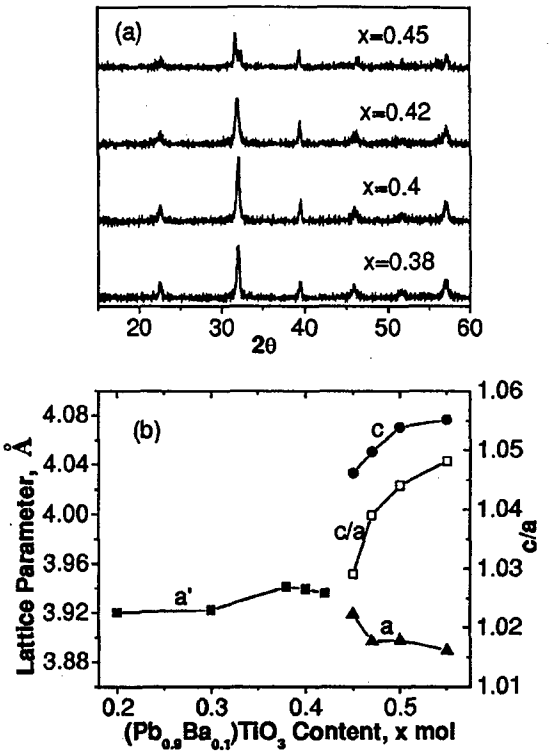

FIG. 1. (a) XRD patterns and (b) lattice parameters of $(1-x)$BLGF-xPBT as a function of x content.

Figure 2 presents the insulation resistivity of $(1-x)$BLGF-xPBT and $(1-x)$BLGF-xPT as a function of x content. For $0.3<x<0.45$, the resistivity ρ of modified BF-PT is in the order of 10^{12} Ω cm indicating that specimens are highly insulated. The maximum resistivity through compositions was observed for $x=0.4$. It is noticed that the value of ρ for BLGF-PBT is higher than that for BLGF-PT, indicating that addition of Ba contribute to increasing the insulation resistivity of BF-PT. The internal stress originated from the crystalline distortion was conjectured to suppress the reduction of $Fe^{3+} \rightarrow Fe^{2+}$ lowering the oxygen vacancy concentration and, subsequently, lowering the conductivity. Evidences of internal stress can be detected from SEM images. Figures 3(a) and 3(b) show the fresh fracture morphology of $(1-x)$BLGF-xPBT for $x=0.4$ and 0.45, respectively.

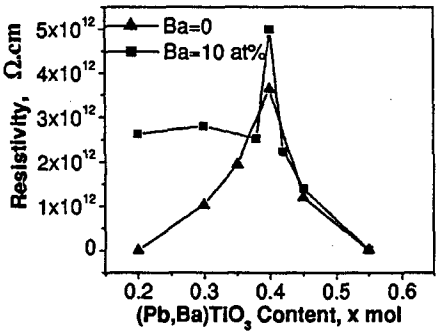

FIG. 2. Electrical resistivity of $(1-x)$BLGF-xPBT and $(1-x)$BLGF-xPT as a function of x content.

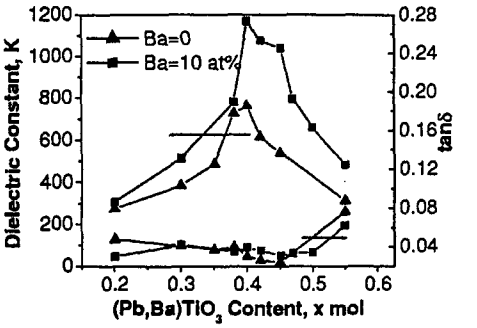

FIG. 4. Dielectric constant K and tan δ of $(1-x)$BLGF-xPBT and $(1-x)$BLGF-xPT as a function of x content at room temperature.

Figure 3(a) indicated that the fracture was more transgranular rather along the grain boundary, implying the existence of stronger internal stress. This is in agreement with the maximum resistivity of $(1-x)$BLGF-xPBT appearing for $x=0.4$. However, we do not have the detailed investigation at this point. It has been known that unstable $A^{3+}B^{3+}O_3$-type perovskite became more stable when it was synthesized under high-pressure environment.[18] It is sure that the stress has great effects on the solid-state reaction. The internal stress might provide a similar high-pressure environment to stabilize the perovskite, and reduce the conductive vacancy.

The dielectric constant K and tan δ of the poled specimens were measured at room temperature. Figure 4 shows the value of K and tan δ of $(1-x)$BLGF-xPBT and $(1-x)$BLGF-xPT as a function of x content, using the measurement frequency of 1 kHz. Through the compositions investigated, both $(1-x)$BLGF-xPBT and $(1-x)$BLGF-xPT can be seen to have dielectric maxima for $x=0.4$, however, the maximum value of K is of 1168 and 763, respectively. In the vicinity of dielectric peak, tan δ is of less than 4% reflecting the good electrical insulation of BLGF-PBT and BLGF-PT. It can be seen that addition of Ba caused K to increase greatly, especially in the region of $x \geqslant 0.4$. In addition, K did not drop quickly over $x=0.4$, remaining high in a broaden region of $0.4 \leqslant x \leqslant 0.47$ for $(1-x)$BLGF-xPBT. However, $(1-x)$BLGF-xPT was observed to have a narrow dielectric peak in the corresponding compositions.

The Curie temperature T_c of our specimen was determined by measuring dielectric constants in the temperature range of 30–600 °C. T_c is the temperature through which the dielectric maxima appeared due to the phase transformation from ferroelectric to paraelectric phase. Our modified BF-PT was detected to have the dielectric peak reflecting the strong ferroelectricity. With increasing the content of bismuth end member, the dielectric peak was widened reflecting the more relaxor characteristics. Combining with XRD analysis and electrical measurements, the phase diagram shown in Fig. 5 roughly summarizes the relationship among composition, transformation temperature, and phase structure of $(1-x)$BLGF-xPBT and $(1-x)$BLGF-xPT. The MPB was determined in the vicinity of $x=0.4$, at which modified BF-PT had the bottom T_c. The vertical line in the middle of phase diagram was drafted to illustrate the MPB, not from the experimental data. We now lack the high-temperature XRD analysis to confirm the true shape of MPB. To the left of the MPB, the perovskite phase has rhombohedral symmetry (FE_r), whereas to the right, it has tetragonal symmetry (FE_t). Above the T_c-x boundary line, the perovskite phase may be in the pseudocubic style. Interestingly, the modified BF-PT did not have a monotonous relationship between T_c and composition, as found for PZT. Rather, a V-shaped boundary between the paraelectric and ferroelectric phases was observed. This suggests that the oxygen octahedron might be twisted near the MPB, and that the high-temperature symmetry might not be the ideal prototypic cubic. Addition of Ba substituent caused T_c of $(1-x)$BLGF-xPBT to decrease relative to $(1-x)$BLGF-xPT, and the difference is about 40 °C in the vicinity of the MPB. This is one of the reasons that $(1-x)$BLGF-xPBT had higher dielectric constant than that of $(1-x)$BLGF-xPT. It can be seen that the bottom T_c for $(1-x)$BLGF-xPBT is around 340 °C, changing little in the region of $0.4<x<0.5$. This is in agree-

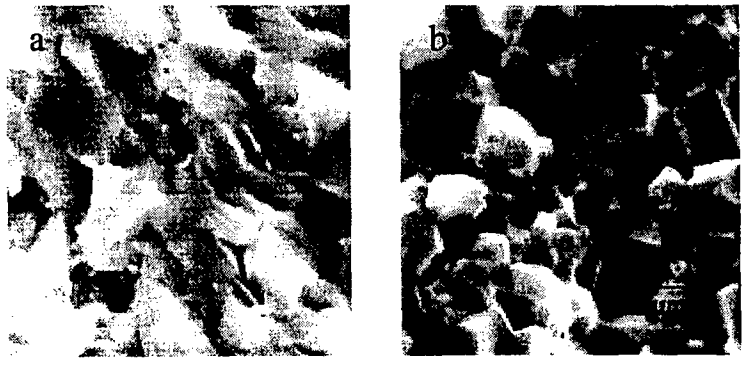

FIG. 3. SEM images of $(1-x)$BLGF-xPBT for (a) $x=0.4$ and (b) $x=0.45$.

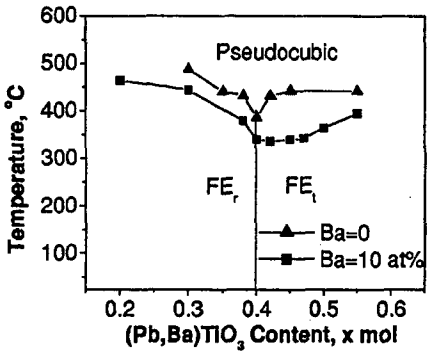

FIG. 5. Phase diagram of $(1-x)$BLGF-xPBT and $(1-x)$BLGF-xPT.

ment with the broaden dielectric peak through compositions for $(1-x)$BLGF-xPBT at room temperature. It might be one of the explanations that the value of K remained high rather than drop fast over the dielectric peak for $(1-x)$BLGF-xPBT.

Figure 6(a) shows the induced polarization of $(1-x)$BLGF-xPBT and $(1-x)$BLGF-xPT for $x=0.4$ as a function of electric field (i.e., the P-E response). The measurement frequency was 10 Hz. The P-E response reveals the strong ferroelectric switching behavior for modified BF-PT. No significant conductivity can be observed from P-E hysteresis loops. The remnant polarization P_r and coercive field E_c of 0.6BLGF-0.4PBT are of 26 μC/cm^2 and 28 kV/cm, respectively. It is indicated that modified BF-PT achieved the comparable ferroelectric properties with conventional PZT, with the relatively larger E_c and dielectric strength. The Ba modification can be seen to lower E_c and to contribute a nicer shape of P-E hysteresis loop for 0.6BLGF-0.4PBT. The corresponding unipolar strain as a function of electric field (ε-E response) is shown in Fig. 6(b). The strain level of specimens is achieved around 0.2% under the field of 60 kV/cm. The ε-E response of 0.6BLGF-0.4PBT had a smaller hysteresis than that of 0.6BLGF-0.4PT. The relatively fat shape of ε-E loop for 0.6BLGF-0.4PT might attribute to the domain switching under the high electrical field. With Ba modification, 0.6BLGF-0.4PBT revealed stronger piezoelectric responses.

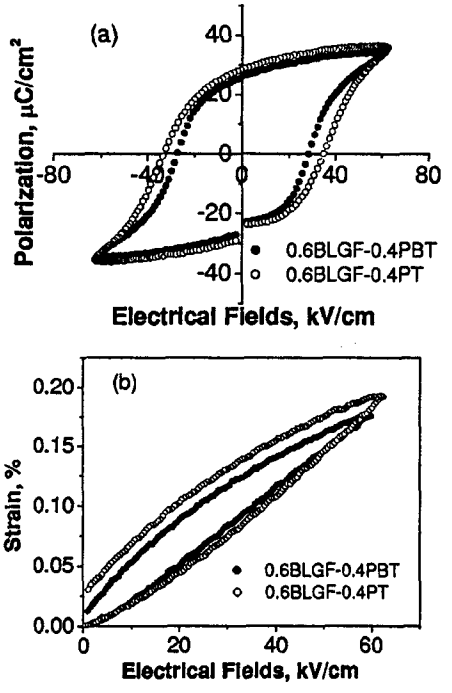

FIG. 6. Induced (a) polarization and (b) strain as a function of electric field for 0.4BLGF-0.6PBT and 0.6BLGF-0.4PT.

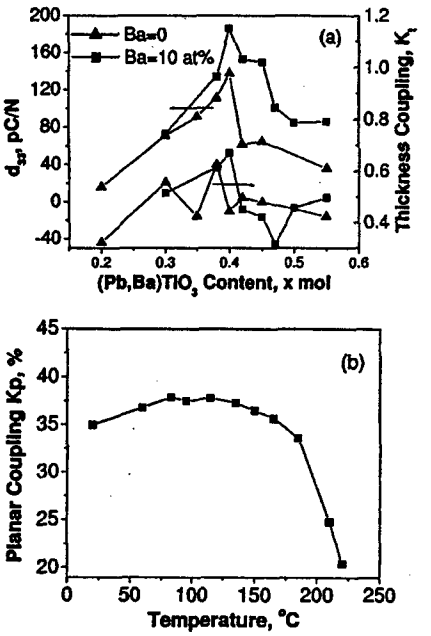

FIG. 7. Weak-field piezoelectric properties of (a) d_{33} constant and thickness coupling factor K_t of $(1-x)$BLGF-xPBT and $(1-x)$BLGF-xPT as a function of x content and (b) planar coupling factor K_p of 0.6BLGF-0.4PBT at the elevated temperatures.

Figure 7(a) shows the weak-field piezoelectric d_{33} constant and thickness coupling factor K_t of $(1-x)$BLGF-xPBT and $(1-x)$BLGF-xPT as a function of x content. K_t was determined using a HP4194 impedance meter with the IEEE resonance and antiresonance method. The formula used to calculate K_t is as follows: $K_t^2 = \pi/2 f_r/f_a \tan \pi/2\Delta f/f_a$, where f_r and f_a represent the resonance and antiresonance frequency, respectively. It can be seen that the variation of d_{33} and K_t with x is similar to the relationship between K and x. There are peaks appearing in the vicinity of $x=0.4$. The corresponding maximum d_{33} and K_t are of 186 pC/N and 67%, respectively, for 0.6BLGF-0.4PBT. Modified BF-PT with Ba had the higher value of d_{33}. In order to investigate the temperature dependence of piezoelectric response, the planar coupling factor K_p was measured at the elevated temperatures. Figure 7(b) shows the relationship of K_p versus temperature for the specimen of 0.6BLGF-0.4PBT. It can be seen that K_p started to drop when T was increased above 170 °C, about half of T_c. Usually, the working temperature of normal piezoelectric ceramics can reach half of T_c.

IV. CONCLUSIONS

Modified $(1-x)(Bi_{0.9}La_{0.1})(Ga_{0.05}Fe_{0.95})O_3$-$x(Pb_{0.9}Ba_{0.1})TiO_3$ crystalline solutions have been developed to be piezo-

electric materials with the MPB in the vicinity of $x=0.4$. Addition of 10 at. % Ba improved the dielectric and electromechanical responses of $(1-x)$BLGF-xPBT. In addition, the dielectric and piezoelectric peak through compositions was broadened due to the Ba modification. $(1-x)$BLGF-xPBT close to the MPB revealed competitive piezoelectric properties with conventional piezoelectric materials. The lead content of modified BF-PT has been significantly reduced.

ACKNOWLEDGMENTS

The authors are pleased to acknowledge support from the Office of Naval Research (ONR) under Contract No. N00014-99-1-1011, the Chinese National Science Foundation under Grant No. 50302006 and 50472098, Shanghai Rising Star Program under Grant No. 04qmx1440, and the key subject construction project (Material Science) of Shanghai Educational Committee

[1]B. Jaffe, W.R. Cook, and H. Jaffe, *Piezoelectric Ceramics* (Academic, New York, 1971).
[2]S.-E. Park and T.R. Shrout, J. Appl. Phys. **82**, 1804 (1997).
[3]G.A. Smolensky, V.A. Isupov, A.I. Agranovskaya, and N.N. Krainik, Sov. Phys. Solid State **2**, 2651 (1961).
[4]C.F. Buhrer, J. Chem. Phys. **36**, 798 (1962).
[5]A. Herabut and A. Safari, J. Am. Ceram. Soc. **80**, 2954 (1997).
[6]J.-K. Lee, K.S. Hong, C.K. Kim, and S.-E. Park, J. Appl. Phys. **91**, 4538 (2002).
[7]S. Hong, S. Trolier-McKinstry, and G.L. Messing, J. Am. Ceram. Soc. **83**, 113 (2000).
[8]H. Yilmaz, G.L. Messing, and S. Trolier-McKinstry, U.S. Navy Workshop on Acoustic Transduction Materials and Devices, Pennsylvania State, 2003.
[9]T. Takenaka, K. Sakata, and K. Toda, Ferroelectrics **106**, 375 (1990).
[10]J. Cheng and L.E. Cross, J. Appl. Phys. **94**, 5188 (2003).
[11]J. Cheng, N. Li, and L.E. Cross, J. Appl. Phys. **94**, 5153 (2003).
[12]C.A. Randall, R. Eitel, B. Jones, T.R. Shrout, D.I. Woodward, and I.M. Reaney, J. Appl. Phys. **95**, 3633 (2004).
[13]R.E. Eitel, C.A. Randall, T.R. Shrout, P.W. Rehrig, W. Hackenberger, and S.-E. Park, Jpn. J. Appl. Phys., Part 1 **40**, 5999 (2001).
[14]T. Kanai, S. Ohkoshi, A. Nakajima, T. Watanabe, and K. Hashimoto, Adv. Mater. (Weinheim, Ger.) **7**, 487 (2001).
[15]Y.F. Popov, A.M. Kadomtseva, S.S. Krotov, D.V. Belov, G.P. Vorob'ev, P.N. Makhov, and A.K. Zvezdin, Low Temp. Phys. **27**, 478 (2001).
[16]M.M. Kumar, A. Srinivas, S.V. Suryanarayana, and T. Bhimasankaram, Phys. Status Solidi A **165**, 317 (1998).
[17]V.V.S.S. Sai Sunder, A. Halliyal, and A.M. Umarji, J. Mater. Res. **10**, 1301 (1995).
[18]Y. Inaguma, A. Miyaguchi, M. Yoshida, T. Katsumata, Y. Shimojo, R. Wang, and T. Sekiya, J. Appl. Phys. **95**, 231 (2004).

APPENDIX 3

High-field and high-T_c piezoelectric ceramics based on $Bi(Ga,Fe)O_3$-$PbTiO_3$ crystalline solutions

Jinrong Cheng and Zhongyan Meng
School of Materials Science and Engineering, Shanghai University, Shanghai, 200072, People's Republic of China

L. Eric Cross
187 Materials Research Institute, The Pennsylvania State University, University Park, Pennsylvania 16802

(Received 30 August 2004; accepted 6 September 2005; published online 19 October 2005)

The gallium-modified bismuth ferrite-lead titanate compositions of $0.4Bi(Ga_{0.4}Fe_{0.6})O_3$-$0.6PbTiO_3$ (0.4BGF-0.6PT), has been investigated for the potential as a high-field and high-temperature piezoelectric ceramic. The crystalline solutions of 0.4BGF-0.6PT were fabricated by using the solid-state reaction method. X-ray diffraction analysis revealed that 0.4BGF-0.6PT has a tetragonal perovskite structure. The Curie temperature T_c of 0.4BGF-0.6PT was determined to be 540 °C. Our 0.4BGF-0.6PT ceramic specimens could withstand the electric field of >250 kV/cm, reflecting the excellent dielectric breakdown strength. The remanent polarization (Pr) and induced strain (ε) achieved were 30 $\mu C/cm^2$ and 0.2%, respectively, revealing the strong ferroelectricity of 0.4BGF-0.6PT. The specimen could be poled into the piezoelectric state under a poling field of 240 kV/cm, giving a weak-field piezoelectric constant d_{33} of 52 pC/N. © *2005 American Institute of Physics*. [DOI: 10.1063/1.2103414]

I. INTRODUCTION

Bismuth ferrite, $BiFeO_3$, has been of interest due to its simple perovskite structure in which ferroelectric and antiferromagnetic orderings coexist at high temperature.[1–4] Bismuth ferrite is stable in the perovskite form having a Curie temperature of 850 °C and an antiferromagnetic Néel temperature at 310 °C. The unique structure-related properties make $BiFeO_3$ potentially of high interest for high-temperature multifunctional applications. However, the piezoelectric and dielectric properties of $BiFeO_3$ and $BiFeO_3$-based materials were limited or unknown for many decades, due to their high electrical conductivity, which prevented proper exploration of low-frequency dielectric properties. Recent studies of $BiFeO_3$-based solid solutions have focused upon exploring cation dopants to control the ceramic conduction. It has been reported that Ga^{3+} partial substitutions for Fe^{3+} in $BiFeO_3$-$PbTiO_3$ (BF-PT) solid solutions could generate resistivities up to $10^{12}\ \Omega\cdot$cm. At the same time, while the addition of La^{3+} made BF-PT easier to be poled into the piezoelectric state, it also caused T_c to decrease. The piezoelectric coefficient d_{33} of 300 pC/N was achieved for the La^{3+} and Ga^{3+} co-modified BF-PT at the morphotropic phase boundary (MPB) between the rhombohedral (R) and tetragonal (T) phases.[5,6] The Curie temperature T_c of 650 °C was obtained for the Ga^{3+} modified BF-PT. These results indicated that the modified BF-PT had comparable piezoelectric properties to conventional $Pb(Zr,Ti)O_3$ (PZT) piezoelectric ceramics. The advantages of bismuth-contained perovskites over PZT family materials are the relatively high mechanical and electrical strengths, and high Curie temperatures.

The objective of this work was to explore high T_c and high-field piezoelectric materials based on 0.4BGF-0.6PT. The Ga^{3+} was introduced into BF-PT to improve the insulation resistance and maintain high T_c simultaneously. Specifically, the phase structure evolution and microstructural information were obtained from the temperature-dependent x-ray diffraction (XRD) analysis and scanning electron microscopy (SEM) characterization. The ferroelectric properties were examined under the high electrical field. The effect of stresses on ferroelectric polarization was briefly discussed. We found that 0.4BGT-0.6PT had giant dielectric strength, which had never been previously reported.

II. EXPERIMENTAL PROCEDURE

Specimens were fabricated by the mixed oxide method. The starting materials used were Bi_2O_3, Fe_2O_3, Ga_2O_3, $PbCO_3$, and TiO_2, with the purity of >99%. Before batching, the loss on ignition of all raw materials was established to obtain the accurate stoichiometry. The oxide powders were batched in appropriate quantities according to the general formula of $0.4Bi(Ga_{0.4}Fe_{0.6})O_3$-$0.6PbTiO_3$. This was followed by ball milling for 24 h and subsequently calcining for 4 h at 750 °C. The calcined powders were vibratory milled for an additional 24 h, and then were granulated with an acryloid polymer (binder) and pressed into pellets. The binder was removed by heating the green pellets at 600 °C for 1 h. Specimens were sintered at 1050 °C for 0.8 h in a sealed crucible. Finally, disks were additionally sintered under pressure to increase the densification. The sintering was carried out in a hot isostatic press (HIP) operated at the pressure of 21 GPa, and at the temperature of 950 °C for 1 h in oxygen ambient. For comparison purposes, specimens of $0.4BiFeO_3$-$0.6PbTiO_3$ without Ga substitutions were also prepared following the similar steps.

For the high-temperature XRD measurement, sintered pellets were crushed into powders, and then annealed at $T > T_c$ to remove the remanent grinding stress. Powders were

placed on the platinum holder. The x-ray diffractometer (Sintag 2) was operated at a scanning rate of 1°/min at 2θ of 15–45 °. XRD data were collected from room temperature to 630 °C. The SEM (Hitachi S-3000H) observation was performed on the freshly fractured surface of ceramics. The chemical homogeneity of specimens was examined by energy-dispersive x-ray analyzer (EDX, EDAX/TSL, Phoenix). Specimens were electroded by using a postfired silver paste (Dupont 6160) for electrical measurements. Dielectric capacitance and loss were measured at room temperature using an HP4194 impedance analyzer. The temperature-dependent dielectric properties were measured between 25 and 650 °C using the HP4284 multifrequency *LCR* meter interfaced with a computer to control the temperature and heating rate. The field-induced polarization and strain were measured at room temperature using a modified Sawyer-Tower circuit with a linear variable differential transducer (LVDT) to obtain induced strain data. Specimens were poled in a silicon oil bath at room temperature by applying a one-cycle unipolar ac field at the frequency of 1 Hz. The piezoelectric constant d_{33} was measured using a Berlincount (ZJ-2) d_{33} meter. For the polarization and d_{33} measurements, specimens were ground into 0.08 mm in thickness. A 2.89–mm-diam platinum electrode was sputtered in the center of some specimens. The ferroelectric and piezoelectric measurements were conducted on both fully and partially electroded specimens. Before the electrical measurement, specimens were annealed to remove the remanent processing stresses.

III. RESULTS AND DISCUSSIONS

The sintering quality was maintained by controlling the sintering shrinkage of about 18% in diameter and the weight loss of less than 1 wt %. The relative density of ceramics was of >96% after HIP sintering. Figure 1(a) shows the SEM image of 0.4BGF-0.6PT ceramics taken from the freshly fractured surface. It can be seen that ceramics were well densified, not containing residual porosity. We found that 0.4BGF-0.6PT prepared under these conditions was a fine grain material with square-shaped grains of 500–1000 nm in size. The EDX compositional analysis was performed at three different points. Figure 1(b) shows the representative EDX pattern of 0.4BGF-0.6PT. The half-quantitative element calculation indicated that the ceramics had chemical homogeneity. The average atom ratio of Ga to Fe was 0.675, close to the chosen stoichiometry.

Figure 2(a) shows the lattice parameter of 0.4BGF-0.6PT as a function of temperature. These data were derived from XRD patterns of 0.4BGF-0.6PT taken from 25 to 630 °C [examples are shown in Fig. 2(b)]. According to XRD results, 0.4BGF-0.6PT revealed the pure perovskite structure through the temperature range investigated. No pyrochlore phases could be found. The diffraction peak of Pt(111) was detected from the powder holder. At 25 °C, 0.4BGF-0.6PT showed the tetragonal symmetry with the c/a ratio of 1.09. The strong crystalline distortion for Ga-modified BF-PT is even higher than that of 1.06 for $PbTiO_3$. It has been known that the Curie temperature T_c of tetragonal

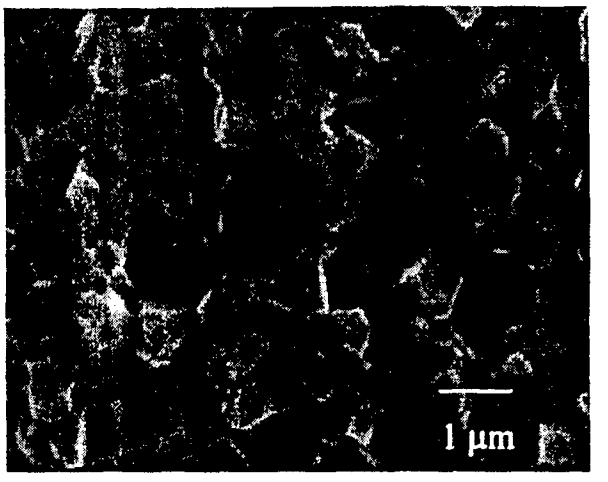

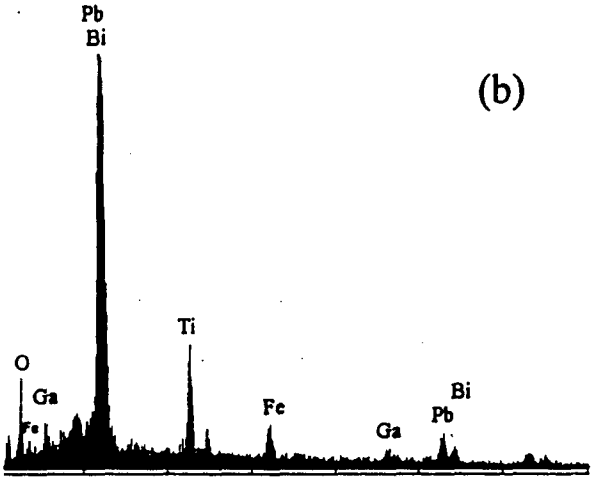

FIG. 1. Cross-sectional (a) SEM image and (b) EDX pattern for 0.4BGF-0.6PT.

ABO_3 family perovskites is proportional to the c/a ratio.[7] The highly distorted lattice symmetry required high temperature to remove the crystalline distortion, implying a high T_c for this material. With increasing the measurement temperature, the c/a ratio decreased gradually to 1.02 at about 470 °C. It can be seen that the peak splitting at 2θ of 31° disappeared at $T>500$ °C indicating the transformation from tetragonal to cubic phases. Therefore, the phase structure evolution with temperatures is an evidence of ferroelectric (FE) to paraelectric (PE) phase transition in the Ga-modified BF-PT.

The resistivity measured of 0.4BGF-0.6PT was of $>10^{12}\ \Omega\cdot$cm at room temperature reflecting highly insulating characteristics. Thus, the dielectric capacitance and loss could be measured using standard methods. The dielectric constant was calculated from the capacitance using a parallel plate approximation. Figure 3 shows the room-temperature dielectric coefficient K and tan δ as a function of frequency. The values of K and tan δ were 207 and 0.02, respectively, for 0.4BGF-0.6PT at 1 KHz, changing little with frequencies over the range of 10^2-10^6 Hz. The values of tan δ were comparable with those of highly insulated PZT ceramics.

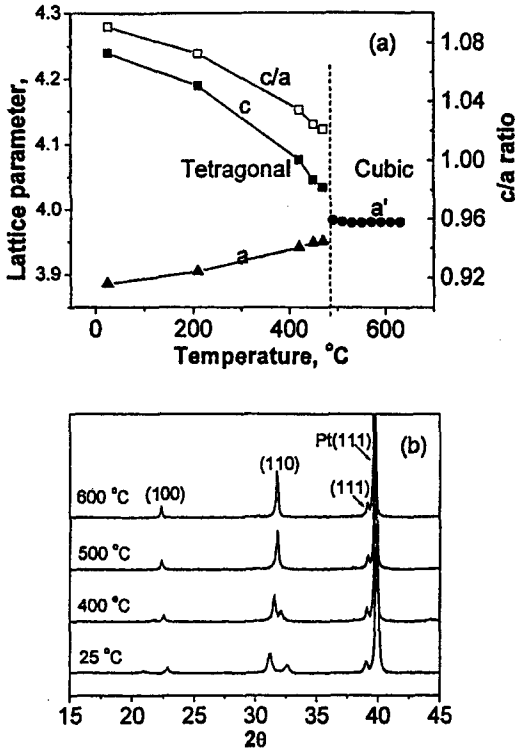

FIG. 2. (a) Lattice parameter and (b) XRD patterns as functions of temperature for 0.4BGF-0.6PT ceramic powders.

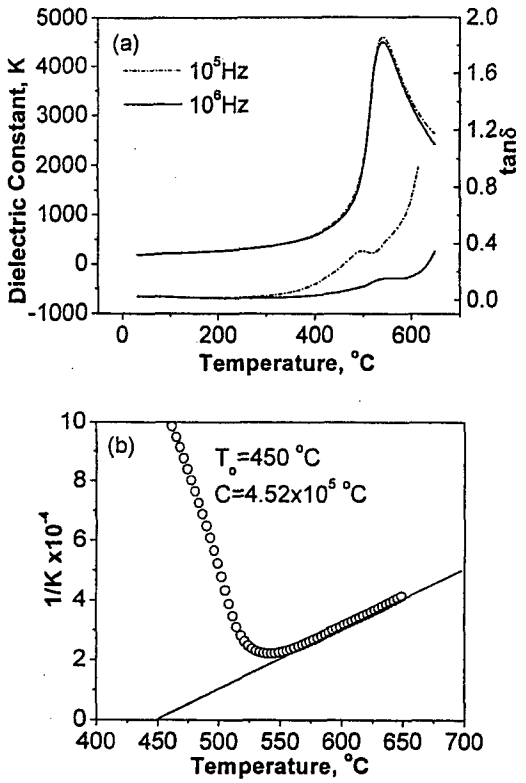

FIG. 4. (a) Dependence of K and tan δ on temperature and (b) reciprocal K vs temperature for 0.4BGF-0.6PT.

However, the value of tan δ was as high as 0.19 at 1 KHz for 0.4BF-0.6PT without Ga^{3+} substitution, and decreased significantly with increasing frequency. Therefore, Ga^{3+} substitution caused tan δ to decrease strongly. Similarly, the dispersion in K due to space charge evident in Fig. 3 for x =0.4 is also eliminated by the addition of Ga^{3+}. Detailed investigations of the effect of Ga^{3+} on the conduction control of BF-PT have been reported in a previous paper.[8]

Figure 4(a) shows K and tan δ of 0.4BGF-0.6PT as functions of temperature using the measurement frequencies of 10^5 and 10^6 Hz. The relationship of reciprocal K versus T is given in Fig. 4(b). The dielectric constant K slightly increases with temperature at $T<400$ °C, then rises rapidly, reaching the maximum near 540 °C. The temperature at the peak permittivity determined the Curie temperature T_c, over which the ferroelectric to paraelectric phase transition occurred. It can be seen that T_c of 0.4BGF-0.6PT was some 200 °C higher than that of bulk PZT. No frequency dispersion was observed, reflecting that 0.4BGF-0.6PT is a ferroelectrics rather than a relaxor. With increasing the temperature to 400 °C, tan δ maintained less than 0.02 at 10^6 Hz, indicating no significant conductivity problems. Usually, the working temperature of a piezoelectric ceramics could reach half of T_c. Thus, 0.4BGF-0.6PT would work well beyond 250 °C, about 100 °C higher than that of PZT.

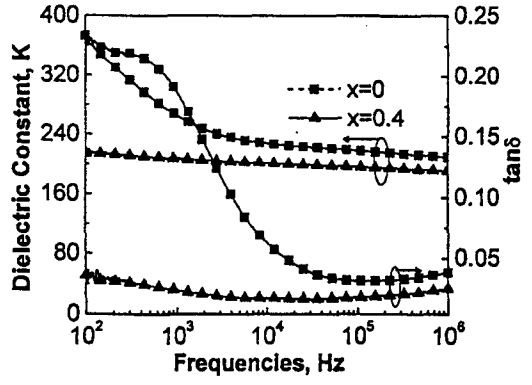

FIG. 3. Dielectric-constant K and tan δ of 0.4BGF-0.6PT as functions of frequency at room temperature.

For classic ferroelectrics, the Curie-Weiss law of $1/K=(T-T_0)/C$ is obeyed at the high temperature, where T_0 is the Curie-Weiss temperature and C is the Curie constant. According to Fig. 4(b), the dielectric constant K follows the Curie-Weiss law at $T>550$ °C. The values of C and T_0 are of 4.52×10^5 °C and 450 °C, respectively. That of $T_0<T_c$ suggests that the FE-PE phase transition is of the first-order type. Thus, the strong ferroelectric character of 0.4BGF-0.6PT is also evident in the high-temperature dielectric measurement.

High-T_c bismuth containing piezoelectric ceramics generally have very large coercive fields (E_c) at room temperature.[9,10] Figure 5(a) shows the induced polarization of 0.4BGF-0.6PT as a function of the driving field. At E =100 kV/cm, only a slim polarization–electrical field (P–E) hysteresis loop was observed, indicating that the applied field was not enough to make the domain switch. With increasing the driving field, the P–E loop developed over the range of 150-250 kV/cm. At E=250 kV/cm, a well-saturated P–E loop developed having the square shape and sharp corners. No significant leakage conduction could be observed at this field. The relationship of induced strain (ε) versus bipolar

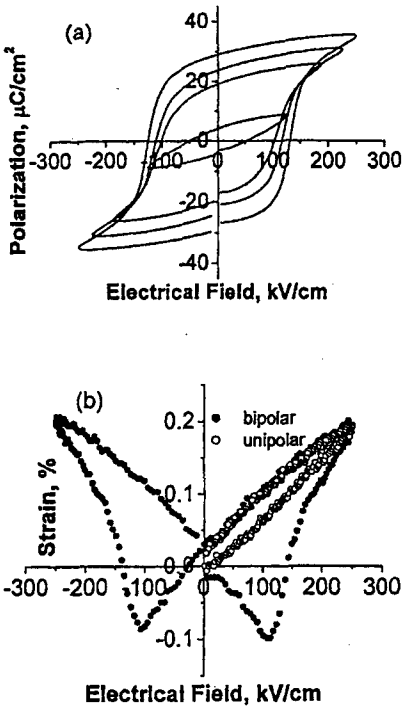

FIG. 5. Induced (a) polarization and (b) strain of 0.4BGF-0.6PT as functions of electrical field, using the measurement frequency of 10 and 1 Hz, respectively.

and/or unipolar electrical field (ε-E curve) is shown in Fig. 5(b). A typical butterfly ε-E curve was obtained, and the unipolar strain changed almost linearly with electrical fields. According to Fig. 5(a) and 5(b), the remanent polarization P_r and strain jump were of 30 μC/cm^2 and 0.2%, respectively. The coercive field E_c was of 130 kV/cm, about 20 times greater than that of bulk PZT. According to the formula of $U=0.5\varepsilon_0\varepsilon E^2$, the energy density U is proportional to E^2. Such a high E_c and saturated field of 0.4BGF-0.6PT have been thought amazing for bulk ceramics, producing a giant U and PE product. Therefore, 0.4BGF-0.6PT would be a promising composition for high-power and high-voltage electromechanical applications, if the coupling to strain could be further improved.

To achieve the very high E fields required for the hysteresis measurements it was necessary to thin the sample to <100 μm. A thin specimen reduced the influences of intrinsic defects allowing a higher break down E fields. As we observed from the SEM image, the grain size of ceramics was very fine, which was a contribution to the high breakdown strength. As detected by XRD, 0.4BGF-0.6PT had strong tetragonal distortion. This can stabilize the domain configuration and reduce the mobility of domain walls. Thus, 0.4BGF-0.6PT became less responsive but more stable, revealing a lower dielectric constant K and very high E_c, however, this is not the complete story.

A very puzzling feature is the electrode influence on the ferroelectric properties of 0.4BGF-0.6PT. In Fig. 6, curves (a) and (b) represent the P–E hysteresis loops for a partially and a fully electroded specimen, respectively. Under a similar electrical field, curve (a) is a well-developed P–E loop reflecting the strong ferroelectric response, whereas curve (b)

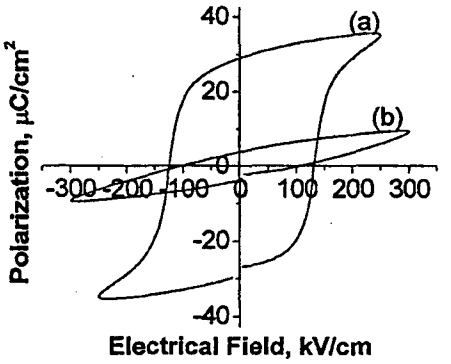

FIG. 6. Induced polarization of (a) partially and (b) fully electroded 0.4BGF-0.6PT specimens as a function of electrical field, using the measurement frequency of 10 Hz.

is very slim indicating that the specimen was barely switched. Consistent results of this type have been observed for several different specimens. The fully electroded specimen could not be completely switched at E=300 kV/cm. Thus, the large ferroelectric polarization was associated with the partially electroded specimen.

When the electrical field was applied on the specimen, the electroded area was switched, however, the bare area was not poled. Stresses were naturally produced between the switched and nonswitched areas. We conjectured that the combination of a high (001) E field and a very strong biaxial (100), (010) tension might break the magnetic symmetry, force a change to rhombohedral symmetry, and unlock the polarization. As in the PZTs, switching would be much easier in the rhombohedral form if broken from the strong antiferromagnetic magnetoelectric coupling. Stresses, such as intrinsic biaxial or applied uniaxial, have been known to influence the ferroelectric transformation and piezoelectric activity of piezoelectric materials.[11,12] Additional investigations are necessary to check out our hypotheses, which will be reported in an additional paper.

Figure 7 shows the high- and weak-field piezoelectric coefficient d_{33} of 0.4BGF-0.6PT for the different poling fields. The weak-field d_{33} was measured by using a quasistatic d_{33} meter at the frequency of 100 Hz, whereas the

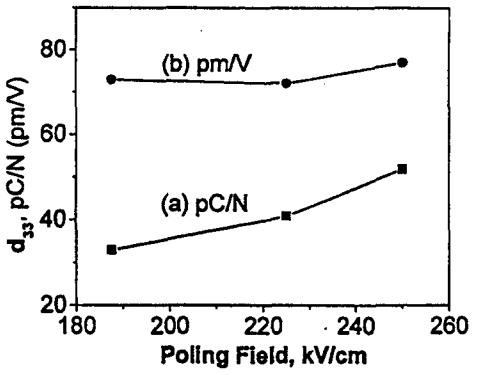

FIG. 7. Piezoelectric coefficient d_{33} of 0.4BGF-0.6PT under different poling fields. (a) Weak-field d_{33} constant measured by using a quasistatic d_{33} meter at the frequency of 100 Hz. (b) High-field d_{33} constant determined by taking the average slope of the unipolar ε-E curves, which were measured under the driving field of 180-250 kV/cm using the measurement frequency of 1 Hz.

high-field d_{33} constants were determined by taking the average slope of the unipolar ε-E curves, which were measured under the driving field of 180-250 kV/cm using the measurement frequency of 1 Hz. The value of weak-field d_{33} can be seen to increase slightly with increasing the poling field E_p, achieving 52 pC/N at an E_p of 240 kV/cm. The high-field d_{33} constant was determined to be 80 pm/V at the same poling field. The differences between the high- and weak-field d_{33} constants were caused by the increased activity of domain walls under the high electrical field.

IV. CONCLUSIONS

The solid solutions based on 0.4BGF-0.6PT have been developed to be highly insulating piezoelectric ceramics. Crystalline 0.4BGF-0.6PT had the perovskite structure with strong tetragonal distortion. The Curie temperature T_c of 0.4BGF-0.6PT was as high as 540 °C. The breakdown strength was of >250 kV/cm. In addition, 0.4BGF-0.6PT could be poled into the piezoelectric state at room temperature. For the same composition of 0.4BGF-0.6PT, the partially electroded specimen revealed greater improvement of ferroelectric polarizations, relative to the fully electroded one. Our results indicate that 0.4BGF-0.6PT offers great advantages for high-temperature and high-field electromechanical components.

ACKNOWLEDGEMENTS

We are pleased to acknowledge support from the National Nature Science Foundation of China under Grants Nos. 50472098 and 50302006, the Office of Naval Research (ONR) under Contract No. N00014-99-1-1011, the Shanghai Rising Star Program under Grant No. 04qmx1440, and the Key Subject Construction Project (Material Science) of the Shanghai Educational Committee.

[1]Y. F. Popov, A. M. Kadomtseva, S. S. Krotov, D. V. Belov, G. P. Vorob'ev, P. N. Makhov, and A. K. Zvezdin, Low Temp. Phys. **27**, 478 (2001).
[2]M. M. Kumar and V. R. Palkar, Appl. Phys. Lett. **76**, 2764 (2000).
[3]G. Smolenskii, B. Isupov, A. Agranovskaya, and N. Krainik, Sov. Phys. Solid State, **2**, 2651 (1961).
[4]P. Fisher, M. Polomskya, I. Sosnowska, and M. Szymanski, J. Phys. C **13**, 1931 (1980).
[5]J. Cheng and L. E. Cross, J. Appl. Phys. **94**, 5188 (2003).
[6]J. Cheng, R. Eitel, and L. E. Cross, J. Am. Ceram. Soc., **86** (12) 2111 (2003)
[7]V. V. S. S. Sunder, A. Halliyal, and A. M. Umarji, J. Mater. Res., **10**, 1301 (1995).
[8]J. Cheng and L. E. Cross, J. Appl. Phys. **94**, 5153 (2003).
[9]G. A. Smolensky, V. A. Isupov, A. I. Agranovskaya, and N. N. Krainik Sov. Phys. Solid State **2**, 2651 (1961).
[10]A. Herabut and A. Safari, J. Am. Ceram. Soc., **80**, 2954 (1997).
[11]G. A. Rossetti, Jr. and L. Eric Cross, Appl. Phys. Lett. **59**, 2524 (1991).
[12]D. Viehland, J. Li, E. McLaughlin, J. Powers, R. Janus, and H. Robinson, J. Appl. Phys. **95**, 1969 (2004).

APPENDIX 4

Mat. Res. Soc. Symp. Proc. Vol. 784 © 2004 Materials Research Society

Dielectric and Ferroelectric Properties of Modified $BiFeO_3$-$PbTiO_3$ Thin Films Derived from Sol-gel Processing

JinRong Cheng[1,2] and L.Eric Cross[1]
[1]Materials Research Institute, The Pennsylvania State University
University Park, PA 16802
[2]School of Materials Science and Engineering, Shanghai University
Shanghai 201800, P.R.China

ABSTRACT

In this paper, thin films of La- modified (Bi,La)FeO_3-$PbTiO_3$ (BLF-PT) morphotropic phase boundary (MPB) solid solutions have been prepared by using sol-gel processing. A thin $Pb(Zr,Ti)O_3$ (PZT) template layer was introduced to make BLF-PT thin films adhere tightly to the platinized silicon ($Pt/Ti/SiO_2/Si$) substrate. X-ray diffraction (XRD) analysis revealed that BLF-PT thin films were of the perovskite structure without detectable pyrochlore phase annealing at 650-750°C. The cross sectional and plain view images of or our specimen were observed by using the scan electrical microscope (SEM). The room temperature dielectric constant K and tanδ were of ~800 and 4% respectively, for BLF-PT thin films using a measurement frequency of 1 kHz. Our preliminary experiments indicated that the sol-gel derived BLF-PT thin films have good insulation resistance and measurable dielectric and ferroelectric responses.

INTRODUCTION

$BiFeO_3$ based thin films have received recent interests due to the unique properties relative to their bulk forms.[1,2] The epitaxial $BiFeO_3$ thin films have been currently deposited on the single crystal (100) $SrTiO_3$ substrate by using the pulsed laser deposition (PLD) techniques. No conductivity problem was observed for $BiFeO_3$ thin films. A giant spontaneous polarizations Ps of ~60 $\mu C/cm^2$ have been achieved, which is 10 times greater than that of $BiFeO_3$ single crystal. However, the coercive field of the films is as high as 200 kV/cm. In addition to pure $BiFeO_3$ perovskite thin films, bismuth contained solid solutions have also been developed in the thin film form.[3] For example, epitaxial 1 μm thick $BiScO_3$-$PbTiO_3$ thin films on (100) $LaAlO_3$ single crystal substrate exhibited good ferroelectric and piezoelectric properties, which was similar to their excellent performances of the bulk ceramics at the same compositions. Thin films of bismuth-contained materials were attracted due to their potentials for higher Curie temperature materials and stronger polarizations caused by Bi^{3+} cation.

Most recently, we first made excellent piezoelectric ceramics of $BiFeO_3$-$PbTiO_3$ (BF-PT) solid solutions by using La substituents.[4] This was our motive to prepare BLF-PT into the thin film form. In this paper, the conventional sol-gel technique was used to prepare the lanthanum modified BF-PT thin films on the widely used platinized silicon substrate. As mentioned above, pure $BiFeO_3$ has a large value of Ec. Our objective was to decrease Ec by making $BiFeO_3$ thin film solid solutions with $PbTiO_3$. We succeeded in dissolving multiple components into a stable solution. A template layer of PZT was introduced to improve the sintering property. The crystallized BLT-PT thin films were determined to be the single-phase perovskite with reliable dielectric and ferroelectric properties.

EXPERIMENT

The chemical solution of $0.57(Bi,La)FeO_3$-$0.43PbTiO_3$ (BLF-PT) and PZT were prepared by dissolving source materials into the 2-methxyethanol (2-MOE) solvent. Bismuth and iron nitrate was used as the source of Bi^{3+} and Fe^{3+} cations. Lanthanum and lead acetate were used to provide La^{3+} and Pb^{2+} cations. Zr^{4+} and Ti^{4+} cations came from zirconium n-propoxide and titanium tetrabutoxide alkoxide respectively. La^{3+} of 20 at% was used to substitute Bi^{3+} cations, while $Bi^{3+}$and Pb^{2+} of 10 at% excess was added to compensate the sintering volatility. The batched solutions were in the transparently red color. PZT solution was first spin-coated onto $Pt/Ti/SiO_2/Si$ and then annealed at 650°C for 30 minute. BLF-PT thin films were then repeatedly coated on the top of PZT template layer until the desired thickness. Finally, the specimens were annealed at 650, 700 and 750 °C individually.

The crystal structure was examined by using x-ray diffraction analysis (Diffractomer, Sintag 2) techniques. Scanning electrical microscope (SEM, Hitachi S-3000H) was utilized to observe the grain morphology. The thin films were sputtered top Pt electrodes with a diameter of 0.8 mm. The dielectric and ferroelectric properties of BLF-PT were characterized using HP4192 and HP4284 impedance analyzer and RT 66 ferroelectric measurement system. The leakage current density was measured by using the Keithley 6517 meter.

RESULTS AND DISCUSSION

Figure 1(a) and 1(b) show the plain view and cross sectional SEM images for a 0.93 μm-thick BLF-PT thin films. The grain size was observed about 150 nm. It was interesting to see a lot of cubes that appeared in the surface of thin films. The more detail analysis, such as compositions was required to detect the origin of cube. Both the plain view and cross sectional images show that BLF-PT thin films were densified without porosity. Layers including the Pt electrode layer and PZT template were observed between the substrate and BLF-PT thin films, It can be seen that the good adhesion of BLF-PT thin films to PZT thin layer. However, the film did not grow in the column form through thickness, rather in a discontinuous distribution of round grains.

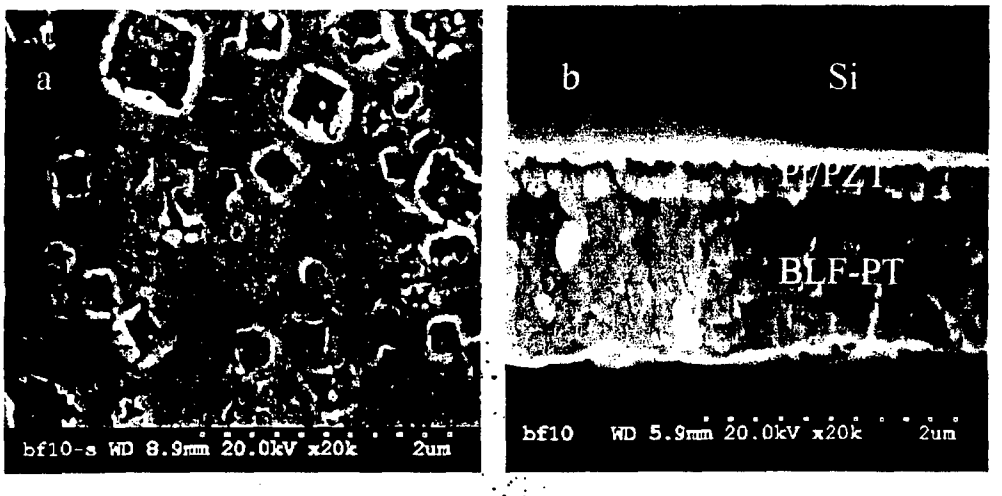

Figure 1 SEM images for the 0.93 μm-thick BLF-PT thin films taken from (a) plain view surface and (b) cross sectional surface

The annealed BLF-PT thin films were examined by XRD analysis. Figure 2 shows XRD patterns of a 0.45 μm-thick BLF-PT thin films annealed at 650°C. For the comparison purpose, the corresponding XRD pattern of bulk at the same composition is also shown in the figure. It can be seen that the thin films were crystallized, as revealed by diffraction peaks, i.e. (100), (110) and (111) at 2θ of 23°, 32° and 39° respectively, at which the corresponding bulk ceramics had peaks. All these are in agreement to prove the perovskite structure of BLF-PT thin films. The second phase has not been detected from the XRD patterns. The intensity of diffraction peaks for BLF-PT thin films was much lower than that of BLF-PT bulk ceramics. It conjectured that a higher annealing temperature might contribute to the better crystallinity.

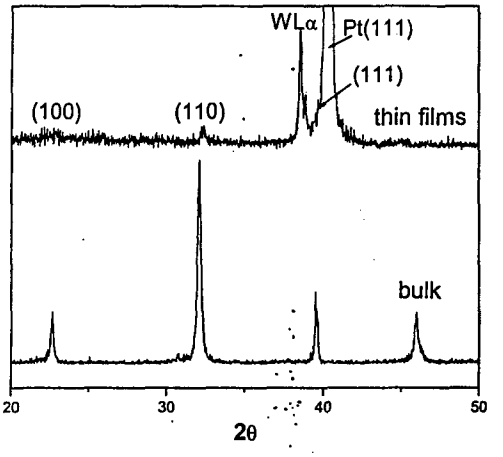

Figure 2 XRD patterns of BLF-PT materials in the thin film and bulk form respectively

The dielectric constant K and tanδ were measured at room temperature. Figure 3 shows K and tanδ as a function of frequency for BLF-PT thin films annealed at 650, 700 and 750 °C respectively.

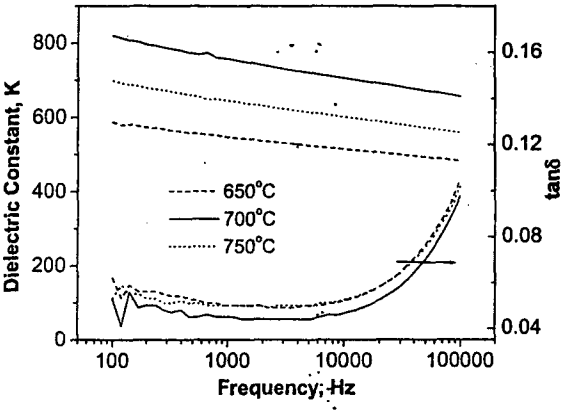

Figure 3 Dielectric constant K and tanδ of BLF-PT thin films as a function frequency at room temperature

It can be seen that BLF-PT thin films annealed at 700 °C had the relatively larger K than those of the films annealed at 650 and 750 °C. The values of K and tanδ were measured to be

~800 and 4% respectively, at the frequency of less than 10^5 Hz. No significant conductivity can be observed from the relationship of frequency and tanδ. The effect of the firing temperature on K might ascribe to the different crystallinity. The firing temperature of 650 °C was not enough to ensure the good crystallinity resulting in a lower value of K. This was in agreement to the lower intensity of diffraction peaks shown in figure 1. The annealing temperature of 750 °C might cause the volatility of bismuth and lead resulting in K to decrease. It has been reported that the value of K for BLF-PT ceramics at the same composition was about 1700.[4] The decrease of K might result from the fine grain of thin films, and the discontinuous growth of grains identified from the SEM image.

The leakage current density J of BLF-PT thin films as a function of electrical fields is shown in figure 4. The value of J is in the order of 10^{-9} A/cm^2 under E<25 kV/cm, which increased with increasing the applied electric field. One of reasons to produce the leakage current flowing through the metal-insulator-metal (MIM) structure was related to the contact barrier. Under the relatively lower field, the contact barrier limited the current injection, and consequently thermally excited electrons. With increasing the electric field, electrons were released from trap centers, and the charge injection was a space-charge-limited conduction. [5]

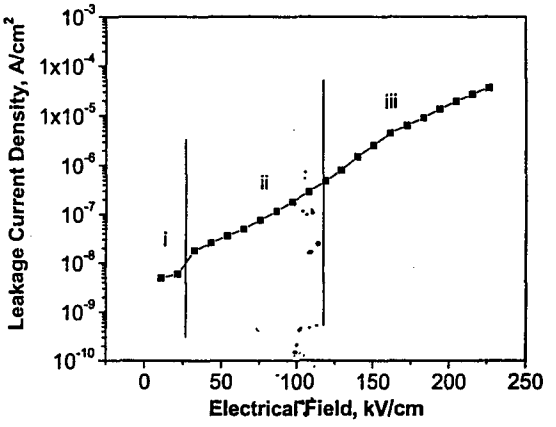

Figure 4 Leakage current density of BLF-PT thin films as a function of the applied electric field

The ferroelectric hysteresis loop was measured to identify the ferroelectricity of BLF-PT thin films. Figure 5(a) displays a polarization-electric-field (P-E) loop, indicating that BLF-PT thin films are sure of ferroelectricity. The P-E loop of the BLF-PT ceramics at the same composition is given in figure 5(b). The different shape of figure 5(a) and 5(b) implied the different performances between the thin film and bulk. The P-E loop in figure 5(a) revealed that the remnant polarization Pr and coercive field Ec were about 20 μC/cm^2 and 100 kV/cm respectively, under E<400 kV/cm. It seems that the P-E loop might be saturated at E>400 kV/cm, however the conductivity was the limitation to increased E. An internal electric field was determined to be ~20 kV/cm according to shift of the P-E loop to the negative field. No significant leakage current was observed from the P-E loop. We attributed the slim shape of P-E response to the fine grain and inhomogeneous compositions of the film, which also provided the breakdown strength of around 8× times higher than that of bulk ceramics.

CONCLUSIONS

BLF-PT thin films have been prepared onto Pt/Ti/SiO_2/Si substrate by using the sol-gel technique. The role of a thin PZT template layer was to improve the sintering properties and the interfacial contact between the BLF-PT thin films and substrate. The firing temperature of 700 °C was preferred to obtain BLF-PT thin films with good crystallinity and prominent dielectric and ferroelectric properties. The leakage current density is in the order of 10^{-7} A/cm^2 under E<100 kV/cm. No significant conductivity could be observed from the standard dielectric and ferroelectric measurement. A slim P-E loop of BLF-PT thin films was related to the fine grain size and inhomogeneous compositions in films.

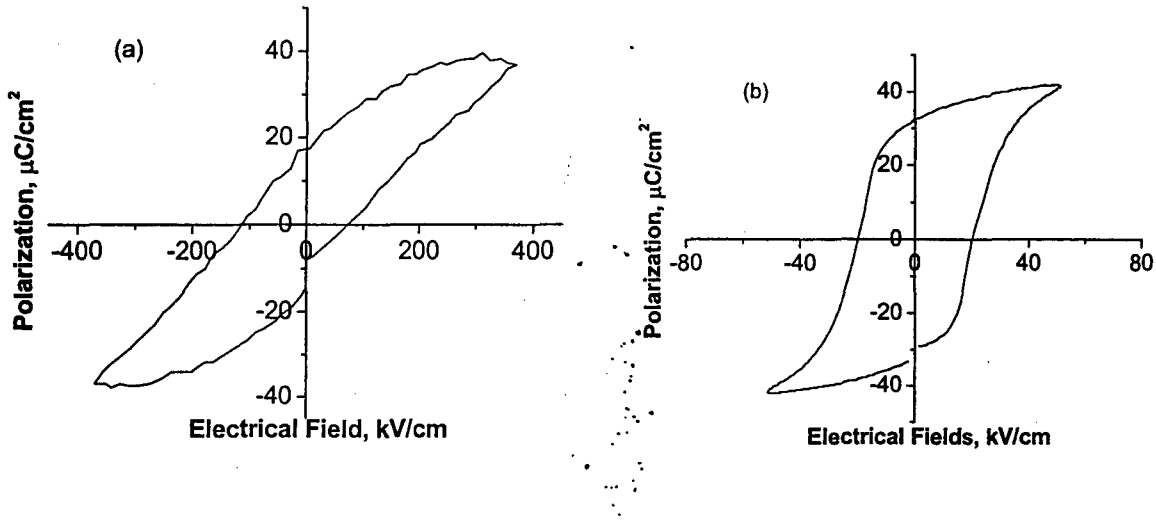

Figure 5 Induced polarizations as a function of electrical field of (a) BLF-PT thin films and (b) BLF-PT ceramics at the same composition

ACKNOWLEDGEMENTS:

The authors are pleased to acknowledge support from the office of Naval Research (ONR) under contract No. N00014-99-1-1011. They thank Nan Li for his great work on the thin film processing.

REFERENCE

1. J. Wang, J. B. Neaton, H. Zheng, V. Nagarajan, S. B. Ogale, B. Liu, D.Viehland, V. Vaithyanathan, D. G. Schlom, U. V. Waghmare, N. A. Spaldin, K. M. Rabe, M. Wuttig, and R. Ramesh, Science **299**, 1719 (2003)
2. Kwi Young Yun,a) Minoru Noda, and Masanori Okuyama, Appl. Phys. Let., **83,** 3981 (2003).
3. T. Yoshimura and S. T-McKinstry, Appl. Phys. Let., **81,** 2065 (2002).
4. J. Cheng and L.Eric Cross, J. Appl. Phys., **94,** 5188 (2003).
5. Xixin Qu, Thin Film Physics (in Chinese), Shanghai Sci. and Techn. Press, 124 (1986).

APPENDIX 5

BISMUTH-BASED PEROVSKITE STRUCTURE SOLID SOLUTIONS WITH FERROELECTRIC MORPHOTROPIC PHASE BOUNDARIES FOR PIEZOELECTRIC APPLICATIONS

L. Eric Cross and Jinrong Cheng
187 Materials Research Institute
The Pennsylvania State University
University Park, Pa 16802 USA

ABSTRACT

This article summarizes a range of studies exploring solid solutions in the $BiBO_3$:$PbTiO_3$ family, where the B site cations are chosen to enhance the ferroelectric Curie Temperature with the objective of expanding the temperature range of morphotropy and the corresponding range of high piezoelectric properties. Recent studies have focused upon $BiFeO_3$ - based compositions as the ferrite has the highest Curie Point for any known perovskite. Heretofore ceramics in this family have been plagued by low electrical resistivity, rendering them useless for piezoelectricity. This work has shown that minor additions of gallium can enhance the resistivity up to 10^{13} ohm cm, providing ceramics with excellent high field dielectric properties. Even for compositions close to the Morphotropic Phase Boundary (MPB) the high coercivity of the ferrite solid solution makes them difficult to pole and it has been necessary to sacrifice some Curie range in the ceramic by lanthanum addition to achieve polability and piezoelectric properties. Parallel work at Penn State (See the chapter by Randall et al.) has focused upon $BiScO_3$:$PbTiO_3$: and shown MPB composition ceramics closely comparable in properties to PZT. Further it has been shown that single crystals of the MPB compositions can be grown and cut to yield d_{33} ~1,250 pC/N and k_{33} ~ 90% up to 300° C. In the ferrite compositions under study, the next step will be to grow single crystals. It is important to note that even at the MPB the tetragonal compositions have c/a larger than 1.05, promising large switchable strain.

INTRODUCTION

In ferroelectric material systems which will be of importance for practical uses as strong piezoelectrics in applications such as actuation or power transduction some of the following attributes will be essential. High dielectric permittivity coupled with strong spontaneous electric polarization, implying a high ferroelectric Curie temperature together with high paraelectric prototypic symmetry. Large permittivity in a strongly polar state implies proximity to a ferroelectric: ferroelectric phase transition, and to retain such proximity over a wide temperature range mandates the engineering of a solid solution system which incorporates a morphotropic phase boundary (MPB) in a part of the phase space accessible by conventional processing either for ceramic forming or single crystal growth. The material must be of a good insulator with high dielectric breakdown strength to permit poling and actuation at high field levels.

This brief review will summarize several years of work in the Materials Research Laboratory/Institute at Penn State exploring bismuth based perovskite structure ferroelectrics as end members in solid solutions with lead titanate. The venture was initially very high risk for two reasons. Firstly, the Bi^{3+} cation is too small to comfortably occupy the A site in ABO_3 perovskite. If formed they would be expected to be rhombohedral ferroelectrics with high Curie point. Several can be stabilized in solid solution with lead titanate ($PbTiO_3$) and the risky

question is starting from the $PbTiO_3$ end of the solid solution which is surely stable can one achieve the tetragonal:rhombohedral (MPB) before the loss of structural stability. A system where success was achieved is the $BiScO_3$:$PbTiO_3$ solid solution where the MPB composition can just be achieved. In $BiGaO_3$:$PbTiO_3$ in spite of intense efforts the MPB could not be realized, and it was necessary to move to $BiGa_xSc_{1-x}O_3$:$PbTiO_3$ to achieve a stable boundary.

A system where the problem does not obtrude is $BiFeO_3$:$PbTiO_3$ solid solution. Bismuth ferrate is a stable perovskite with Tc at 850° C and thus the expectation of massive Ps. However now a second problem evidences, it is that of achieving and maintaining high insulation resistance against the easy valence change Fe^{3+} to Fe^{2+}. A useful accidental consequence of the gallate program was the finding that small additions of $BiGaO_3$ had a profound effect in the raising the missing breakdown strength of $BiFeO_3$ and associated solid solutions.

EXPERIMENTAL PROCEDURE

The crystalline solid solutions explored were largely fabricated using convention mixed oxide ceramic processing. The starting material were Bi_2O_3, Ga_2O_3, Sc_2O_3, Fe_2O_3, $PbCO_3$ and TiO_2, all with purities greater than 99%. For each composition of the different solid solutions suitable fractions of the appropriate components were mixed by ball milling for 24 hours with stabilized ZrO_2 media, then calcined at 750°–850°C for 2 to 4 hours. After Calcining the powders were vibratory milled for an additional 24 hours to ensure uniformity, then uniaxially pressed into pellets with 12.7 mm diameter and 1.5 mm thickness. Final forming was in a sealed crucible under protective atmosphere in the temperature range from 950° to 1100°C for times of order 0.8 to 1.5 hours according to composition. The sintered weight loss and radial shrinkage were of order 1% and ~ 18% respectively.

Structure and phase evolution as a function of composition and temperature were characterized by X-ray diffraction (XRD) (Sintag-1). Microstructure was explored using freshly fractured surfaces of sintered pellets examined by scanning electron microscopy (SEM) (Hitachi S-3000H).

For electrical studies polished disks were annealed then electroded with a post fire silver paste (Dupont 6160) Temperature dependent weak field dielectric measurements were made using a controlled HP-4284 impedance analyzer with the sample housed in a Delta Design environmental control chamber. Electrical insulation resistance was measured using a Keithley 6517 meter. The ferroelectric hysteresis and induced elastic strain were measured simultaneously using a modified Sawyer Tower setup with strain measurement by a linear variable differential transformer. Piezoelectrics properties were characterized by Berlincourt d_{33} meter and checked by the IEEE resonance-antiresonance method with an HP-4194A impedance analyzer.

BISMUTH GALLATE:LEAD TITANTE SOLUTIONS

In spite of using every stratagem consistent with conventional ceramic processing it was not possible to produce a stable single phase perovskite structure in solid solution with more than 25% $BiGaO_3$. [1] At this composition the structures is still clearly tetragonal (Fig.1) with no evidence of a rhombohedral ferroelectric phase. As expected both differential thermal analysis Fig. 2a and dielectric permittivity measurements (Fig. 2b) show evidence of a ferroelectric phase change in the vicinity of 490°C confirming the high Curie temperatures in this solid solution system. It is probable that compositions up to and including the morphotropic phase boundary could be stabilized under high pressure conditions, but this was beyond the scope of the present program.

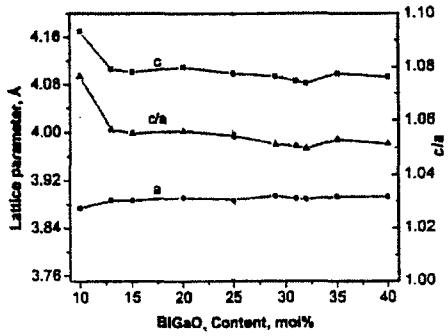

Fig. 1: Lattice constants of BG-Pt as the function of GB content

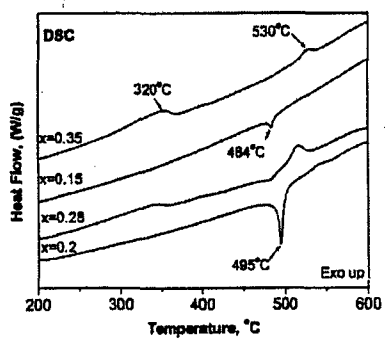

Fig 2a: DSC curves of BGPT ceramic powders with various compositions

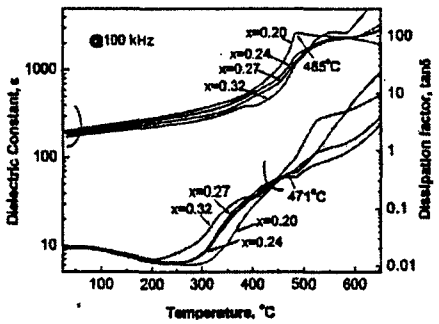

Fig. 2b: The temperature dependent dielectric spectrum taken at 100 kHz.

BISMUTH SCANDATE: LEAD TITANATE SOLID SOLUTIONS

A more extensive sequence of studies of the $BiScO_3$:$PbTiO_3$ solid solution systems has been carried forward in the MRI at Penn State, and in a joint program with Dr. T. Sekiya's group at NIRIN in Nagoya, now part of the Smart Structures Research Center at NAIST in Tsukuba. Evidence is that by careful processing in sealed atmosphere controlled crucibles.[2] [3] It was possible to produce single phase perovskite structure ceramics up to 47% $BiScO_3$ and that a tetragonal rhombohedral boundary is clearly evident at 37.5% $BiScO_3$. (Fig. 3) Unlike PZT the Curie Temperature first rises with $BiScO_3$ addition to $PbTiO_3$ and is over 400°C at the MPB composition (Fig 4.a) leading to very high values of the remanent polarization (Fig. 4b) and large values of d_{33} comparable to soft PZT. (Fig. 5)

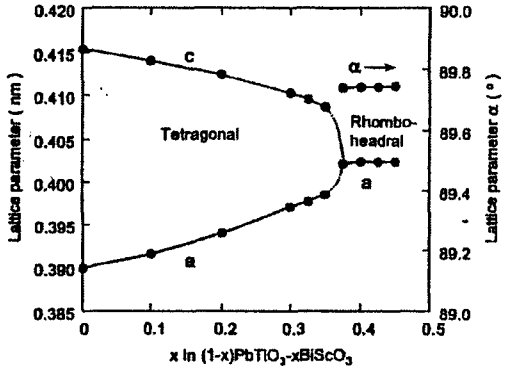

Fig. 3: Plot of lattice parameters vs. composition for $(1-x)$PT-xBS perovskites

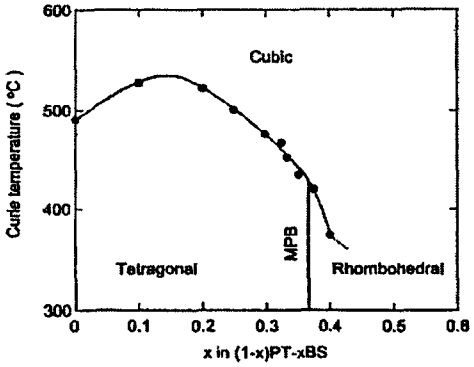

Fig. 4a: Phase diagram in the PT-BS system

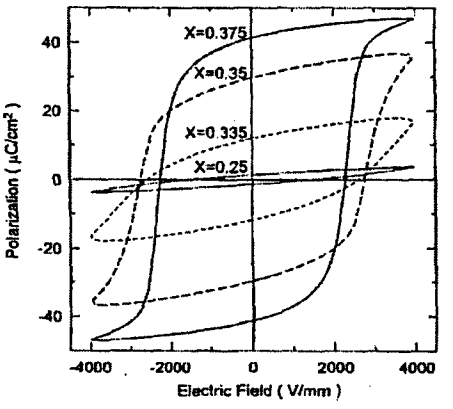

Fig. 4b: D-E hysteresis loop of $(1-x)$ PT-xBS ceramics at room temperature

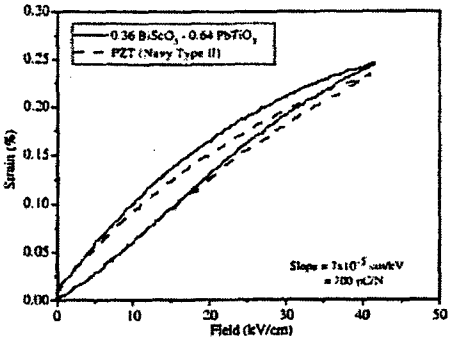

Fig. 5: Unipolar strain-electric field behavior of poled 36% $BiScO_3$ -64% $PbTiO_3$, contrasted to a Navy Type II PZT, showing a high field d_{33} of 700 pC/N

Clearly a cogent reason for exploring alternative MPB systems with high Curie Temperature and corresponding large polarization is that unlike PZT they may be tractable for single crystal growth and thus offered opportunity to explore oriented properties, realizing ultra high values of d_{33} and k_{33} as in the 001 poled PZN:PT and PMN:PT crystals. Recent studies at Penn State [4] have shown that indeed it is possible to grow single crystals at the 43% $BiScO_3$ composition, that 001 oriented specimens do have very high $d_{33} \sim 1{,}200$ pC/N and coupling coefficient $k_{33} \sim 90\%$ maintained to over 330° C (Fig. 6a) with strain capability over 0.12% at 10kV/cm corresponding to the weak field $d_{33} \sim 1{,}200$ pC/n (Fig. 6b). The single crystal BS:PT data is of critical importance as it does suggest that the polarization tilting mechanism which gives the ultra high response in PZN:PT is general and likely to be possible in other high Curie Temperature solid solution systems with MPBs.

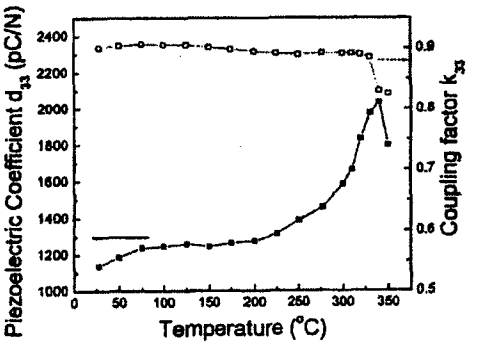

Fig. 6a: Longitudinal electromechanical coupling factors k_{33} and piezoelectric coefficients d_{33} as a function of temperature

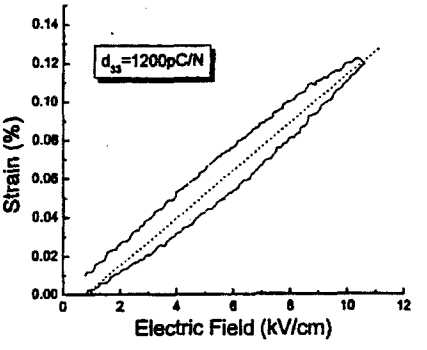

Fig. 6b: Unipolar S-E loop for <001) –oriented BSPT (43/57) single crystals

BISMUTH SCANDATE GALLATE:LEAD TITANATE SOLID SOLUTION

The success achieved with the bismuth scandate based solid solutions suggests that it should be interesting to explore gallate:scandate combination where the scandium may stabilize the solid solution with lead titanate sufficiently to achieve the MPB phase boundary compositions. Initial studies using (1-x)Bc $(Ga_{1/4}Sc_{3/4})O_3$-x$PbTiO_3$ suggests that this may be the limit for gallium substitution. The potential advantage for the mixed systems is shown in Fig. 7 where it is evident that the Curie Temperature is raised into the range 465 to 510°C however, this is at the cost of some second phase contamination in the rhombohedral phase compositions below 60% $PbTiO_3$.[5] It will be interesting to see how minor additions of $BiGeO_3$ effect crystal growth of $BiScO_3$ crystals and if the addition has the same effect on conduction and dielectric strength.

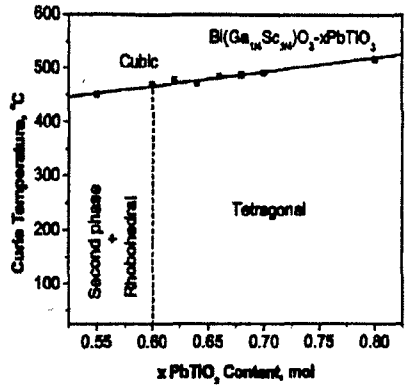

Fig. 7: Draft of a phase diagram of BGS-PT as a function of the PT content

BISMUTH FERRATE: LEAD TITANATE BASED SOLID SOLUTIONS:

Introduction

Bismuth Ferrate $BiFeO_3$ is an obvious end member candidate for solid solution with $PbTiO_3$. It is quite stable in the perovskite form with a Curie point at 850° C [6] and an antiferromagnetic Néel temperature at 310°C. [7] The first Penn State studies focused upon exploring "dopants" to control conduction. This work showed that Ga^{3+} additions could generate resistivities up to 10^{13} ohm cm in compositions of $BiFeO_3$:$PbTiO_3$ close to the MPB (near 0.3 mole $PbTiO_3$). Not only were these ceramics of very high resitivity, but they also had excellent breakdown characteristics, supporting fields up to 250 kV/cm.[8] Even at these very high field levels it proved difficult to pole samples of ceramic even at compositions near the MPB so a range of lanthanum modified compositions was explored, where some of the high Tc and high strain were sacrificed but ceramics poling could be achieved.

Composition chosen for initial study

In gallium modified $Bi(Ga_xFe_{1-x})O_3$:$PbTiO_3$ compositions chosen for initial study were 0.7 BGF:0.3PT for x in the range $0 \leq x \leq 0.1$ and 0.4 BGF:0.6PT for x in the range of $0 \leq x \leq 0.5$. For the lanthanum modified compositions, studies were focused upon (1-x) $(Bi_{1-y}La_y)(Ga_{0.05}Fe_{0.95})O_3$: x $PbTiO_3$ (BLGF:PT) for x values in the range $0.2 \leq x \leq 0.65$ and for y values in the range $0.2 \leq x \leq 0.65$ and for y values in the range $0 \leq y \leq 0.20$. Earlier studies had shown that the level 0.05 Ga was adequate to maintain high insulation resistance in the interesting MPB compositions.

Characterization

The effects of Ga substitution on the phase evolution in $Bi(Ga_xFe_{1-x})O_3$:$PbTiO_3$ (BGF:PT) ceramics were identified by XRD analysis. Figures 8 (a) and (b) show the diffraction patterns for 0.7 BGF: 0.3PT with Ga concentration $x \leq 0.10$ and for 0.4 BGF:0.6 PT with x in the range $x \leq 0.5$.

Coexistence of rhombohedral and tetragonal phases was observed for 0.7 BGF:0.3PT as marked in Fig. 8(a) showing that the 0.3PT composition lies very close to the MPB. Peak intensities suggest that for 0.7BGF:0.3PT with Ga (x) = 0 the dominant phase is rhombohedral. However, with increasing x the tetragonal fraction appears to increase and the rhombohedral to decrease up to the stability limit $x \leq 0.1$ above which secondary, non-perovskite phases begin to appear. It is interesting to note the very large tetragonal distortion (separation of <001> and <100> peaks) at the MPB corresponding to a (c/a) ratio ~ 1.16 for 0.7 BGF:0.3PT with x = 0.1.[6]

For the tetragonal phase region, 0.4 BGF:0.6PT, a higher Ga (x) content was required to maintain high resistivity and the values of x in the range $0 < x < 0.5$ were explored. The <100> peak splitting shows that c/a first increases with Ga content up to x ~ 0.25, decreasing with further increments of x. However, for compositions above x = 0.25 there is evidence of secondary non-perovskite phases.

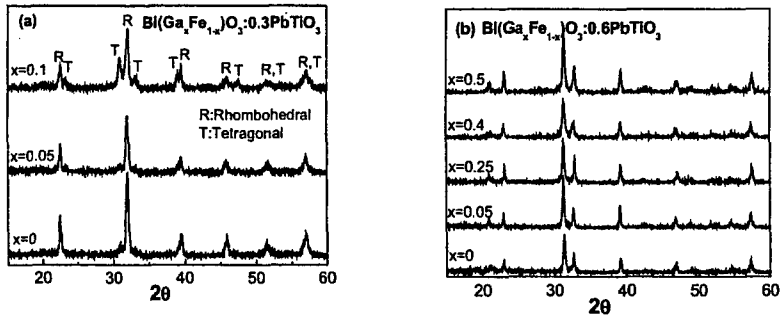

Fig. 8: XRD patterns of (a) BGF:0.3PT and (b) BGF:0.6PT for different Ga concentrations

For the lanthanum substituted composition BLGF:PT with just 5 mole % gallium substitution, phase pure perovskite structures with no secondary pyrocholore were observed for PT contents above 0.1 ($x \geq 0.1$). The structure changes from rhombohedral to tetragonal at the MPB. Figures 9 (a – c) show the lattice parameters as a function of PT content for various La concentrations, indicating how the rhombohedral to tetragonal transition moves to higher PT concentration with increasing La incorporation. It is very interesting to note the large overlap of rhombohedral and tetragonal phases around 0.3 PT in the La = 0 (x = 0) composition and the very large value of tetragonal c/a ~ 1.16 at this composition. High values persist up to La (x ~ 0.10) but drop markedly for x ~ 0.20 where c/a ~ 1.02. A tentative family of phase diagrams for the location of MPBs in the La modified family is given in Fig. 10 where the high temperature extreme were taken from dielectric measurements. At the lower La content the phase boundary is taken as the mid composition of the mixed phase region. At higher La concentration, as is evident in Fig. 9, the boundary is more clearly defined.

Perhaps the most important result of these studies is that depicted in Fig. 11 showing the manner in which electrical resistivity is improved in the 0.7 BGF:0.3PT and in the 0.4BGF:0.6PT.

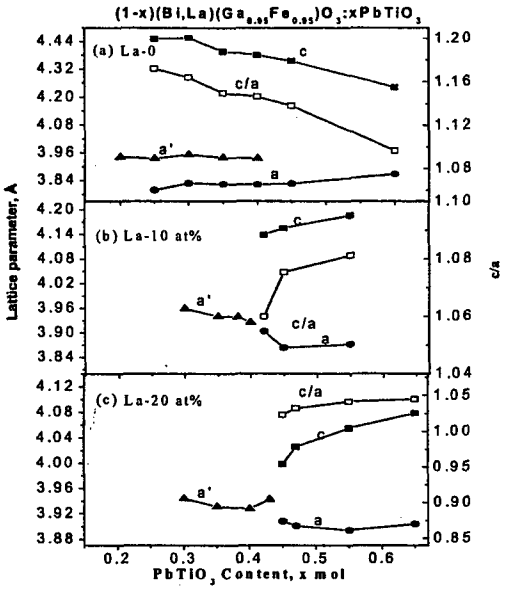

Fig. 9: Lattice parameters of BLGF:PT as a function of PT

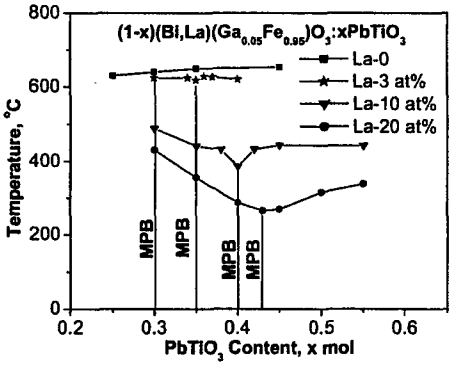

Fig. 10: Location of MPB in the BLGF:PT solid solutions for La concentration of 0, 3, 10 and 20 atom%

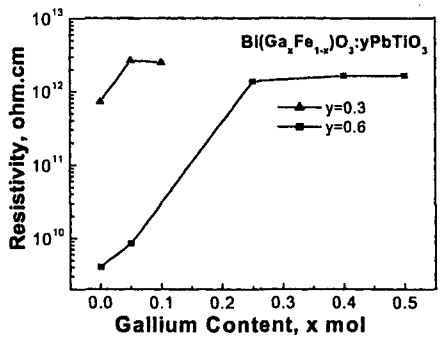

Fig. 11: Electrical resistivity of BGF:0.3PT and BGF:0.6PT as a function of Ga concentration

For the lanthanum substituted composition, it was possible to maintain an insulation resistance of over 10^{10} ohm cm with just 5 atom % gallium substitution with values of order 10^{13} ohm cm for the interesting range of the MPB compositions. This permitted excellent weak field dielectric permittivity measurements over the interesting range of PT as in shown in Fig. 12. As could be expected, the samples show weak dielectric dispersion, but clear peaks in K which track the composition of the MPB as determined by XRD.

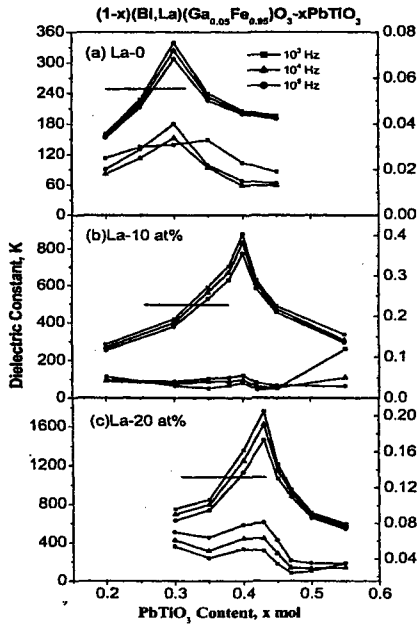

Fig. 12: Room temperature dielectric constant K and tanδ of BLGF:PT as a function of PT content for (a) 0; (b) 10; and (c) 20 atom % La.

High field dielectric hysteresis measurements are summarized in Fig. 13 taken on the modified Sawyer Tower circuit with a bipolar sinusoidal field at 10 Hz, up to 80kV/cm. Ferroelectric hysteresis is clearly evident in the samples with 10 and 20 atom % lanthanum with remanent polarization $P_r \sim 30\mu C/cm^2$, but E_c is still high at 20 kV/cm.

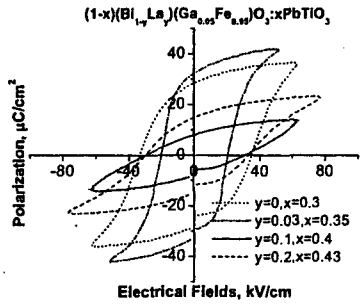

Fig.13: Dielectric hysteresis in BLGF:PT solid solutions taken with bipolar sinusoidal waves at 10 Hz

High field bipolar and unipolar strain S_{33} vs. E_3 are shown in Fig. 14. MPB compositions of BLGF-PT with 10 and 20 atom % of Lanthanum have similar strain levels of 0.35% and 0.2% under fields of 60 kV/cm. Estimating a large amplitude d_{33} value from a linear approximation to the slope gives $\Delta S_{33}/\Delta E_3 \sim 380$ pm/V. Measurement by Berlincourt meter and standard IEEE resonance method yield d_{33} values as a function of PT content for compositions with 10 and 20% La shown in Fig 15. Maximum values occur at the MPB compositions of 295 pC/N (20% La) and 163 pC/N (10% La) with planar coupling coefficients of order 0.36, confirming the response comparable to that of PZT ceramic.

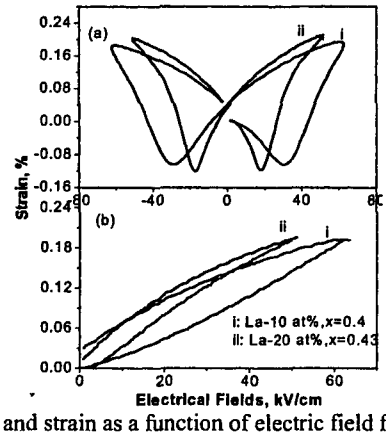

Fig. 14: Induced polarization and strain as a function of electric field for MPB compositions of BLGF:PT, (a) bipolar S –*E* response and (b) unipolar S –*E* response. Curves i and ii are corresponding to compositions of La-10 at%, x=0.4 and La-20 at%, x=0.43 respectively.

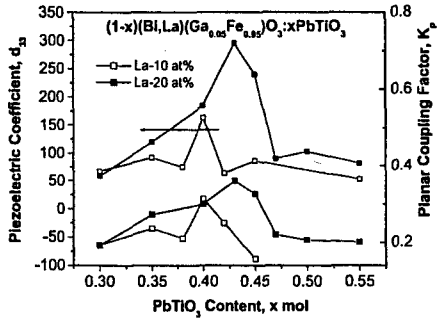

Fig. 15: Piezoelectric constant d_{33} and planar coupling factor K_p of BLGF:PT as a function of PT content with La concentrations of 10 and 20 atom %.

DISCUSSION

It is clear from the experimentation described that the BGF:PT solid solution can be fabricated as a single phase perovskite across the whole composition range and that it encompasses a ferroelectric rhombohedral to tetragonal phase transition. Small additions of gallium of order 5 atom % enhance the resistivity to ~ 10^{12} ohm cm and the currently processed ceramics will withstand very high electric fields up to 250 kV/cm. An unusual feature of the phase change in the BGF:PT system is the very broad composition range of co-existence of rhombohedral and tetragonal forms. A second unusual feature, which may be connected, is the truly massive c/a ratio of the tetragonal form of order of 1.16 at the MPB composition. In spite of the high breakdown field and the co-existence of rhombohedral and tetragonal forms it proved impossible to pole the 0.7 BGF:0.3PT composition for piezoelectric study.

Softening the composition as in PLZT by the addition of lanthanum, to form a BLGF:PT sequence, sacrifices some Curie Temperature but does sharpen the phase transition and at 10 atom % La the transition to cubic still occurs at 400°C and the c/a ratio of the tetragonal form is of order 6%. The purpose of the studies presented were to scope out some of the bounds and possible flexibilities in the properties which could be generated for compositions with morphotropic phase boundaries in the bismuth based perovskite family. Obviously now electrical conductivity is not a 'show stopping' problem, and strong piezoceramics with performance comparable to PZT and lower lead content can be generated. Clearly, the next step, as has now been accomplished for the bismuth scandate:lead titanate MPB composition, is to explore the growth of single crystals. With the very high Curie temperature of the ferrate, the parameter space available in the BLGF:PT system is much larger than in $BiScO_3$:PT compositions and the fact that very high tetragonal strain is preserved even in heavily La modified compositions gives confidence that even higher switchable strain may be possible.

An initial concern that the high coercivity persisting even in the La modified system might preclude the rotational instability which is essential for the high [001] activity in the crystals has been alleviated by the scandate studies, where even though the coercivity for ceramics switching is 20 kV/cm, as in BLGF:PT at the MPB, d_{33} ~ 1,250 pC/n and k_{33} ~ 90 % are shown to be achieved in <001> poled single crystals.[4]

Very recent studies in cooperation with Drs. Viehland and Dong in Virginia Tech show that the La modified BLGF:PT have substantial magneto-electric properties which will be the subject of further studies.

REFERENCES

[1]J. Cheng, W. Zhu, N. Li, and L. E. Cross, "Fabrication and Characterization of $xBiGaO_3$-(1-x)$PbTiO_3$: A High Temperature Reduced Pb-content Piezoelectric Ceramic", *Mater. Lett.* **57,** 2090 (2003).

[2]C.A. Randall, R.E. Eitel, T. R. Shrout, D. I. Woodward, and I. M. Reaney, "Transmission electron microscopy investigation of the high temperature $BiScO_3$–$PbTiO_3$ piezoelectric ceramic system", *J. Appl. Phys.* **93,** (11) 9271 (2003).

[3]Y. Shimojo, R. Wang, T. Sekiya, T. Nakamura, and L.E. Cross, "MPB Phase Diagram and Ferroelectric Properties in the $PbTiO_3$ System" Ferroelectrics, Vol **284**,121-128 (2003)

[4]S. Zhang, C. A. Randall, and T. R. Shrout, "High Curie temperature piezocrystals in the $BiScO_3$-$PbTiO_3$ perovskite system" *Appl. Phys. Lett.* **83** (15), 3150 (2003).

[5]Jinrong Cheng, Richard Eiel, Nan Li, and L.E. Cross, "Structural and electrical properties of $(1-x)Bi(Ga_{1/4}Sc_{3/4})O_3 - xPbTiO_3$ piezoelectric ceramics" *Journal of Applied Physics*, **Vol** 94 (1), 605-609 (2003)

[6]G. Smolenskii, B. Isupov, A. Agranovskaya, and N. Krainik, "New Ferroelectrics of Complex Composition", *Sov. Phys. Solid State* **2,** 2651 (1961).

[7]P. Fisher, M. Polomskya, I. Sosnowska, and M. Szymanski, "Temperature dependence of the Crystal and Magnetic Structures of $BiFeO_3$", *J. Phys. C.* **13,** 1931, (1980)

[8]Jinrong Cheng, L.E. Cross, "Effects of La Substituent on Ferroelectric rhombohedral/ tetragonal morphotropic phase boundary in $(1-x)(Bi,La)(Ga_{0.05}Fe_{0.95})O_3 - xPbTiO_3$ piezoelectric ceramics" Journal of Applied Physics, **Vol** 94 (8) 5188-5192, (2003)

APPENDIX 6

APPLIED PHYSICS LETTERS 86, 072905 (2005)

Flexoelectric effect in ceramic lead zirconate titanate

Wenhui Ma[a)]
Department of Physics, Shantou University, Shantou, Guangdong 515063, People's Republic of China

L. Eric Cross
Materials Research Laboratory, Pennsylvania State University, University Park, Pennsylvania 16802

(Received 7 September 2004; accepted 30 December 2004; published online 11 February 2005)

Mechanical strain gradient generated electric polarization or flexoelectric effect was investigated in unpoled lead zirconate titanate (PZT) ceramics in the ferroelectric state by using a cantilevered beam based approach. Flexoelectric coefficient μ_{12} at room temperature was measured to be 1.4 μC/m in the PZT ceramic at small level of strain gradient. Temperature-dependent experimental investigations clearly showed that high dielectric permittivity in the ferroelectrics enhanced flexoelectric polarization: essentially a linear relation was found to exist between μ_{12} and dielectric susceptibility χ at lower permittivity level (2100–2800), while μ_{12} versus χ curve started to deviate from the straight line at the $\chi \sim 2800$ and nonlinear enhancement of μ_{12} with χ was observed, with μ_{12} value reaching 9.5 at $\chi \sim 11\,000$. The nonlinearity in the flexoelectric effect was associated with domain-related processes. It is suggested that flexoelectric effect can have a significant impact on epitaxial ferroelectric thin films and mesoscopic structures. © *2005 American Institute of Physics.*
[DOI: 10.1063/1.1868078]

Flexoelectric effect is the coupling between mechanical strain gradient and electric polarization and can be described by

$$P_l = \mu_{ijkl} \frac{\partial \varepsilon_{ij}}{\partial x_k}, \tag{1}$$

where P_l is the flexoelectric polarization, μ_{ijkl} the flexoelectric coefficient, ε_{ij} the elastic strain, and x_k the position coordinate. μ_{ijkl} is a fourth-rank polar tensor and therefore has nonzero components in dielectric solids of any crystal symmetry. Theoretical estimations predicted that flexoelectric coefficients in simple dielectrics are generally small (of the order e/a or $\sim 10^{-10}$ C/m, where e is the electron charge and a the dimension of unit cell).[1–3] Earlier experimental work on polymers[4] supported the theoretical predictions. Recently we developed a cantilevered beam based approach[5] to perform reliable measurements of flexoelectric effect. Experimental investigations using the approach showed that flexoelectric coefficients in the ferroelectric materials are many orders of magnitude higher (10^{-6} to 10^{-4} C/m).[6,7] The cantilevered beam based approach is generally used for dynamic flexoelectric measurements at lower level of strain gradient. To investigate the flexoelectric effect at higher strain gradient we developed another approach based on four-point bending and used the approach in static measurements of the flexoelectric coefficients in ferroelectric materials.[8]

Based on flexoelectric effect, ideas for developing new types of piezoelectric composites[9] were proposed, where none of the components is piezoelectric. If we understood flexoelectric effect well and there were database of flexoelectric coefficients available, a range of properly engineered flexoelectric composite structures could provide completely new piezoelectric capability.

Ferroelectric thin films and mesoscopic structures have exhibited a lot of potential for device applications such as FERAM and MEMS.[10] Misfit strain certainly exists at the interface between the epitaxially grown thin film ferroelectric and the substrate or electrode material. Nonuniform relaxation of the misfit strain in the thin films can lead to strain gradient,[11] which can then influence the dielectric and polarization behaviors of the ferroelectrics. Experimentally, some new phenomena recently observed in the thin film ferroelectrics were suggested to be due to the consequences of flexoelectric effect, such as the mechanical stress induced imprint in PZT capacitor structures[12] and pyroelectricity in highly stressed quasiamorphous $BaTiO_3$ films.[13] Recently a phenomenological model[14] of flexoelectricity was also proposed, showing that flexoelectric effect could play an important role in reducing the dielectric maximum in ferroelectric thin films. Ferroelectric PZT based ceramics and thin films are a family of technologically important functional materials.[15] In this letter, we report experimental investigations of the flexoelectric effect in ceramic PZT.

The PZT samples are the same as those used before,[8] with dimensions 60 mm long, 7 mm wide, and 3 mm thick. Flexoelectric effect was investigated using the cantilevered beam based approach and the system used for the flexoelectric measurement is identical to that used in earlier studies of barium strontium titanate (BST) and lead magnesium niobate (PMN).[5–7] A series of 3-mm-diam thin sputtered gold electrodes were prepared on the sample surface along the bar length. The ceramic bar sample is rigidly clamped at one end and driven into transverse vibration at 1 Hz by a small moving coil loudspeaker. The ac mechanical strain as a function of position along the bar was measured using a Microstrain™ DVRT (differential variable reluctance transducer) and the generated current was measured using an SR830 DSP Lock-in amplifier. The measured mode shape was then used to calculate the strain gradient at positions of the electrodes using the free bar model.[5]

For an unpoled PZT ferroelectric ceramic at the morphotropic phase boundary, although individual grains may have lower symmetry (tetragonal or rombohedral) which permits

a)Electronic mail: mawenhui_usa@yahoo.com

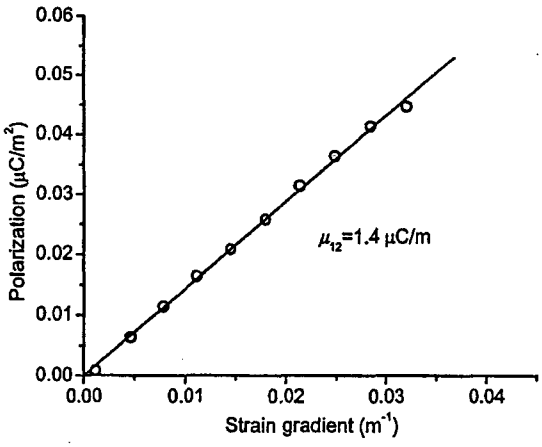

FIG. 1. Room temperature flexoelectric polarization vs strain gradient for unpoled PZT ceramic measured at 1 Hz near the clamped end (x_1/L =0.18) of the cantilevered beam.

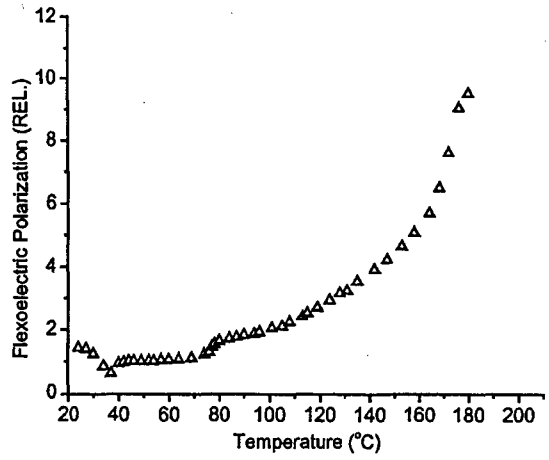

FIG. 2. Flexoelectric polarization (arbitrary unit) measured as a function of temperature in the ferroelectric state for the unpoled PZT ceramic.

piezoelectricity, in the volume of the ceramic one may expect a macroscopic symmetry of $\infty\infty m$, so the nonzero components for the flexoelectric tensor μ_{ijkl} should be μ_{1111}, μ_{1122}, and μ_{1212}, or in matrix notation μ_{11}, μ_{12}, and μ_{44}. In the unpoled PZT ceramic, no residual piezoelectricity could be detected by Berlincourt d_{33} meter and no evidence of piezoelectric resonance could be found in the impedance trajectory from 1 kHz to 1 MHz. By using the cantilevered beam based approach, any remnant piezoelectricity from the top and bottom halves of the sample bar is well balanced during the flexoelectric measurements. That some unbalance was affecting the measured value was however ruled out by the simple experiment of inverting the sample and noting that the measured signal did not change either in amplitude or phase. Clearly in ferroelectrics the free surface breaks the symmetry of the bulk and may affect the polarization behavior, however, in the present studies the effect of surface ferroelectricity[16] is unlikely due to the highly conductive metal electrodes on both free surfaces. Thus we believe that the measured electric polarization P_3 is solely due to the strain gradient in the x_3 thickness direction and can be written as

$$P_3 = \mu_{12}\frac{\partial \varepsilon_{13}}{\partial x_1}. \tag{2}$$

Figure 1 presents the room temperature (24 °C) flexoelectric polarization as a function of the transverse strain gradient obtained near the clamped end (x_1/L=0.18) of the bar by using the cantilevered beam based dynamic approach. It is clear that the generated electric polarization is linearly proportional to the elastic strain gradient and the slope of the line gives a magnitude of μ_{12} of 1.4 μC/m, close to the early data of 0.5 μC/m[8] obtained by static measurements using a four-point bend fixture. Figure 2 presents the measurements of μ_{12} in the PZT ceramic as a function of temperature (24–180 °C). When heating up from room temperature (24 °C), unexpectedly the μ_{12} initially drops before it becomes stabilized at 40 °C, then flexoelectric polarization basically keeps flat at the temperature range of 40–70 °C but starts to rise prominently at 70 °C.

Clearly high dielectric permittivity in the ferroelectric materials can enhance flexoelectric coefficients[6,7] and μ_{12} can be related to dielectric susceptibility χ by

$$\mu_{12} = \gamma\chi\frac{e}{a}, \tag{3}$$

where γ is a scaling factor. In order to evaluate the impact of dielectric property on the flexoelectric effect, dielectric spectra from the PZT ceramic were measured and shown in Fig. 3, where a strong but rounded dielectric maximum suggests a diffuse phase transition around 220 °C. The plot of μ_{12} versus χ is shown in Fig. 4. Comparison of experimental data obtained in BST, PZT, and PMN reveals that, at similar level of relative dielectric permittivity, μ_{12} in BST is roughly one order of magnitude higher than that in PMN or PZT. It remains unclear as to why the Pb-based ferroelectrics should have lower values of flexoelectric coefficients.

As shown in Figs. 2 and 4, the initial drop of μ_{12} with χ is unexpected but may correspond to the increase of loss tangent (Fig. 3) in the temperature range (24–50 °C). A linear relation between μ_{12} and χ with γ=1 is seen to exist in the χ range of 2100–2800 (or temperature range of 40–74 °C). The μ_{12} versus χ curve deviates from the γ=1 line at the $\chi\sim$2800 and the rise of μ_{12} with χ becomes essentially nonlinear, with μ_{12} reaching 9.5 at $\chi\sim$11 000.

Nonlinearity in flexoelectric coefficient was found in temperature-dependent experimental investigations of BST,[7] where μ_{12} was raised to 100 μC/m when approaching the dielectric peak from the paraelectric state. Such nonlinear

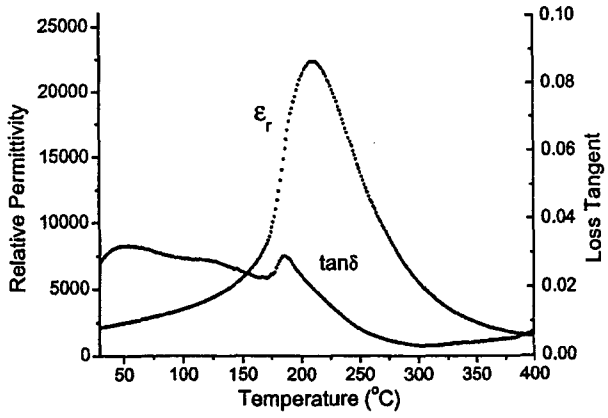

FIG. 3. Dielectric permittivity and loss tangent for the unpoled PZT ceramic measured as function of temperature at a frequency of 1 kHz.

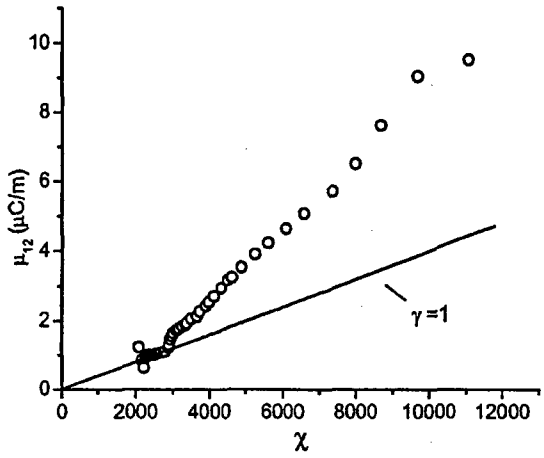

FIG. 4. Flexoelectric coefficient μ_{12} vs dielectric susceptibility χ for the unpoled PZT ceramic. The dotted line shows a linear relation between μ_{12} and χ at lower level of dielectric permittivity with a $\gamma=1$.

enhancement was suggested to be due to the survival of some ferroelectric domains in the BST ceramic above the Curie transition temperature T_C. In the previous studies of ceramic PMN,[6] nonlinear enhancement of μ_{12} with χ was also observed and found to be closely associated with the pre-existing polar microdomains in this prototypic relaxor ferroelectric material.[17] Apart from the nonlinear behavior of flexoelectric coefficient with dielectric permittivity, previous static investigations[8] in PZT ceramic revealed nonlinear relation between flexoelectric coefficient and mechanical strain gradient, where the jump of μ_{12} from 0.5 μC/m at lower strain gradients to 2 μC/m at much higher strain gradients was shown to be associated with the onset of domain wall motion induced by the very high level of inhomogeneous strain achievable with the four-point bend fixture. As discussed earlier, nonlinearity in the flexoelectric effect can be tentatively attributed to the domain-related processes in ferroelectrics and the scaling factor γ in Eq. (3) depends on the materials investigated, the level of dielectric permittivity, and the magnitude of strain gradient. The experimental findings of nonlinear phenomena are in good agreement with the theoretical studies by Catalan *et al.*,[14] where it was shown that flexoelectric coefficient is only a linear function of the strain gradient or permittivity when the induced flexoelectric polarization is small. In addition to the extrinsic influence of domain-related processes discussed earlier, it is possible that a part of the nonlinearity in the flexoelectric effect may also be of intrinsic origin as shown in the theoretical work of Catalan *et al.*[14]

In epitaxial ferroelectric thin films and mesoscopic structures, Curie phase transition temperature T_C or dielectric peak can be adjusted to around room temperature where ultrahigh dielectric permittivity becomes available, by appropriate selection of lattice misfit and film thickness as shown in recent theoretical[18] and experimental[19] studies. Likewise, strain gradient in these ferroelectric structures can also be adjusted by tailoring the structure dimensions or controlling the relaxation of the misfit strain. The nonlinear enhancement of flexoelectric coefficients with the dielectric permittivity and strain gradient can lead to a significant impact of flexoelectric effect in these properly engineered thin film ferroelectric heterostructures.

In summary, flexoelectric effect was investigated in the ferroelectric state of unpoled lead zirconate titanate (PZT) ceramics. Temperature-dependent flexoelectric investigations showed that μ_{12} essentially increases with relative dielectric permittivity and the nonlinear phenomenon was found at higher level of dielectric permittivity, which is suggested to be associated with domain-related processes.

[1]Sh. M. Kogan, Sov. Phys. Solid State **5**, 2069 (1964).
[2]V. L. Indenbom, E. B. Loginov, and M. A. Osipov, Sov. Phys. Crystallogr. **26**, 656 (1981).
[3]A. K. Tagantsev, Sov. Phys. JETP **61**, 1246 (1985).
[4]M. Marvan and A. Havránek, Prog. Colloid Polym. Sci. **78**, 33 (1988).
[5]W. Ma and L. E. Cross, Appl. Phys. Lett. **78**, 2920 (2001).
[6]W. Ma and L. E. Cross, Appl. Phys. Lett. **79**, 4420 (2001).
[7]W. Ma and L. E. Cross, Appl. Phys. Lett. **81**, 3440 (2002).
[8]W. Ma and L. E. Cross, Appl. Phys. Lett. **82**, 3293 (2003).
[9]J. Fousek, L. E. Cross, and D. B. Litvin, Mater. Lett. **39**, 287 (1999).
[10]N. Setter and R. Waser, Acta Mater. **48**, 151 (2000).
[11]P. Imperatori, F. J. Lamelas, and P. H. Fuoss, J. Appl. Phys. **80**, 5723 (1996).
[12]A. Gruverman, B. J. Rodriguez, A. I. Kingon, R. J. Nemanich, A. K. Tagantsev, J. S. Cross, and M. Tsukada, Appl. Phys. Lett. **83**, 728 (2003).
[13]V. Lyahovitskaya, I. Zon, Y. Feldman, S. R. Cohen, A. K. Tagantsev, and I. Lubomirsky, Adv. Mater. (Weinheim, Ger.) **15**, 1826 (2003).
[14]G. Catalan, L. J. Sinnamon, and J. M. Gregg, J. Phys.: Condens. Matter **16**, 2253 (2004).
[15]B. Jaffe, W. Cook, and H. Jaffe, *Piezoelectric Ceramics* (Academic, New York, 1971).
[16]A. M. Bratkovsky and A. P. Levanyuk, arXiv: cond-mat/0402100.
[17]L. E. Cross, Ferroelectrics **76**, 241 (1987).
[18]N. A. Pertsev, A. G. Zembilgotov, and A. K. Tagantsev, Phys. Rev. Lett. **80**, 1988 (1998).
[19]J. H. Haeni, P. Irvin, W. Chang, R. Uecker, P. Reiche, Y. L. Li, S. Choudhury, W. Tian, M. E. Hawley, B. Craigo, A. K. Tagantsev, X. Q. Pan, S. K. Streiffer, L. Q. Chen, S. W. Kirchoefer, J. Levy, and D. G. Schlom, Nature (London) **430**, 758 (2004).

APPENDIX 7

APPLIED PHYSICS LETTERS VOLUME 85, NUMBER 16 18 OCTOBER 2004

A strong magnetoelectric voltage gain effect in magnetostrictive-piezoelectric composite

Shuxiang Dong,[a] J. F. Li, and D. Viehland
Materials Science & Engineering, Virginia Tech, Blacksburg, Virginia 24061

J. Cheng and L. E. Cross
Materials Research Laboratory, Pennsylvania State University, State College, Pennsylvania 16802

(Received 9 April 2004; accepted 6 July 2004)

A magnetoelectric laminate composite consisting of magnetostrictive Terfenol-D ($Tb_{1-x}Dy_xFe_{2-y}$) and piezoelectric $Pb(Zr,Ti)O_3$ layers has an extremely high voltage gain effect of ≈300 at its resonant state, offering potential for high-voltage miniature transformer applications. © *2004 American Institute of Physics*. [DOI: 10.1063/1.1786631]

The magnetoelectric (ME) effect is a polarization response to an applied magnetic field H, or conversely a spin response to an applied electric field E.[1] Ferroelectromagnetic materials of single phase, multiple phases, and laminate composites have been studied.[2–15] However, to date, investigations of ME laminate composites have focused on passive sensors,[6,12,14] rather than high-power device applications. Also, previously, only ME materials with low coupling have been found.

It is possible that ME laminates could operate under high-power drive in solid-state transformers. This is because both magnetostrictive Terfenol-D ($Tb_{1-x}Dy_xFe_{2-y}$) and piezoelectric $Pb(Zr,Ti)O_3$ (PZT) layers exhibit significant magneto-mechanical and electro-mechanical energy densities, respectively.[16–18] Recently, we have developed laminate composite designs that have significantly higher magnetoelectric coupling effects.[13,14] Our approach was based on energy analysis and laws of motion, and not simply constitutive equations.[9,11] The analysis was developed for a long plate type piezoelectric/magnetostrictive laminate composite; and was based upon the piezoelectric and piezomagnetic equations of state, in a longitudinal-mode vibration. Our analysis revealed the possibility of an extremely high magnetoelectric voltage gain, suitable for high-voltage miniature transformer applications.

Figure 1 illustrates the composite geometry chosen for this investigation. It is a long plate type piezoelectric/magnetostrictive laminate composite, in which the piezoelectric layer is sandwiched between two magnetostrictive ones. More complicated multilayer geometries of this general type are possible, but that given in Fig. 1 readily allows for equivalent circuit analysis. The conductive magnetostrictive layers are separated by an insulating piezoelectric one, and thus eddy currents are effectively eliminated if the thickness of the magnetostrictive layers is sufficiently thin. This magnetoelectric laminate design differs from previous ones, as its aspect ratio is high, favoring the longitudinal direction along which fields are applied. The piezoelectric layer consists of two elements, both of which are longitudinally poled and placed in reverse directions with respect to each other about the mid-section of the laminate. This maximizes the voltage and power outputs of the device.

The working principle is as follows. A harmonic ac magnetic field H_{ac} is applied along the longitudinal direction of the composite. This causes the two magnetostrictive layers to shrink/expand in response to H_{ac}. The magnetostrictive strain acts upon the piezoelectric layer that is bonded between the two magnetostrictive layers, causing the piezoelectric layer to strain, producing a voltage output between the end and middle electrodes. This transduction of magnetic to electrical energy is what we designate as the magnetoelectric coupling effect.

A solenoid with N turns around the laminate that carries a current of I_{in} was used to excite an ac magnetic field H_{ac}, as shown in Fig. 1. The input ac voltage applied to the coils was V_{in}, and its frequency was f. This excites an H_{ac} of the same frequency f, along the longitudinal direction of the laminate. When the frequency of H_{ac} is equal to the resonance frequency ($\omega_s=2\pi f_s$) of the laminate, the magnetoelectric coupling effect is sufficiently strong that the output ME voltage (V_{out}) induced in the piezoelectric layer is much higher than V_{in}, in particular when a suitable dc magnetic bias H_{dc} is applied. Thus, under resonant drive, our ME laminate exhibits a strong voltage gain, due to the magnetoelectric effect.

At the first longitudinal resonance frequency, this laminate is a half-wavelength ($\lambda/2$) ME resonator. A node line is located at the middle position of the laminate, where the vibration velocity (i.e., mechanical current) is zero. Assuming a symmetric vibration of the laminate and that the polarization of the piezoelectric layer is symmetric about the node line, the ME voltage induced across each end and middle electrode in the layer is equivalent. The magneto-elasto-electric equivalent circuits can be derived by using the piezoelectric and piezomagnetic constitutive equations, and by applying Newton's second law of motion to the laminate and

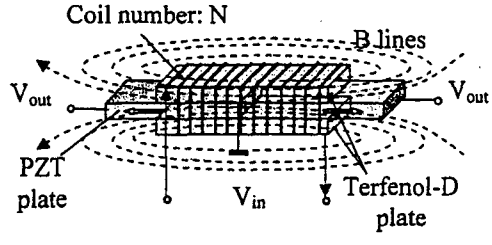

FIG. 1. Configuration and operation principle of magnetoelectric transformer.

[a]Electronic mail: sdong@vt.edu

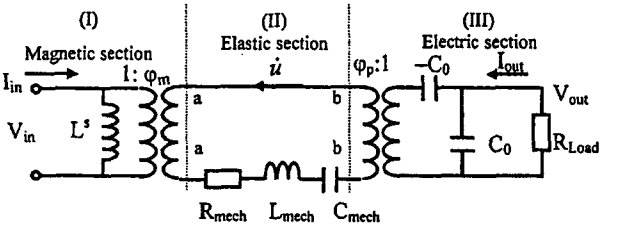

FIG. 2. Equivalent circuit of the ME transformer, where $R_m = \pi Z_0/4Q_m, L_m = \pi Z_0/4\omega_s$, and $C_m = 1/\omega_s^2 L_m$ are the motional mechanical impedance, inductance, and capacitance, respectively; $\varphi_m = \lambda_{33}/j\omega N$ is the magneto-elastic coupling factor; $\varphi_p = 2A_1 g_{33p}/l s_{33}^D \bar{\beta}_{33}$ is the elasto-electric coupling factor; $C_0 = 2A_1/l\bar{\beta}_{33}$ is the clamped capacitance of the piezoelectric layer; and $L^s = 2A_m \mu_{33}^s N^2/l$ is the clamped inductance of the coils around Terfenol-D layers.

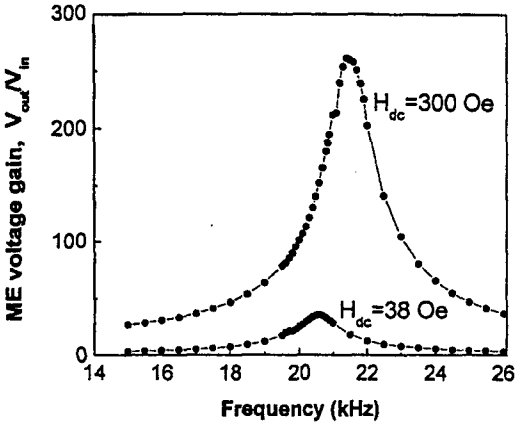

FIG. 3. Measured ME voltage gain as a function of operational frequency.

subsequently finding analogous electrical parameters.[16,17] See Fig. 2.

The magnetoelectric voltage gain was determined by analysis of the equivalent circuit in Fig. 2. Assuming that the circuit is unloaded and by applying Ohm's law, the maximum voltage gain can be estimated as

$$V_{\text{gain,max}} = \frac{4Q_{\text{mech}}\varphi_p^2}{\pi\omega_s C_0 Z_0}, \tag{1}$$

where Q_{mech} is the mechanical quality factor of the piezoelectric layer, φ_p is the elasto-electric coupling factor, C_0 is the clamped capacitance of piezoelectric layer, and Z_0 is the mechanical impedance of the laminate. From this relationship, it can be seen that the maximum voltage gain at the resonance frequency is mainly related to the piezoelectric section of the equivalent circuit in Fig. 2. The voltage gain is directly proportional to Q_{mech} and φ_p^2 (or $g_{33,p}^2$, piezoelectric voltage constant) in the piezoelectric layer. This is because the output voltage V_{out} is generated by this section. The function of the magnetic section of the circuit is to transduce the magnetic energy into a mechanical vibration. The piezoelectric one subsequently transduces this vibration to an electrical output.

Calculations were performed using Eq. (1), assuming a laminate length of 70 mm, width of 10 mm, and thickness of 6 mm. The voltage gain for a value of $Q_m = 100$ was only 18.5. However, for $Q_{\text{mech}} = 500$, the gain was 92.5. A typical value of Q_{mech} for PZT-8 is 1400 (see Table I): using this value, a maximum voltage gain of 259 can be estimated. This voltage gain is significantly larger than that of other voltage gain devices, such as electromagnetic and piezoelectric transformers.[19–21] Thus, the high voltage gain of our laminate could be quite purposeful for power electronics, such as transformer applications.

We can estimate the maximum efficiency ($\eta_{\max}$) of the magnetoelectric transformer, using the equivalent circuit in Fig. 2. To do this, we neglect the electrical losses (mainly eddy current loss in magnetoelectric material) by assuming that the laminate (i) is a multi-thin-layer type; (ii) is operated at relative low-frequency; and (iii) has only mechanical contributions to the total loss factor. Thus, if the load of the circuit is optimum, $R_{\text{load,opt}} = 1/\omega_s C_0$, the value of $\eta_{\max}$ of the laminate at resonance is

$$\eta_{\max} = \frac{\varphi_p^2}{\varphi_p^2 + \dfrac{\pi Z_0 C_0 \omega_s}{2Q_{\text{mech}}}}. \tag{2}$$

Clearly, a higher Q_{mech} will result in higher efficiencies. Using the material parameters shown in Table I and by assuming that $Q_{\text{mech}} = 1000$, the maximum efficiency of our ME transformer can be estimated using Eq. (2) as $\eta_{\max} > 95\%$ when the eddy current loss in magnetostrictive material can be neglected. When eddy current losses cannot be neglected, the parameters in the magnetic and elastic section will need to be complex coefficients. Correspondingly, the efficiency shall be less than $\eta_{\max}$, and Eq. (2) will need to be modified further.

A laminate composite consisting of a longitudinally poled piezoelectric $Pb(Zr,Ti)O_3$(PZT) layer and two longitudinally magnetized magnetostrictive Terfenol-D ones was fabricated as shown in Fig. 1. In our design, the Terfenol-D layers were 40 mm in length, and the piezoelectric layer was 80 mm in length. A long and thin piezoelectric layer helps to achieve higher ME voltages, as it has larger vibration amplitudes at both ends. The ME voltage gain was measured. A voltage generator was used as an input source to the coils, and an oscilloscope was used for monitoring both input and output voltages. Figure 3 shows the measured voltage gain $V_{\text{out}}/V_{\text{in}}$ of our ME transformer as a function of the drive frequency f. A maximum voltage gain of ~260 was found at a resonance frequency of 21.3 kHz. In addition, at the resonance state, the maximum voltage gain of the ME transformer was strongly dependent on an applied dc magnetic bias H_{dc}, which is due to the fact that Terfenol-D has a large

TABLE I. Electromechanical and magnetoelastic materials parameters for Terfenol-D and PZT ceramics.

	$g_{33} \times 10^{-3}$	$d_{33,m}$ or $d_{33,p}$	$d_{31,m}$ or $d_{31,p}$	S_{11}^Hor $S_{11}^E \times 10^{-12}\text{m}^2/\text{N}$	S_{33}^Hor $S_{33}^E \times 10^{-12}\text{m}^2/\text{N}$	k_{33}	k_{31}	Q_m
Terfenol-D[a]		1.1×10^{-8}Wb/N	-5.8×10^{-9} Wb/N	125	40	0.7		<10
PZT-8[b] piezoceramic	25.5	290 pC/N	−125 pC/N	11.8	17.4	0.68	0.33	1400

[a]Cited from Ref. 17.
[b]Cited from APC company, Pennsylvania.

effective piezomagnetic coefficient only under a suitable H_{dc}. For $H_{dc} \approx 300$ Oe, our prototype exhibited a maximum voltage gain of ≈ 300, which is slightly higher than the predicted value using Eq. (1). It is because the piezoelectric layer is longer than the Terfenol-D layers. Because the effective operational working frequency (assuming neglible eddy currents) for a bulk Terfenol-D is less than 10 kHz,[17] the efficiency of a magnetoelectric transformer consisting of a Terfenol-D/PZT bulk laminate is much lower ($\leqslant 0.5\eta_{max}$) than that predicted by Eq. (2). However, by using a multithin-layer type configuration, we believe that it may be possible to obtain a higher efficiency, as predicted by Eq. (2).

Compared with conventional electromagnetic transformers, our ME transformer does not require secondary coils with a high-turns ratio in order to obtain a step-up voltage output. Compared with piezoelectric transformers, it has significantly higher voltage gains and a notably wider bandwidth. Also, it has the additional advantage of low input impedance, thus low-voltage current driving for the magnetostrictive Terfenol-D layers, and a high output impedance for the PZT one. Finally, Terfenol-D has a very high energy density[17] of 4.9–25 kJ–m^3, which is notably higher than that of PZT used in conventional piezoelectric transformers. The combination of these advantages offers potential for applications in new solid-state transformer devices.

In summary, a strong magneto-electric voltage gain effect has been found in laminate composites of piezoelectric PZT and magnetostrictive Terfenol-D. We believe these results have important ramifications, potentially offering applications in miniature solid-state power transformers.

The authors gratefully acknowledge the support of the Office of Naval Research under Grant Nos. N000140210340, N000140210126, and MURI N000140110761.

[1]L. D. Landau and E. Lifshitz, *Electrodynamics of Continuous Media* (Pergamon, Oxford, 1960), p. 119.
[2]M. Avellaneda and G. Harshe, J. Intell. Mater. Syst. Struct. **5**, 501 (1994).
[3]T. Wu and J. Huang, Int. J. Solids Struct. **37**, 2981 (2000).
[4]K. Mori and M. Wuttig, Appl. Phys. Lett. **81**, 100 (2002).
[5]J. Ryu, A. V. Carazo, K. Uchino, and H. Kim, J. Electroceram. **7**, 24 (2001).
[6]J. Ryu, A. V. Carazo, K. Uchino, and H. Kim, Jpn. J. Appl. Phys., Part 1 **40**, 4948 (2001).
[7]J. Ryu, S. Priya, K. Uchino, H. Kim, and D. Viehland, J. Korean Ceramic Soc. **39**, 813 (2002).
[8]C.-W. Nan, M. Li, and J. H. Huang, Phys. Rev. B **63**, 144415 (2001).
[9]C. W. Nan, L. Liu, N. Cai, J. Zhai, Y. Ye, and Y. H. Lin, Appl. Phys. Lett. **81** 3831 (2002).
[10]M. Avellaneda and G. Harsche, J. Intell. Mater. Syst. Struct. **5**, 501 (1994).
[11]G. Srinivasan, E. Rasmussen, B. Levin, and R. Hayes, Phys. Rev. B **65**, 134402 (2002).
[12]Y. Li, Vol. 1 (sensors online: http:/sensorsmag.com/articles/1000/52/index.htm).
[13]S. Dong, F. Bai, J. F. Li, and D. Viehland, IEEE Trans. Ultrason. Ferroelectr. Freq. Control **50**, 1236 (2003).
[14]S. Dong, J. F. Li, and D. Viehland, Appl. Phys. Lett. **83**, 11 (2003).
[15]G. Srinivasan, E. T. Rasmussen, J. Gallegos, R. Srinivasan, Y. I. Bokhan, and V. M. Laletin, Phys. Rev. B **64**, 214408 (2001).
[16]W. Mason, *Physical Acoustics, Principles and Methods* (Academic, New York, 1964), Part 1A.
[17]G. Engdahl, *Magnetostrictive Materials Handbook* (Academic, San Diego, 2000).
[18]T. Ikeda, *Fundamentals of Piezoelectricity* (Oxford University Press, New York, 1990).
[19]C. Rosen, Seventh Electronic Components Symposium, Washington, DC, 1956, pp. 205.
[20]J. S. Yang and W. Zhang, Int. J. Appl. Electromagn. Mech. **10**, 105 (1999).
[21]J. S. Yang, X. Zhang, Int. J. Appl. Electromagn. Mech. **16**, 29 (2002).

APPENDIX 8

ELSEVIER

Microelectronic Engineering 66 (2003) 574–583

MICROELECTRONIC ENGINEERING

www.elsevier.com/locate/mee

Domain phenomena in single crystalline and ceramic ferroics: unresolved and attractive problems

J. Fousek[a,b], L.E. Cross[b,*], J. Nosek[a]

[a]*Department of Electrical Engineering and Electromechanical Systems, International Center for Piezoelectric Research, Liberec Technical University, Liberec, Czech Republic*

[b]*Materials Research Institute, The Pennsylvania State University, University Park, PA 16802, USA*

Abstract

Domain-related properties of ferroic materials offer a number of application aspects. However, some of the involved domain characteristics have not been fully explained and may initiate an interesting field of further research. Here we specify and discuss several such still unresolved problems related to single crystalline and ceramic samples. Those concerning static domain pattern include the topic of domain wall thickness and of possible macroscopic wall properties, macroscopic properties of ceramic samples *depoled* in different ways and application of multidomain systems in surface acoustic wave devices. Discussed problems related to dynamic domain phenomena include the issue of visibility and thickness of moving domain walls, the effect of nucleation and the topic of extrinsic contributions to macroscopic properties of multidomain samples.

Keywords: Domains in ferroics; Domain wall thickness; Depoling ceramics; Surface acoustic waves; Moving domain walls; Nucleation; Extrinsic contributions

1. Introduction

Samples of ferroic materials can be produced in a number of assemblage types; as single crystals, ceramics, polymers, glass ceramic, composites and thin (thick) films. All of them may contain domains since the existence of the latter is dictated by the symmetry reduction specifying the phase transition. Here we address only single crystals and ceramics. Understandably, most unsolved problems in single crystals indicate open questions even in ferroics of other systems. In contrast, many essential domain-related problems in non-single-crystalline types of samples are connected with boundary conditions or composition-nonhomogeneity aspects that are irrelevant in single crystals.

Some interesting domain-related features remain unsolved; some are very difficult to be solved,

*Corresponding author. Tel.: +1-814-865-1181; fax: +1-814-863-7846.

0167-9317/02/$ – see front matter
doi:10.1016/S0167-9317(02)00968-1

some have not been readdresses because there are no application-related aspects; and some were not accessed because no proper experimental techniques were available, etc.

Out of a number of such problems we have selected just a few which we believe would be worth addressing whether experimentally and/or theoretically. Roughly speaking, all open issues can be also classified into those connected with static aspects of domain patterns and those related to dynamic aspects of wall motion and switching. Here we have made a narrow selection of problems related to both these viewpoints.

2. Domain walls and domains at rest

2.1. Domain wall thickness

The problem of wall thickness d_w was repeatedly addressed starting from the early stages of ferroelectric domain investigations. From the recent points of view of application aspects it may play a substantial role: when using specific properties of walls their thickness d_w would be essential, in addition to the domain density.

Here we shall concentrate on nonferroelastic walls in ferroelectrics; the problem was probably first discussed for the classical ferroelectric $BaTiO_3$. The early models [1] and calculations [2] indicated that d_w of its 180° walls is just a few lattice parameters; in most discussions of properties of multidomain samples this extremely small wall thickness is generally assumed. And indeed a very large number of TEM investigations (see, e.g., Ref. [3,4]) of this material indicated the d_w values between 10 and 100 Å. Also in some other perovskites this small wall thickness was confirmed. For TGS, a ferroelectric of a significantly different composition, a similar value $d_w \cong 80$ Å was reported [5], based on atomic force microscopy data.

The mentioned information on d_w has been primarily based on observations of either extremely thin samples or of thin surface regions of crystals. Repeatedly, much thicker domain walls have been detected using X-ray topography which can reveal walls inside a sample; e.g., d_w of the order of 1 μm was reported for $NaNO_2$ [6], $SC(NH_2)_2$ [7] or TGS [8,9]. While data based on this method have been disputed because of its possible limited spatial resolution, we have to admit that reliable reports on d_w values inside samples based on other methods are missing.

We wish to mention two examples indicating the possibility of existence of thick nonferroelastic walls. Kawata et al. [10] investigated 180° domains in thick *a*-oriented plates of defect-free $BaTiO_3$ by surface reflection topographs and optical micrographs. Their data refer to static situations. Antiparallel domains terminate by *oblique* optically visible 180° walls. The analysis of X-ray and optical data showed that d_w values were of the order of 1 μm. The ε_{23} strain component was found to be responsible for the optical contrast of oblique walls in which **P** makes an angle 1–2° with $\mathbf{P}_S$. The origin of the significantly increased thickness cannot be of a simple mechanical-compatibility origin. It could be related either to the structural aspects of walls of $(h,k,l \neq 0)$ orientation or to the fact that they may be charged. The latter possibility seems to be less probable since the mentioned investigations did not proceed fast and charge compensation could be assumed. Thus these results seem to indicate that an inclined mechanically fully compatible wall can be in fact significantly thicker than generally assumed.

It has been assumed from the early stages of investigations that wall thickness could be strongly

influenced by lattice defects; either walls can be assumed to prefer locations with high density of defects or defects could diffuse into the existing walls. The problem was repeatedly addressed for ferroelastic walls. Darinskii and Sidorkin [11] were probably the first to address theoretically the influence of defects on the observed d_w of a nonferroelastic 180° wall. They defined the effective wall thickness $d_{w.eff}$ as the width of a layer containing the domain wall which is locally deformed by point defects. For defect concentration 10^{18} cm^{-3} $d_{w.eff}$ increased from a few unit cells to 300 Å, and for linear defects parallel to the polar direction $d_{w.eff}$ might reach the value of 3000 Å. When the charge of local defects is specifically taken into account [12], the broadening of walls has distinctive features; in particular, the wall can contain extended areas of curved sections where it makes an angle with the $\mathbf{P}_S$ direction.

Much more recently the problem was finally addressed also experimentally, by Gupta and co-workers [13,14]. Indeed it has been shown that the thickness of 180° nonferroelastic wall can be considerably influenced by the presence of lattice defects. In congruent crystals which are Li-deficient, the 180° walls formed at room temperature have been reported to reveal very specific properties: large birefringence within regions of thickness of the order of 1 μm [13,14]. Based on these and some macroscopic properties, strain components connected with walls were evaluated [15] and the existence of strong local electric fields was suggested. In stoichiometric crystals strain and birefringence tend to disappear; thus these effects and the large wall width are clearly connected with lattice defects. Kim et al. [16] used X-ray synchrotron diffraction imaging to study strain components when crossing the wall and found that they represent wall thickness of several μm in both congruent $LiNbO_3$ and $LiTaO_3$.

To summarize briefly, we can state that two features have been proved to influence considerably the thickness of a static 180° nonferroelastic wall: the wall orientation and lattice defects. Although representative types and properties of defects resulting in wide domain walls do not seem to have been specified, the latter feature in particular may open a new field of applications of ferroelectric crystals with a large wall density; a new area of domain wall engineering [17,18]. $LiNbO_3$ samples with appropriate non-stoichiometry and with engineered dense domain pattern might offer macroscopic properties new in the sense of symmetry and/or in the sense of values of some material coefficients.

2.2. Domain wall symmetry

Let us now pay attention to the 'ideal' wall structures, uncharged and uninfluenced by defects. Can they offer some macroscopically detectable properties differing from those of a single domain material? It would be an interesting question from the practical point of view if the wall width and/or their density would provide a non-negligible sample volume. The lowest-order tensor which could represent the macroscopic properties of walls is a vector, polarization. Thus one asks the question whether a domain wall in a nonferroelectric sample can carry a dipole moment. A positive answer to this question was suggested by Walker and Gooding [19] who showed theoretically that domain walls in the room temperature phase α of quartz can carry a dipole moment. Between the parent phase β and phase α there exists an incommensurate phase containing triangular domain systems of two variants; in one variant domain walls carry dipole moments along the 3-fold axis, in the other the dipoles are of opposite direction. Snoeck et al. [20] showed that applied field results in changes of this domain pattern and could be interpreted as a result of sidewise motion of the polar walls. Another indirect proof of polar walls was presented by Jorio et al. [21] for crystals of Cs_2HgBr_4. Raman

scattering and infrared reflectivity dates led to the conclusion that domain walls carry a dipole moment lying in the wall plane. We are not aware of other data representing polar walls; symmetry-based analyses [22,23] indicate that they may be present in both nonferroelastic and ferroelastic nonferroelectric species and recent theoretical study [24] predicted that even antiphase domain walls may be polar, in $SrTiO_3$ crystals in particular.

Polarity of domain walls in defect-free samples of classical ferroics does not seem to have been unambiguously proved. However, when an attribute is allowed by symmetry, it may be just a matter of time and of finding the proper material to demonstrate its existence.

2.3. Applications of static domain systems: SAW

Let us now mention two specific domain-related application aspects. Surface acoustic waves play an important role in some applications of piezoelectric crystals and $LiNbO_3$ plays an essential role. Since two domain states of this material differ in elastic coefficients and in signs of piezoelectric constants, different domain geometries can be considered influencing the propagation of SAW. Here we wish to point out that even a simple system of two domains D1 and D2 (Fig. 1) can offer properties which may be useful for SAW applications. The SAW propagates from the interdigital transducer IDT1 to IDT2. Each domain is provided with electrodes (A1, A2) so that electric fields perpendicular the the propagation direction of SAW can be applied. As shown before [25], by static or slowly changing electric field it is possible to influence the group velocity of SAW in either of the domains and this can be achieved in each domain in a different way. The effect can be described by the change of elastic and piezoelectric coefficients: $c^* = c + aE$, $e^* = e + bE$. As a result, two time delay lines are produced on one substrate. On the domain wall considered here to be perpendicular to the signal propagation, significant reflection of the surface acoustic wave can occur [26]. Interference of the original and reflected SAW can be influenced by the electric field in domain D1. The whole system can be used for signal processing.

2.4. Static domain systems in depoled ceramic samples

Another interesting domain-related aspect concerns ferroelectric ceramics. Consider we wish to depole a previously poled ceramic sample. This can be achieved in several ways; the resulting

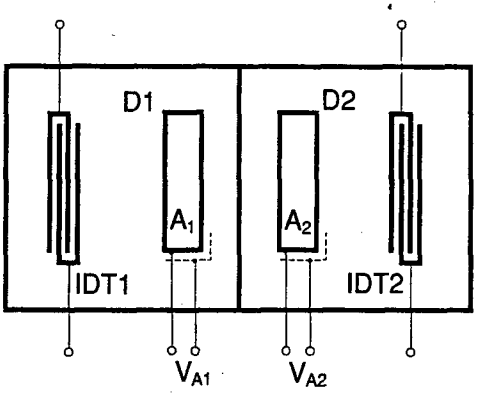

Fig. 1. A two-domain system for SAW applications; see text.

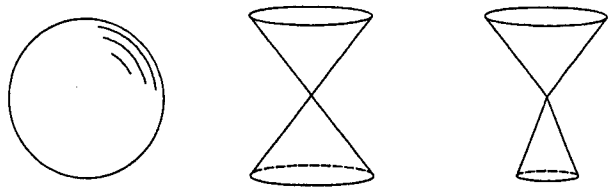

Fig. 2. Representation of symmetries of depoled ceramic samples: (a) thermally depoled sample; (b) sample depoled by ac field; (c) sample depoled when traversing the hysteresis loop.

symmetries are represented in Fig. 2. Thermal depoling (a) would result in the $\infty\infty m$ symmetry with zero piezoelectricity. When a low frequency ac field is applied whose amplitude is reduced with time, it can be expected that the arrangement of $\mathbf{P}_S$ directions results in zero value of $\bar{P}$ but does not return to a homogeneous distribution of spherical symmetry; we would rather expect the vector distribution corresponding to a double-cone of symmetry ∞/mm. Tensorial properties of a sample depoled in this way (b) do not seem to have been investigated. Let us note that tensorial properties in the samples depolarized by the two mentioned ways would differ, by symmetry; e.g., in tensors of symmetries V^2, $[V^2]$, $\varepsilon V[V^2]$, $V[V^3]$ and $[[V^2]^2]$ [27].

Yet a ceramic sample can be depolarized in still another manner: a $P(E)$ hysteresis loop is slowly traversed. When the loop crosses the horizontal axis ($\bar{P}=0$), it can be expected that the domain geometry in this state will differ significantly from those depoled by the above mentioned methods. Can a ceramic sample depoled in this way be piezoelectric? This question was discussed by Luchaninov and co-workers [28,29]; and the answer is positive. Here we present the simplest approach to the problem. Obviously, in this state the $\mathbf{P}_S$ distribution could be represented by an asymmetric double cone: the distribution of $\mathbf{P}_S$ vectors around the previous poling direction can be narrower than the distribution around the opposite direction. Thus the ∞mm symmetry would still be retained although in the arrived state $\bar{P}=0$. The sample could still exhibit piezoelectric properties. Investigations of ceramic samples depoled in the three mentioned ways might offer interesting information.

3. Dynamic aspects: moving domain walls and nucleation

3.1. Visibility and thickness of moving 180° walls

Above we have addressed the problem of the thickness of 180° walls at rest. However, the issue of the thickness and structure of moving 180° walls may be found even more interesting. It was discussed a long time ago and seems to be an almost forgotten issue although it can play a substantial role in ferroelectric memories.

If nonferroelastic 180° walls in a high quality $BaTiO_3$ crystal were as thin as discussed above, they could not be observed optically. However, Miller and Savage [30] reported that during polarization reversal 180° domains are visible when viewed along the *c*-axis between crossed polaroids. Nakamura et al. [31] showed that when a field is applied to an *a*-oriented $BaTiO_3$ crystalline plate, slightly oblique static walls can be observed for a short time in a polarizing microscope as bright lines.

Theoretical discussion [32] showed that the effective thickness of a moving wall with average (*hk*0) orientation may be very large because of the nucleation process. However, it did not include any aspects which would lead to an optical contrast; either a modified symmetry of domain walls or an inclined wall orientation. The visibility of sidewise moving walls viewed along the *c*-axis was discussed in detail by Kobayashi et al. [33]. They showed that the optical contrast in the zones of moving walls indicated birefringence which increased when the wall moved faster; after the wall had stopped moving, it took some time for the contrast to disappear. Using X-ray diffraction they confirmed that the symmetry of a moving wall is influenced by a monoclinic deformation which results also in optical visibility of the wall. We may note that the shear strain specified by Kawata et al. [34] in a static wall is about one order of magnitude smaller than that observed by Kobayashi for the moving wall. Independently, Kobayashi [35] also demonstrated that moving 180° walls in $BaTiO_3$ are visible even when viewing along the *a*-axis.

In the observations referred to above, $BaTiO_3$ crystals were used grown by the original Remeika's method. It might be interesting to readdress the problem using crystals grown by Linz's top-seeded flux method.

It appears that the presently applied theories of switching do not take into account the specific structure and thickness of moving domain walls. This applies in particular to switching in thin films where the moving wall thickness may in fact be comparable to the sample thickness. In fact we miss even some basic experimental data on antiparallel switching processes in thin film samples of materials presently used in memory devices.

3.2. Nucleation

It was accepted in the early of investigations that polarization reversal in classical ferroelectrics proceeds in three steps: nucleation of domains with antiparallel polarization and their forward growth followed by sidewise expansion. Experimental data on which the switching models are based are of two kinds: macroscopic properties—hysteresis $P(E)$ or switching current $i(t)$ dependencies—and observations of domains during the switching process. We now address the question whether the nucleation process, meaning random formation of small domains with antiparallel $\mathbf{P}_S$, really plays a role.

It is well known that Landauer [36] pointed out in the early stages of investigations of $BaTiO_3$ that the critical nucleation energy ΔU^*, in fact a potential barrier to be overcome to form a stable nucleus with antiparallel polarization, is too high ($10^8 kT$) to allow for any realistic nucleation rate. It is a result of combined contributions of depolarizing field energy and surface energy of the nucleus. Even if the depolarizing field were compensated by free charges from the electrodes, the surface energy term alone is too large ($10^5 kT$) for nucleation aided by thermal fluctuations to be possible. Only in applied field orders of magnitude higher [37] than the real field required for switching the activation energy could be reduced to $10kT$. For PZT, in the applied field 100 kV/cm, Tagantsev's estimation (A.K. Tagantsev, personal communication) of the barrier was $10^3 kT$. To solve this problem, a number of experimental investigations were performed and some theoretical approaches were proposed.

Understandably, many attempts have been devoted to analyzing the nucleation stages experimentally. Stadler and Zachmanidis [38] used etching to reveal domains formed in $BaTiO_3$ after the application of several pulses of field; to each cylindrical domain a nucleus was attributed. Depending on the sign of the 'internal bias', 10–30% of observed domains were 'repeaters', indicating nucleation

occurring at predetermined sites. Thus the remaining percentage of nuclei might be formed chaotically, based on statistical probability. Total nucleation rate dn/dt was found to be proportional to $E^{1.4}$. It has to be pointed out these results were obtained by etching the samples a long time after the application of field. Therefore the obtained data, while interesting, need not represent the nucleation process.

Much more recently, Gruverman et al. [39] investigated nucleation in lead germanate; the specific advantage of this material is that its species $\bar{6}$–Pd–3 allows for optical observation of nonferroelastic domains in real time, due to optical activity. The authors specified three time intervals: t_d in which the first 'through' domains appear; it was found to depend on the quality of sample surface; t_{tr} during which the nucleation rate increases till a steady state regime (constant value of dn/dt) is reached; this regime lasted for more than 2 ms. The essential point is that the authors used stroboscopy to observe the nucleated and grown domains. The possibility to use this method indicates that the nuclei occurred repeatedly at the same spots which must have been predetermined by defects. It would be interesting to study crystals of the same material grown with the aim to control their defect structure and to reach maximum purity.

The fact that nucleation has been repeatedly observed at surfaces of samples need not be connected with the ideal nucleation energy considerations. Preparation of samples usually includes mechanical modification of their surfaces which may lead to facilitating the nucleation or even to built-in nuclei. It is interesting that this may play a substantial role even in nonferroelastic samples. Venables [40] showed that surface polishing of $LiTaO_3$ samples leads to formation of dislocations with [001] oriented Burgers vectors, which served as nuclei of antiparallel domains; their densities reached a value of 10^7 per cm^2.

Other data are available concerning the number of nuclei and its time dependence. However, because of the limited spatial and time resolution to obtain information on the *real* nucleation process is difficult. To refer to small observed domains as to nuclei may be questionable.

The mentioned estimations and data point to the question whether the nucleation process plays an essential role in the observed macroscopic properties, like hysteresis loops or switching currents. It was shown already by Janta [41] that to interpret the $P(E)$ loop does not really require the nucleation stage. In his model, the presence of lattice defects results in the existence of residual domains. Using the $\exp(-\alpha/E)$ law for wall velocities together with the domain coalescence described by the Avrami theorem, hysteresis loops can be calculated whose amplitude and frequency dependencies agree well with experimental data. Ishibashi and Takagi [42] developed a phenomenological theory of the switching current in pulse field. They solved the problem under two different assumptions: (a) the nucleation rate is constant throughout the switching period; (b) latent nuclei of a given number are assumed to exist and no further nucleations occur. The available experimental data did not allow to reach ultimate conclusions regarding the role of the nucleation process; however, the assumption of latent nuclei did not contradict any observed properties.

The problem of nucleation is still repeatedly addressed. A new theoretical approach was offered by Molotskii et al. [43]. They consider the following mechanism for the formation of nuclei. When E is applied, electrons tunnel from an electrode to states of neutral defects aggregates. Those captured by defects form single-electron fluctuons; a fluctuon is a bound state of an electron (or a hole) with a fluctuation of local polarization. The coalescence of such fluctuons leads to the appearance of stable multielectron fluctuons which may be regarded as repolarization nuclei. While the energy of an equilibrium fluctuon is found to be negative, there is still a barrier of the order of several eV which is

expected to be overcome by thermal fluctations. Let us stress that even the fluctuon model assumes that lattice defects play a role in the whole process.

Recently, Urenski et al. [44] referred to the offered models [36,43] of how the activation energy could be reduced by assuming domain nucleation on the polar crystal surface where the required charge carriers may be injected from the switching electrodes. They pointed out that when studying $KTiOPO_4$ crystals we have the possibility to compare two situations. At room temperature the material possesses superionic conductivity (mobile K ions) allowing for compensation of depolarizing field. This may lead to easy nucleation in the bulk of the crystal. In contrast, at low temperatures the material is a true dielectric for which nucleation at the electrodes may be more probable. Indeed an obvious difference was observed in these two temperature regions: In the dielectric state the domains are nucleated at the electrodes and grow straightforwardly from the top to the bottom surface. In the superionic state the observed domains appear in the crystal bulk and on growing are strongly widened. These interesting observations do not rule out the possibility of built-in nuclei.

To conclude, all results support or at least do not exclude the assumption that in the observed switching processes the ideal defect-independent nucleation is irrelevant. However, the possibility cannot be excluded that in different materials the nucleation processes are of different origins. It would be of interest to concentrate further research on one crystalline material grown with well defined concentrations of defects and working with samples whose surfaces would be prepared in a well controlled way.

At the end of this section, we wish to point out that the problem of nucleation is closely related to the aspect of 'writing' domains which is essential for memory applications of thin films. Eng et al. [45] addressed the issue also for thick samples, using scanning force microscopy. They showed that local polarization reversal can be induced by applied field in any required spot (specified with the accuracy of about 10 nm). Till now such a nucleation process in a highly nonhomogeneous field has not been addressed theoretically. It has been suggested [46] that even higher order ferroic effects might be involved.

3.3. Modes of extrinsic contributions

The last problem we wish to mention is the classical issue of domain wall (extrinsic) contributions to small-signal macroscopic properties of ferroics. In a nonferroelastic ferroelectric, wall shifts by Δx increase the measured permittivity. Assuming the applied field amplitude $E_0 = 1$ V/cm and a realistic density of walls at room temperature, in typical crystals of TGS Δx at 1 kHz is of the order of 0.1 Å. In a ferroelastic ferroelectric, wall shifts by Δx lead to extrinsic parts of permittivity, elastic constant and piezoelectric coefficient. Estimations for RbH_2PO_4 based on the data of all three properties lead to Δx of the order of 0.1–1 Å [47], again for $E_0 = 1$ V/cm, at a below the resonance frequency.

Let us consider the 'ideal' wall thickness just a few unit cells, referring to TEM observations or to wall theories, both macroscopic or microscopic. Then such small values of shifts Δx represent rather a change of the structure of walls rather than their uniform displacements. The problem can be solved in two different ways. First, the walls inside thick samples may be actually much thicker; this would be in agreement with some observations mentioned above. Alternatively, the walls can be pinned by defects and the mentioned Δx represents just a spatially averaged value. Yang et al. [48] used near field scanning optical microscope to investigate domain walls in thick samples of $LiTaO_3$. When electric field was applied, curved sections of 180° walls were clearly observed, demonstrating that

even nonferroelastic walls can be pinned by defects. The curvature radius corresponded to the applied field.

This observation showed clearly that—at least in nonferroelastic ferroelectrics—the Δx calculated from the measured macroscopic quantities is an averaged value. In addition, because the internal structure of a bent wall may be different from that of a planar wall, the extrinsic contributions may combine two aspects—volume changes of positively and negatively oriented domains as well as changes of the internal wall structures, due to bending.

The problem of extrinsic contributions has been repeatedly addressed for several decades; yet it still offers an area of interesting research which might also open new and essential application aspects.

4. Concluding remark

At the end we wish to stress that in many issues mentioned above the role of crystal lattice defects is expected to be essential; yet we still know very little about the background of defect-induced phenomena. Growing defect-free and defect-defined samples will be expensive but surely very interesting.

We have mentioned only a small selection of interesting and open problems related to domain phenomena in ferroics. There are many other issues worth addressing. They offer interesting physical aspects and material properties and we expect that the domain research will belong to very active and strongly supported research areas in the coming years.

Acknowledgements

This project was supplied with the subvention from Ministry of Education of the Czech Republic, project MSM 242200002.

References

[1] W. Känzig, R. Sommerhalder, Helv. Phys. Acta 26 (1953) 603.
[2] V.A. Zhirnov, Zh. Eksp. Teor. Fiz. 35 (1958) 1175.
[3] M. Tanaka, G. Honjo, J. Phys. Soc. Jpn. 19 (1964) 954.
[4] H. Blank, S. Amelinckx, Appl. Phys. Lett. 2 (1963) 140.
[5] L.M. Eng, J. Fousek, P. Günter, Ferroelectrics 191 (1997) 211.
[6] M. Takagi, S. Suzuki, J. Phys. Soc. Jpn. 63 (1994) 1580.
[7] J. Aoyama, S. Suzuki, M. Takagi, J. Phys. Soc. Jpn. 61 (1992) 3613.
[8] J.F. Petroff, Phys. Stat. Sol. 31 (1969) 285.
[9] D.Y. Parpia, Phil. Mag. A 46 (1982) 691.
[10] H. Kawata, S. Suzuki, M. Takagi, J. Phys. Soc. Jpn. 50 (1981) 3398.
[11] B.M. Darinskii, A.S. Sidorkin, Sov. Phys. Solid State 26 (1984) 2048.
[12] A.S. Sidorkin, B.M. Darinskii, Sov.Phys.- Solid State 28 (1986) 157.
[13] V. Gopalan, M.C. Gupta, J. Appl. Phys. 80 (1996) 6099.
[14] T.J. Yang, U. Mohideen, M.C. Gupta, Appl. Phys. Lett. 71 (1997) 1960.
[15] T.J. Yang, U. Mohideen, Phys. Lett. A 250 (1998) 205.

[16] S. Kim, V. Gopalan, B. Steiner, Appl. Phys. Lett. 77 (2000) 2051.
[17] J. Fousek, D.B. Litvin, L.E. Cross, J. Phys. Condens. Matter 13 (2001) L33.
[18] J. Fousek, L.E. Cross, Ferroelectrics 252 (2001) 171.
[19] M.B. Walker, R.J. Gooding, Phys. Rev. B 32 (1985) 7408.
[20] E. Snoeck, P. Saint-Gregoire, V. Janovec, C. Roucau, Ferroelectrics 155 (1994) 371.
[21] A. Jorio, P. Echegut, N.L. Speziali, M.A. Pimenta, Ferroelectrics 221 (1999) 79.
[22] J. Prívratská, V. Janovec, Ferroelectrics 222 (1999) 23.
[23] V. Janovec, L. Richterová, J. Pøívratská, Ferroelectrics 232 (1999) 73.
[24] A.K. Tagantsev, E. Courtens, L. Arzel, Phys. Rev. B 64 (2001) 224107.
[25] J. Nosek, in: Proc. European Frequency and Time Forum 1997, Neuchatel, Switzerland. March 1997, 1997.
[26] D.V. Roschupkin, M. Brunel, R. Tucoulou, E. Bigler, N.G. Sorokin, Appl. Phys. Lett. 64 (1994) 164.
[27] Y.I. Sirotin, M.P. Shaskol'skaya, in: Foundations of Crystal Physics, Nauka, Moscow, 1979.
[28] A.G. Luchaninov, A.V. Shil'nikov, Sov. Phys. Tech. Phys. 25 (1980) 364.
[29] A.G. Luchaninov, A.V. Shil'nikov, L.A. Shuvalov, Ferroelectrics 41 (1982) 181.
[30] R.C. Miller, A. Savage, Phys. Rev. Lett. 2 (1959) 294.
[31] T. Nakamura, H. Ogihara, J. Kobayashi, J. Phys. Soc. Jpn. 18 (1963) 1716.
[32] A. Fousková, Czech. J. Phys. B 20 (1970) 790.
[33] J. Kobayashi, N. Yamada, T. Nakamura, Phys. Rev. Lett. 11 (1963) 410.
[34] H. Kawata, S. Suzuki, M. Takagi, J. Phys. Soc. Jpn. 50 (1981) 3398.
[35] J. Kobayashi, Phys. Stat. Sol. 21 (1967) 151.
[36] R. Landauer, J. Appl. Phys. 28 (1957) 227.
[37] H.L. Stadler, Ferroelectrics 137 (1992) 373.
[38] H.L. Stadler, P.J. Zachmanidis, J. Appl. Phys. 35 (1964) 2625.
[39] A. Gruverman, N. Ponomarev, K. Takahashi, Jpn. J. Appl. Phys. 33 (1994) 5536.
[40] J.D. Venables, Appl. Phys. Lett. 25 (1974) 254.
[41] J. Janta, J. Phys. Soc. Jpn. 28 (Suppl.) (1970) 340.
[42] Y. Ishibashi, Y. Takagi, J. Phys. Soc. Jpn. 31 (1971) 506.
[43] M. Molotskii, R. Kris, G. Rosenman, J. Appl. Phys. 88 (2000) 5318.
[44] P. Urenski, M. Molotskii, G. Rosenman, Appl. Phys. Lett. 79 (2001) 2964.
[45] L.M. Eng, M. Bammerlin, Ch. Loppacher et al., Ferroelectrics 222 (1999) 153.
[46] M. Abplanalp, J. Fousek, P. Günter, Phys. Rev. Lett. 96 (2001) 5799.
[47] M. Štula, J. Fousek, H. Kabelka et al., J. Korean Phys. Soc. (Proc. Suppl.) 32 (1998) S758.
[48] T.J. Yang, V. Gopalan, P.J. Swart, U. Mohideen, Phys. Rev. Lett. 82 (1999) 4106.

APPENDIX 9

Ferroelectrics, 293: 43–60, 2003

ISSN: 0015-0193 print / 1563-5112 online
DOI: 10.1080/00150190390238108

Taylor & Francis
Taylor & Francis Group

Open Issues in Application Aspects of Domains in Ferroic Materials

J. FOUSEK[a] and L. E. CROSS[b]

[a]*Department of Electrical Engng. and Electromechanical Systems and International Center for Piezoelectric Research; Liberec Technical University, Czech Republic*
[b]*Materials Research Institute, The Pennsylvania State University, University Park, PA 16802, USA*

(Received September 4, 2002; In final form December 15, 2002)

Domain-related application aspects of ferroics are specified. Domains can play both positive and negative roles. Here we concentrate on the first aspect: using particular domain properties in practical devices. Several research areas related to these properties in single crystals are discussed in some detail, with the aim to specify some of the unsolved domain characteristics. The discussion is related to selected fields of applications and concerns various classes of domain engineering, writing domains, the effect of domain nucleation.

Keywords: Domains in ferroics; domain engineering; domain nucleation; writing domains

INTRODUCTION

Investigations of ferroic materials can be classified into two research areas: (a) properties connected with the change of crystal symmetry at the phase transition; (b) properties connected with multiple relation between the symmetry characteristics of the parent and ferroic phases, i.e. properties connected with the existence of domains. Both areas offer wide fields of practical applications. Domains in ferroic samples can play both a positive and a negative role. The latter case is connected with spatial nonhomogeneity and possible instability of macroscopic properties of a multidomain sample.

Here we concentrate on some aspects of practical applications of ferroelectric materials in which domains play an essential positive role. Their schematic overview is shown in Table I. It demonstrates that domain properties offer a wide area of applications including those based on optical, dielectric or electromechanical characteristics and those based on the switching properties. Some of them are real and on the market. Others might be

TABLE I Applications of ferroelectrics in which domains play an essential role

Physical property	Example of device	C.A.
Piezoelectric properties of poled ceramics	Transducers	Yes
	Sensors, actuators	Yes
	Positioners, motors	Yes
	Resonators, filters	Yes
	Transformers	Yes
Piezoelectric prop's of domain-engineered crystals	Transducers	Yes
Permittivity of ceramics	Capacitors	Yes
Polarization bistability	Nonvolatile memories	Yes
Dielectric nonlinearity	Variable capacitors	No
Acoustic prop's of domain-engineered crystals	Transducers	No
Single domain wall motion	Analog recording	No
Electron emission	Ferroelectric cathodes	Yes
Switchable birefringence	Displays	No
	Optical memories	No
	Image processors	No
Electro-optics	Diffraction gratings	No
Nonlinear optics	Frequency multipliers based on quasi-phase matching structure	Yes
Photorefraction	Optical memories	No
	Image processors	No

C.A. = commercial availability.

readdressed using recent advanced techniques or taking into account previously unknown ferroic materials.

Samples of ferroics can be produced in a number of assemblage types: as single crystals, ceramics, thin (thick) films, polymers, glass ceramics and composites and all of them may contain domains. In what follows we concentrate on the properties of single crystals, the basic configuration of ferroics, and discuss several of their application-related domain aspects: various possibilities of domain engineering, domain nucleation and writing nanodomains. Their deeper analysis based on new experimental and theoretical methods could open new areas of aplications or extend those which have been already addressed.

DOMAIN ENGINEERING: CLASSIFICATION

The concept of domain engineering was originally introduced to designate periodic domain patterns in ferroelectrics, offering specific macroscopic

properties [1]. Nowadays we are aware of several distinctive aspects of domain engineering [2]:

(a) *domain-geometry engineering* (further marked as *DGE*) specifies crystals with particular geometries of domain distribution; in samples a defined number n of domain states is represented and two possibilities exist: $n = n_{max} = |G|/|F|$ or $n < n_{max}$ (G, F stand for the order of parent and ferroic phase, resp.). *DGE* can be of two significantly different kinds. In the first variety (a1) a system of domains of a particular geometry covers repeatedly the area (volume) of the sample. In the second kind (a2) a domain or a specified system of domains exists in an otherwise single domain sample.
(b) *domain-average engineering*, when in a sample a defined number $n < n_{max}$ of domain states is represented with irregular geometry;
(c) *phase- and domain-average engineering*, when also different phases can coexist in a crystalline sample;
(d) *domain wall engineering*, based on specific intrinsic properties of domain walls (*DW*'s).

In this classification we consider static domain patterns; thus application aspects related to dynamic properties of *DW*'s (extrinsic contributions and switching processes) are not involved. The field of domain engineering offers a large field of research, on both theoretical and experimental levels. In the two following subsections we wish to specify the open research areas connected with the (a) and (d) domain engineering aspects.

DOMAIN-GEOMETRY ENGINEERING

Domain geometry engineering (*DGE*) has been already succesful in real practice, e.g. (a1) in optical second harmonic generation [1, 3, 4] or (a2) in optical waveguides [5]. Many other application possibilities have been suggested and are under investigation or development, mostly in the area of optical properties (e.g. generation of higher optical harmonics, multicolour lasers, analog-to-digital converters, optical modulators, acousto-optic deflectors, electro-optic shutters, optical parametric oscillators, holographic storage systems) and in the field of acoustics (e.g. acoustic filters, generation of acoustic harmonics, controlling surface acoustic waves). The excellent review of *DGE* of Shi-ning Zhu et al. [6] includes the variety of techniques for *DGE* and this aspect will not be addressed here.

There exist 212 species of ferroics, defined by the change of point symmetry and specified by new properties. The symmetry change determines the number of domain states as well as the existence and orientation of permissible *DW*'s. More than 2300 ferroics (not considering solid solutions or liquid crystals) are known [7]; thus many *DGE* aspects can be addressed experimentally for a large number of materials portraying different species.

Here we shortly discuss the above specified kind (a1) of *DGE* and will come back to the (a2) aspect in connection with "writing domains". Most of the mentioned applications are based on lamelar domain systems and involve just two domain states—whether these are the only ones permitted by symmetry, like in ferroelectric $LiNbO_3$ (species $\bar{3}m$–Pd–$3m$)[1] and ferroelastic NdP_5O_{14} (mmm–εs–$2/m$), or if the two states are selected from a larger number of symmetry-allowed states, like antiparallel domains in $BaTiO_3$ ($m\bar{3}m - P\varepsilon ds - 4mm$).

Even for two domain states, however, there are realistic possibilities to produce samples with more complicated and still geometrically defined patterns. In ferroelastics, the essential role can be played by nonuniform stresses. It was shown [8–10] that in $Gd_2(MoO_4)_3$ bars ($\bar{4}2m - P\varepsilon ds - mm2$) various regular domain patterns can be created when a sample is deformed either by bending or by torsion. They can be changed when additional mechanical force or electric field is applied. In some cases the orientation of *DW*'s was found to differ from theoretical stress-free permissible orientations. All these aspects offer a wide range of possible domain geometries. A frequently observed regular pattern in ferroelastics based on two domain states is characterized by a periodic zig-zag wall. Obviously, such a boundary has not the parameters of a permissible wall and specified sections of the zig-zag boundary produce additional elastic energy. Such patterns can be applied for tunable acoustic reflection gratings [11]. Zig-zag systems embodying just two domain states have been observed also in ferroelastics with a larger number of domain states, e.g. in $Pb_3(PO_4)_2$ ($\bar{3}m$–εs–$2/m$) for which $n_{max} = 3$ [12].

It is obvious that in species with $n_{max} > 2$ a large number of domain geometries can be defined. However, *DGE* has not been adressed for such multi-state systems. This problem would be connected with several basic questions: whether more complicated domain systems can be repeatedly produced, what are their macroscopic properties and how many such systems

[1] Here we use species designation indicating the point symmetries of the parent and ferroic phases. Symbols P, ε, d, s indicate the appearance of new components of polarization, strain, piezoelectric and elastic tensors in the ferroic phase; thus these symbols represent ferroelectric, ferroelastic, ferroelastoelectric and ferrobielastic transitions.

exist with respect to the parent phase. Before specifying these open problems in more detail let us point to several experimentally observed domain geometries. In tetragonal $BaTiO_3$ an interesting complex square-net pattern composed of 90° *DW*'s was first reported by Forsbergh [13]. It may arise in plate-like samples at slow cooling through T_{TR}. First a prismatic group of laminar domains is formed. When a perpendicular group also appears, a square pyramid is formed at their intersection. A regular and reproducible system of such pyramids can arise, connected with a slight curvature of the sample, probably due to a nonhomogeneous distribution of impurities. The pattern can be created also intentionally, by applying an appropriate pressure to a single domain plate.

Other specific domain arrangements were observed and analyzed in ceramic samples of $BaTiO_3$ [14]. The Arlt's α-configuration in a cube-shaped region is built up from domains separated by 90° walls but in addition by "*I*-interfaces" composed of alternating stripes of 180° and 90° walls. Four $\mathbf{P}_S$ vectors out of possible six are represented and the cube carries a nonzero dipole moment. In an alternative β-configuration the *I*-interfaces are complex, containing sections of 90° walls, sections without any wall and sections with head-to-head 180° walls. Both α and β systems can exist in 12 possible orientations.[2]

Regular and fairly complicated domain patterns have been observed also in other species. In the orthorhombic phase of $BaTiO_3$ ($m\bar{3}m$–$P\varepsilon ds$–$mm2$) a symmetric "checkerboard pattern" exists [15]. In ferroelastic $Pb_3(VO_4)_2$ ($\bar{3}m$–εs–$2/m$) several geometries including 3 domain states were observed [16], such as spiral branch configuration and star pattern.

Producing regular patterns can be based also on the phase coexistence at first order phase transitions. It was shown [17] that in $BaTiO_3$ the orientation of the cubic-tetragonal phase boundary can be controlled by the temperature gradient. When the former is properly oriented, regular patterns of 90° domains can be realized, with a required period. Phase transition studies of KD_2PO_4 [18] indicate a similar possibility in this material.

Let's now specify some problems related to the *DGE* of (a1) type which should be addressed theoretically; based on such analyses experimental attempts to produce reproducible patterns with interesting properties could be started. (i) What are possible domain geometries reducing the total energy for specified applied elastic and electric forces; in forces also field and stress gradients should be included; in ferroics with 1st order transitions conditions

[2]G. Arlt, private communication.

at the phase boundary must be considered. (ii) Which of such multidomain systems in a given species are thermodynamically (meta)stable under given external conditions. (iii) What are their symmetries (analyses of geometrically defined complicated domain patterns) and numbers (with respect to the parent phase). (iv) What are their macroscopic properties related to domain sizes. (v) What are their properties for specified k-vectors of propagating optical or acoustic waves. (vi) Defects of which characteristics and distribution can lead to required domain geometries.

DGE systems with more than two domain states necessarily include ferroelastic domain pairs and the problem of elastic coexistence can make the topic more complicated. In fact, the issue of stress-free conjunction of more than two ferroelastic domain states does not seem to have been systematically discussed; some data indicate that such cases do exist. When multidomain systems require additional strains, materials with very small specified components of spontaneous strain would be preferred. The elastic energy of a multidomain sample can be reduced by its deformation (e.g. bending). Other possibility is that another phase is involved in the pattern; indeed the star pattern in lead orthovanadate mentioned above includes a triangular region representing another phase.

Addressing the specified problems could open large areas of new effects; practically each of these issues could be analyzed for any of the 212 species. From the practical point of view, obviously, the most important are species represented by single crystals for which qualified growth methods are available. At this time this aspect supports the analyses of a few ferroics, including perovskites (species *m3̄m–Pεds–4mm*, *m3̄m–Pεds–mm2*, *m3̄m–Pεds–3m*, *m3̄m–εs–* *4/mmm*, *m3̄m–εs–mmm*) and $Bi_4Ti_3O_{12}$ (*4/mmm–Pεds–m*). In materials with a larger number of ferroelastic domain states (up to 24 for several species), it would be really a challenge for experimentalists to specify some basic features of domain geometries.

As already mentioned, to fabricate samples useful for *DGE* a large number of technics can be used. Spatial distribution of defects during the crystal growth has been applied for $LiNbO_3$, $LiTaO_3$ as well as for alanine-doped triglycine sulphate [19] and it can be assumed that patterns realized in this way are stable. In fact, even head-to-head 180° configurations [20] can be realized. However, when other method is used for *DGE*, e.g. applying nonuniform electric or elastic fields close to T_{TR}, the pattern becomes energetically unstable after removing the fields or after cooling. Depolarizing energy and change of the P_S value need not play a substantial role because of bound charge compensation. In contrast, the elastic energy—change of spontaneous strain and elastic coefficients with temperature—can have a substantial

destabilizing effect. This can be solved when the domain pattern is fixed by producing a corresponding geometry of defects, e.g. by irradiation.

DOMAIN WALL ENGINEERING

The available discussions of *DGE* assume that intrinsic properties of *DW*'s do not play any role. We now shortly address the issue (d), *domain wall engineering*. It is based on specific properties of walls and realistic when their density is high and their thickness finite [2].

In a ferroelectric we expect $P = 0$ in the middle of a 180° *DW*; in a ferroelastic, we anticipate a continuous change of strain. Both these aspects result in a change of symmetry inside the wall and thus a domain wall can offer even unexpected properties. This was illustrated theoretically when Dauphiné domain walls in nonpolar quartz were predicted to carry a dipole moment [21]; later it was proven experimentally [22]. It is easy to demonstrate this possibility for ferroelastic walls. If the invariant $\mu_{ijkl}(\partial\varepsilon_{ij}/\partial x_k)E_l$ is allowed by symmetry in the free energy function, a ferroelastic wall will carry polarization $P_l = \mu_{ijkl}(\partial\varepsilon_{ij}/\partial x_k)$ where μ describes the flexoelectric effect. For instance, in crystals of $SrTiO_3$ and $CsPbCl_3$ ($m\bar{3}m$–εs–$4/mmm$) or in tetragonal $BaTiO_3$ ferroelastic walls are, by symmetry, allowed to carry polarization $P_x = P_z = (\mu_{1111} - \mu_{3311})\,(\partial\varepsilon_{xx}/\partial x)$. The symmetry analysis of nonferroelastic domain walls [23] makes it possible to predict their permitted macroscopic properties. Even antiphase boundaries can carry a dipole moment, as predicted recently [24] for $SrTiO_3$.

Except for the mentioned case of quartz (where in the incommensurate phase the wall density is very high), we have no direct data on the polarity of *DW*'s in nonferroelectric materials. The main problem is that the relative volume $\Delta V/V$ occupied by walls should not be negligible. Let us accept that the required value is $\Delta V = 0.1V$. Assume the *DW* thickness 3 nm; no way is known to increase this value for a defect-free sample. Then the required average domain width is 30 nm while the common value is 1 to 10 μm. Thus *DW* density would have to be increased at least by a factor of 30 if wall properties should play a substantial role.

At present there seem to exist several methods how this problem could be addressed experimentally. Materials with an incommensurate phase might offer one possibility. When temperature decreases and the incommensurate—commensurate transition temperature T_l is approached, the structure of discommensurations is close to that of domain walls separating regions with nearly uniform order parameter, close to domains. Near

above T_f their density is still very high but at T_f it is strongly reduced, as demonstrated by dielectric properties [25]. However, by irradiation, the dense quasi-domain systems could be stabilized over a wide temperature range. For applications a material with T_f above room temperature would be required.

Formation of dense ferroelectric (nonferroelastic) domain patterns was also discussed in connection with photorefractive properties. The photorefractive grating is recorded by interfering light beams which form spatially oscillating space charge field, resulting in corresponding distribution of free carriers. It was shown [26, 27] that when a $BaTiO_3$ or $KNbO_3$ crystal is partially depoled before the grating is recorded, the intensity and lifetime of the space charge grating is dramatically increased. This can be explained by the compensation of free charge by bound-charged 180° domain walls. Whether such a dense spatially modulated domain pattern can be stable was analyzed theoretically [28]; under specified material conditions indeed dense partial switching can be expected.

Perhaps the only experimentally proved method of creating very dense domain patterns is based on the application of strongly nonhomogeneous electric fields using atomic force microscopy. The method makes possible to write very small domains of a high density into single crystals; we shall come back to this point in the Subsection "Writing domains."

An intensively studied family of materials is related to crystals of $YBa_2Cu_3O_7$ ($4/mmm$–εs–mmm). In the parent phase of oxygen-reduced samples tweed patterns of extremely high density were observed in a wide temperature interval. They have been connected with composition fluctuations, in particular with correlated distribution of oxygen producing high amplitude shear displacement waves [29]. Thus ferroelastic domain walls occupy a significant part of the sample volume and can be expected to influence essentially macroscopic characteristics of the material depending on tensorial properties of *DW*'s.

The frequently addressed issue of domains in YBCO is in fact an example demonstrating the possible and reproducible role of defects in the density of *DW*'s. In addition, it is obvious that lattice defects can play a substantial role also by affecting the local structure and symmetry of walls. As shown theoretically [30], the wall thickness d_w itself can be significantly influenced by defects. They predicted the increase of d_w from 30 Å up to the effective thickness $d_{w,\text{eff}}$ of 3000 Å, depending on the characters of defects. This is a wall of a new structure and symmetry, but the essential increase of its thickness might strongly reduce the wall density required for a substantial influence on macroscopic properties of the sample.

Only recently the problem of d_w value has been readdressed experimentally. It was found indeed that $d_{w,\text{eff}}$ of 180° nonferroelastic walls can be considerably influenced by the presence of lattice defects [31, 32]. In congruent crystals of $LiNbO_3$ and $LiTaO_3$ which are Li-deficient, walls formed at room temperature have been reported to reveal very specific properties: large birefringence within regions of thickness of the order of 1 μm. Based on these and some macroscopic properties, strain components connected with walls were evaluated [33]. In stoichiometric crystals strain and birefringence tend to disappear; thus these effects and the large wall width are clearly connected with lattice defects. The study of strain components within walls using x-ray synchrotron diffraction imaging [34] showed that in both congruent $LiNbO_3$ and $LiTaO_3$ *DW*'s were several μm thick.

It has to be stressed that defect-influenced thick *DW*'s can be expected to offer other macroscopic properties than those based on symmetry considerations of pure materials. To summarize shortly, we can state that although representative types and properties of defects resulting in wide *DW*'s do not seem to have been specified, further research may open a new field of applications of ferroelectric crystals with a large wall density; a new area of domain wall engineering [35, 36]. $LiNbO_3$ samples with appropriate non-stoichiometry and with engineered dense domain pattern might offer macroscopic properties new in the sense of symmetry and/or in the sense of values of some material coefficients.

NUCLEATION

Till now we concentrated on some open research areas of static domain patterns. We shall come back to a specific aspect of this problem in the following Subsection: "writing" domains at predetermined spots. It is genenerally accepted that polarization reversal in ferrolectrics proceeds in three steps: nucleation of domains with antiparallel polarization and their forward growth followed by sidewise expansion. The first step, random formation of small domains with antiparallel P_S, is of essential importance for writing domains in defined spots to reach the required geometry. We now ask whether such nucleation process really plays a role.

It is generally accepted that the critical nucleation energy ΔU^*, a potential barrier to be overcome to form a stable nucleus with antiparallel polarization, is too high to allow for any realistic nucleation rate: $10^8 kT$ for $BaTiO_3$. Even if the depolarizing field were compensated by free charges from the electrodes, the surface energy contribution alone is too large ($10^5 kT$) to make possible

the nucleation by thermal fluctuations in applied field of realistic values. For PZT, in the applied field 100 kV/cm, the barrier was estimated as $10^3 kT$ [37]. Thus the nucleation process presents a problem.

In fact the nucleation stages were only rarely analyzed by real experiments. It was concluded [38] that in $BaTiO_3$ only 10 to 30% of observed domains were "repeaters," indicating nucleation occuring at predetermined sites. Thus the remaining percentage of nuclei might be formed chaotically, based on statistical probability. However, these data were obtained by etching the samples a long time after the application of field and therefore they need not to represent the nucleation process. Much more recently, nucleation in lead germanate was investigated [39]; its specific advantage is that the species $\bar{6}$–*Pd*–3 allows for optical observation of nonferroelastic domains in real time, due to optical activity. Stroboscopy was used to observe the nucleated domains; this indicates that the nuclei occurred repeatedly at the same spots which must have been predetermined by defects. It would be interesting to study crystals of the same material grown with the aim to control their defect structure and to reach maximum purity. Furthermore, preparation of samples usually leads to mechanical modification of their surfaces which can facilitate the nucleation. This may play a substantial role even in nonferroelastics as demonstrated [40] in samples of $LiTaO_3$.

These estimations and data point to the question whether the nucleation process plays an essential role at all in the observed macroscopic switching properties. Indeed it was shown [41] that to interpret the $P(E)$ loop does not really require the nucleation stage. Assuming the existence of residual domains—due to lattice defects—and using classical laws for *DW* velocity and domain coalescence, hysteresis loops can be calculated whose amplitude and frequency dependencies agree well with experimental data.

It appears that we do not have a clear explanation what kind of lattice defects may be responsible for built-in nuclei; the problem of nucleation is still repeatedly addressed. Even in the new theoretical approach [42] based on tunneling of electrons from an electrode, the aggregates of neutral defects play an essential role. An electron captured by a defect forms a fluctuon, a bound state of an electron with a fluctuation of local polarization. The coalescence of such fluctuons leads to the appearance of stable multielectron fluctuons which may be regarded as repolarization nuclei. In this model there is still a barrier of the order of several eV which is expected to be overcome by thermal fluctations.

Crystals of $KTiOPO_4$ have a specific property which makes it possible to compare two situations [43]. At room temperature the material possesses superionic conductivity (mobile K ions) allowing for compensation of

depolarizing field. This may lead to easy nucleation in the bulk of a crystal. In contrast, at low temperatures the material is a true dielectric for which nucleation at the electrodes may be more probable. Indeed an obvious difference was observed in these two temperature regions. In the dielectric state the domains are nucleated at the electrodes and grow straightforwardly from the top to the bottom surface. In the superionic state the observed domains appear in the crystal bulk and on growing are strongly widened. Even these interesting observations do not rule out the possibility of built-in nuclei.

It thus appears that most of the results support and the others do not exclude the assumption that in the observed switching processes the ideal defect-independent nucleation is irrelevant. However, the possibility can't be excluded that in different materials the nucleation processes are of different origins. It would be of interest to concentrate further research on one crystalline material grown with well defined concentrations of defects and investigating samples whose surfaces would be prepared in a well controlled way.

WRITING (NANO)DOMAINS

The problem of nucleation discussed in the previous paragraph is closely related to the practical aspect of "writing" domains. At present it is connected with two research and application areas. First, *DGE* of the (a2) type: domains of defined geometry and small size can play a role in surface acoustic waves devices or optical waveguides. Second, writing domains of the smallest possible (*nano*) size and high density which are time-stable but can be rewritten: their obvious application aspect are memory devices. At present, most of the research in this field is oriented towards ferroelectric thin films [44]. However, writing domains into ferroelectric single crystals has been also addressed, using several methods: electron beam bombardment, laser beam illumination and atomic force microscopy. Here we concentrate on processes involving only two nonferroelastic domain states.

The concept of writing a domain includes two aspects: the induced nucleation *at a predetermined spot* and the *stability* of the generated domain. In the second point also the size of the written-in domain is involved. Is writing a nanodomain possible without defects? The problem is that the spatial definition of a predetermined spot is complex since it should include the comparison of the size of the written domain and the allowed inaccuracy of its location.

One of the first attempts to induce domain nuclei at defined spots was accomplished by local *illumination* of a TGS sample *by laser beam* [45]. It

was shown to result in the creation of small domains, in "writing" domains. The authors connected the effect with the formation of a depolarizing field but pointed out the complexity of the situation: what should be taken into account in the analysis of the effect are temperature dependencies of P_S, strain ε and piezoelectric coefficients, as well as the role of grad T, grad $\mathbf{P}_S$ and grad ε and heat propagation. The small induced domains were not stable; however, irreversible switching in predefined spots was achieved later [46] in Fe-doped TGS plates. An Ar laser beam of 5 mW power was focused to a 1μ diameter; one pulse was enough to result in local irreversible switching when a *dc* voltage, not high enough to result in switching by itself, was also applied. At even higher illumination intensity no *dc* field was required. The analysis of results led to the conclusion that local heating forms a polarization gradient; the latter results in electric field responsible for reversible [45] or irreversible [46] processes. In TGS crystals defects are known to play a very substantial role in domain formation and it would be interesting to connect these data with crystal quality and compare them with the behaviour of other ferroelectrics.

The writing of domains became a very actual problem in connection with optical waveguides, SHG and surface acoustic waves. In neither case one should speak about nanodomains: the typical required domain width is several μm. For SHG the domain walls cover the whole sample cross-section while for waveguides their depth is of the order of 1 μm. In these topics the mostly addressed materials are $LiNbO_3$ and $LiTaO_3$ because of their macroscopic properties, stability and possibility to grow large homogeneous single crystals. Regularly applied methods for writing surface domains into congruent $LiNbO_3$ crystals are based on *Ti indiffusion* [5] or Li_2O *outdiffusion* [47] processes. Both result in domain reversal on the positive c-face of the sample and have been used also for periodic domain systems.

The problem of writing domains at defined spots was addressed by another technique, *electron beam bombardment*. Crystals of $LiNbO_3$ grown by classical methods are difficult to pole at room temperature and at higher temperatures electrical conductivity as well as the loss of Li and O ions create a problem. However, when a vacancy is temporarily generated in the oxygen triangle, a pathway for Li ions is opened; they can shift and reverse $\mathbf{P}_S$. Based on this fact, the role of an electron beam in poling this material was demonstrated [48], showing that an energetic beam excites the lattice and when even a low electric field is also applied, the ions move orderly, resulting in a poling process at temperatures well below T_C.

While the diffusion techniques mentioned above are active on the positive c-faces of these materials, electron beam bombardment leads to $\mathbf{P}_S$ reversal

on the opposite surfaces with a negative bound charge [49] and this may be preferred for optical waveguides. The usefulness of the method was demonstrated by fabrication of domain gratings in $LiNbO_3$ for SHG. In fact in this material electron beam "litography" allows to write—from the negatively charged surface—domains of required geometry and depth [50]. The method was also applied [51] to $LiTaO_3$ which is known to have a higher optical damage threshold than $LiNbO_3$. Again, in samples with electrons injected on positive c-face no sign of domain inversion was observed. The typical diameter of focused electron beam is between 0.1 and 1 μm; however, in most cases the diameters of written domains tend to increase.

The possible mechanism of domain inversion by electron bombardment may be due to the electric field buildup by the injected electrons [51]. The penetration depth of 25 keV electrons injected into $LiTaO_3$, was estimated as 3 μm. They induce an electric field antiparallel to $\mathbf{P}_S$ on the negative c-face but parallel to $\mathbf{P}_S$ on the positive c-face. The field is higher on the side injected with electrons and decays towards the opposite side of the sample. This may account for nucleation of domains on the negative c-face. Indeed no domain inversion was observed when electrons are injected into positive c-face. Defects are believed to define possible sites for the nucleation of inverted domains.

The above discussed methods refer to formation of domains which are small but do not really represent nanodomains, being of typical width tenths or units of μm. The techniques which allow to write domain one or two orders of magnitude narrower are based on *atomic force microscopy* (AFM). Crystals of guanidinium aluminum sulphate hexahydrate (GASH, species $\bar{3}m$–*Pd*–3*m*) were addressed first; domains of noticeably regular round shapes could be induced [52, 53]. In cleaved plates about 0.3 mm thick antiparallel domains of diameter 100 to 150 nm were written by applying voltage pulses of 3V amplitude and 4 sec duration and it was possible to erase them by pulses of opposite polarity. They have been referred to as *stable* domains; however, their stability features have not been specified. The AFM tips had a curvature radius about 50 nm; taking into account account nonhomogeneity of the electric field around the tip, its magnitude at the surface when a nucleus was formed by the applied voltage of 3 V was estimated as $E_S = 6\times10^5$ V/cm.

In $BaTiO_3$, the next addressed material, it was shown [54] that designed patterns of c-domains can be written into samples 0.5 mm thick by pulses of 10 V applied to the AFM tip. These domains of about 300 nm in diameter were not connected with any changes in surface topography. Theoretical estimations showed that the domain, as it starts to grow under the 10 V

voltage applied to the tip, should stop at a distance about 5–10 μ from the surface, while the radius of its base area on the surface will not exceed 200 nm. As a result, a nonthrough spike-shaped domain will be formed. These estimations are consistent with the observed diameters.

The problem of writing domains using AFM was systematically addressed by Eng et al., first using samples of $BaTiO_3$ and TGS [55] 125 μm and 700 μm thick, resp. The smallest written-in domains were of 500 nm width; they could be in form of lines or dots, depending on time program of the field applied to the tip. In $BaTiO_3$ the stability of written domains was found to be more than 5 days, much longer than in TGS where domains keep their written-in shapes just for tens of minutes. Local switching could be demonstrated by a "nanoscale" hysteresis loop at any spot of the $BaTiO_3$ crystal [56] when the applied field exceeded 1400 V/cm. Thus this field "$E_{C,\text{nano}}$" represents the energy required for nucleation. In the loop no saturation is seen, because as the field grows the domain will grow, both laterally and through the sample. An ultraslow process resulted in large domains of diameter up to 20 μm. Thus domain switching of small structures useful for memories has to be performed very rapidly. The best performance to create small domains was reached with high voltage pulses ($E > 3$ kV/cm) applied for less than 100 μs. Local polarization reversal can be induced by applied field in any required spot specified with the accuracy of about 10 nm [57].

Selected problems of nanoscale domain switching were summarized by Eng [58]. To write domains into a $BaTiO_3$ sample first the selected area was made single domain by scanning with a negative *dc* bias $\geq$ 10 V/cm between the conductive tip and the counter electrode. Then the tip was moved to a desired spot and a positive voltage was applied for time τ_{exp}. This resulted in a written domain; it was imaged in the piezoelectric AFM mode. The domain diameter observed on the surface could be as small as 60 nm. The size and lifetime of such nanodomains depend on the sample thickness and its crystallography. However, much stronger influence on the domain size have the applied field E_{exp} and time τ_{exp}. The analysis of experimental results resulted in the specification of dependence of E_{exp} for which switching was succesful on time τ_{exp}. The important conclusion was that nanoscale domains with diameter below 100 nm result only when applying a strong field $E_{\text{exp}} >$ 50 kV/cm for a short period $\tau_{\text{exp}} < 30$ μs. Such nanosized domains were found to be stable for more than 30 days. It may be expected that much shorter switching times may reduce the spot diameter even more.

From the point of view of real applications the problem of written-in domains stability belongs to the most essential ones. It is obvious that the

energy of depolarizing field and domain walls can result in meta- or instability of written domains. Theoretically the issue has been addressed only recently [59] when the stability of a domain near the electrode-less surface was theoretically analyzed. The approach was based on several assumptions: by an AFM tip $\mathbf{P}_S$ is reversed in a cylinder of radius R and height Z; electrostatic U_{elst} and domain wall U_{dw} energy enter the analysis; the surface bound charge is neutralized; writing is fast and there is no time for space-charge redistribution during writing so that uncompensated P_S charges are associated with a freshly written domains; and after the tip removal the only electrical field is due to these charges and induced polarization charges at the surface. Once the tip is removed, the domain is unstable because of the positive U_{elst} and U_{dw} energies; they result in a restoring force. It is assumed that the wall will not move unless the acting force does not exceed a certain threshold value $f_{\text{thr}} = 2P_S E_C$. Considering $P_S = 30\ \mu C/\text{cm}^2$ and assuming $E_C = 20$ kV/cm, f_{thr} is of the order of 1 MPa. On the basis of a simple model it is shown that for cylindrical domains larger than several nm f_{thr} would not be overcome by the decrease of wall energy U_{dw}. Next the depolarization energy U_{dp} underneath an electrodeless dielectric surface has to be considered; assuming real parameters of a ferroelectric material, it is shown that the force due to U_{dp} is much larger so that f_{thr} can be easily surmounted. The forces required to reduce or erase a domain decrease with increasing domain size. A domain has to reach a certain size in order to become stable. The mentioned model made it possible to specify the "stability region" in the (R, Z) space. Its "nose" corresponds to minimum dimensions of R and Z, namely $R^* = \gamma/E_C P_S$, $Z^* = 6\gamma/\varepsilon\varepsilon_0 E_C^2$. Assuming wall energy density $\gamma = 1\ \text{mJ/m}^2$ and $\varepsilon = 1000$, the minimal ratio Z/R for a stable domain is of the order of 100. Therefore, to stabilize a domain of a modest radius, say 0.1 μm, its depth of 10 μm would be required.

Routinely, stable domains of this or larger radius can indeed be written by AFM; yet it is unlikely that they can reach such depth. This is because the pronounced nonhomogeneity of the field below the AFM tip has not been taken into account. Additional calculations showed that when this is respected, the aspect ratio of the most favourable domain configuration is about 10; such a domain is stable once the tip is removed.

In the just discussed model it is assumed that the bound charge at the top of the written domain cannot be compensated by space charge because of lack of time for diffusion. In contrast, the bound charge on the surface may be instantaneously neutralized by charge transfer from the AFM tip during writing. It was shown experimentally that in fact this charge is even overcompensated, due to an excessive charge transfer from the tip.

If the surface bound charge is neutralized, the $\mathbf{P}_S$ charge at the opposite tip of the domain is no longer attracted to the surface. Instead, it feels repulsion due to its image charge which is of the same sign. This repulsion stress reaches a maximum $2P_S^2/\varepsilon\varepsilon_0$ for $R \gg Z$, about 20 MPa for the above assumed coefficients. Domains are stabilized by this repulsion and even small domains, down to a few nm, should not shrink; rather they should expand in the z-direction. In addition: the larger the domain, the more stable it is, since the repulsive stress increases with R/Z. This is consistent with the general experimental observations that larger domains are more stable after writing.

We have mentioned the basic ideas of this simple theory in some detail since at present it seems to be one of the very few attempts to propose a theoretical viewpoint on the problem how ferroelectric domains can be "written". In this Subsection we have specified several application aspects supporting the research territory of writing domains. There is no doubt that if the issue were experimentally resolved and fully understood, many other practical fields could be addressed in optical, acoustical, electro-optic or elasto-optic areas. However, in "nanoscale domain engineering" there are many open problems. Let us shortly mention some of them.

With some small uncertainty, a domain can be written by atomic force microscopy in any specified spot of a sample. Yet as discussed in the previous subsection, the present understanding of domain nucleation assumes the significant role of crystal structure defects. Detailed high resolution investigations of writing domains could help to classify different kinds of lattice defects from several points of view; in particular, how they influence the local switching field, how the defect polarity is defined, how stable is the written domain. Another issue to be addressed is the depth of introduced domains and their (meta)stability in strongly nonhomogeneous applied field as well as after its removal. Here one of the involved particular problems is the role of fast processes reducing the energy of a written domain, including compensation of bound charges or domain walls shift to positions preferred by local defects.

In the above mentioned discussions writing of domains was connected with the classical energy of a ferroelectric $-(\mathbf{P}_S\mathbf{E})$. Recently, Abplanalp et al. [60] observed specific $\mathbf{P}_S$ reorientation in thin films of $BaTiO_3$ using atomic force microscopy and interpreted the results by ferroelastoelectric switching. For a full understanding of the effect nonhomogeneous spatial distributions of electric field and stress will have to be taken into account. This research area may be opened for thick samples, fully defining the field and stress gradients and specifying the possible role of ferroelastoelectricity.

It is appropriate to mention that Massanell et al. [61] showed that nanolines of the width as small as 60 nm can be written on surfaces of TGS crystals using a scanning near-field optical microscope. However, they were not related to domains and several defect mechanisms have been proposed. This in fact represents a danger: when not appropriate techniques are used, writing of defects in can be performed not connected with $\mathbf{P}_S$ reversal.

In the last decade the problem of writing domains into thin films has been addressed very frequently and we can expect strong activities in this field. There the boundary conditions—role of depolarizing field and elastic energy in particular—are very different from those in bulk crystals; however, a systematic comparison is not yet available.

CLOSING REMARK

Out of possible problems connected with applications based on ferroic domains—see Table I—we have shortly discussed just a few with the aim to demonstrate that very interesting research areas are still open.

This work has been supported from the Thematic Network on Polar Electroceramics POLECER (G5RT-CT-2001-05024) and from the Grant Agency of the Czech Republic (project No. 202/02/1006).

REFERENCES

[1] Duan Feng, Nai-ben Ming, Jing-Feng Hong et al., *Appl. Phys. Letters* **37**, 607 (1980).
[2] J. Fousek and L. E. Cross, *Ferroelectrics* **252**, 171 (2001).
[3] V. Ya. Shur, E. L. Rumyantsev, E. V. Nikolaeva et al., *Ferroelectrics* **236**, 129 (2000).
[4] Z. W. Liu, S. N. Zhu, Y. Y. Zhu et al., *Solid State Commun.* **119**, (2001) 363.
[5] S. Miyazawa, *J. Appl. Phys.* **50**, 4599 (1979).
[6] Shi-ning Zhu, Yong-yuan Zhu, Yan-qing Lu et al., *Phase Transitions* **72**, 239 (2000).
[7] P. Tomashewski, *Phase Transitions* **38**, 127 (1992).
[8] J. Fousek, M. Glogarová, and H. Kürsten, *Ferroelectrics* **11**, 469 (1976).
[9] G. G. Krainyuk, A. I. Otko, and A. E. Nosenko, *Soviet Phys.—Solid State* **26**, 1582 (1984).
[10] A. I. Otko, G. G. Krainyuk, and A. E. Nosenko, *Ferroelectrics* **64**, 147 (1985).
[11] S. W. Meeks, L. Clarke, and B. A. Auld, *Proc. IEEE Ultrasonic Symposium* (1985).
[12] E. F. Dudnik, E. V. Sinyakov, V. V. Gene et al., *Sov. Phys.—Solid State* **17**, 1212 (1975).
[13] P. W. Forsbergh Jr., *Phys. Rev.* **76**, 1187 (1949).
[14] G. Arlt and P. Sasko, *J. Appl. Phys.* **51**, 4956 (1980).
[15] D. P. Cameron, *IBM J. Res. Develop.* **1**, 1 (1957).
[16] C. Manolikas and S. Amelinckx, *Phys. Stat. Sol. (a)* **60**, 607 (1980).
[17] E. G. Fesenko, V. G. Gavrilyatchenko, A. F. Semenchev et al., *Ferroelectrics* **63**, 289 (1985).

[18] J. Bornarel, R. Cach, and Z. Kvitek, *Ferroelectrics* **236**, 117 (2000).
[19] W. Wang and Q. Ming, *J. Crystal Growth* **79**, 758 (1986).
[20] J. Chen, Q. Zhou, J.-F. Hong et al., *J. Appl. Phys.* **66**, 336 (1989).
[21] M. B. Walker and R. J. Gooding, *Phys. Rev. B* **32**, 7408 (1985).
[22] E. Snoeck, P. Saint-Gregoire, V. Janovec et al., *Ferroelectrics* **155**, 371 (1994).
[23] J. Privratska and V. Janovec, *Ferroelectrics* **191**, 17 (1997).
[24] A. K. Tagantsev, E. Courtens, and L. Arzel, *Phys. Rev. B* **64**, 224107 (2001).
[25] V. Novotna, H. Kabelka, J. Fousek et al., *Phys. Rev. B* **47**, 11019 (1993).
[26] R. S. Cudney, J. Fousek, M. Zgonik et al., *Phys. Rev. Letters* **72**, 3883 (1994).
[27] R. S. Cudney, P. Bernasconi, M. Zgonik et al., *Appl. Phys. Letters* **70**, 1339 (1997).
[28] J. Fousek, M. Marvan, and R. S. Cudney, *Appl. Phys. Letters* **72**, 430 (1998).
[29] D. A. Vul, I. Tsatskis, and E. K. H. Salje, *Phil. Mag. Letters* **72**, 277 (1995).
[30] B. M. Darinskii and A. S. Sidorkin, *Sov. Phys.—Solid State* **26**, 2048 (1984).
[31] V. Gopalan and M. C. Gupta, *J. Appl. Phys.* **80**, 6099 (1996).
[32] T. J. Yang, U. Mohideen, and M. C. Gupta, *Appl. Phys. Letters* **71**, 1960 (1997).
[33] T. J. Yang and U. Mohideen, *Physics Letters A* **250**, 205 (1998).
[34] S. Kim, V. Gopalan, and B. Steiner, *Appl. Phys. Letters* **77**, 2051 (2000).
[35] J. Fousek, D. B. Litvin, and L. E. Cross, *J. Phys. Condens. Matter* **13**, L33 (2001).
[36] J. Fousek and L. E. Cross, *Ferroelectrics* **252**, 171 (2001).
[37] A. K. Tagantsev, personal communication.
[38] H. L. Stadler and P. J. Zachmanidis, *J. Appl. Phys.* **35**, 2625 (1964).
[39] A. Gruverman, N. Ponomarev, and K. Takahashi, *Jpn. J. Appl. Phys.* **33**, 5536 (1994).
[40] J. D. Venables, *Appl. Phys. Letters* **25**, 254 (1974).
[41] J. Janta, *J. Phys. Soc. Jpn. Suppl.* **28**, 340 (1970).
[42] M. Molotskii, R. Kris, and G. Rosenman, *J. Appl. Phys.* **88**, 5318 (2000).
[43] P. Urenski, M. Molotskii, and G. Rosenman, *Appl. Phys. Letters* **79**, 2964 (2001).
[44] A. Gruverman, A. Kholkin, A. Kingon et al., *Appl. Phys. Letters* **78**, 2751 (2001).
[45] A. Hadni, X. Gerbaux, D. Chanal et al., *Ferroelectrics* **5**, 259 (1973).
[46] A. Hadni and R. Thomas, *Ferroelectrics* **6**, 241 (1974).
[47] J. Webjorn, F. Laurell, and G. Arvidsson, *IEEE Photonics Technology Letters* **1**, 316 (1989).
[48] P. W. Haycock and P. D. Townsend, *Appl. Phys. Letters* **48**, 698 (1986).
[49] R. W. Keys, A. Loni, R. M. De la Rue et al., *Electronics Letters* **26**, 188 (1990).
[50] M. Yamada and K. Kishima, *Electronics Letters* **27**, 828 (1991).
[51] W.-Y. Hsu and M. C. Gupta, *Appl. Phys. Letters* **60**, 1 (1992).
[52] A. Gruverman, O. Kolosov, J. Hatano et al., *J. Vac. Sci. Technol B* **13** (1995).
[53] O. Kolosov, A. Gruverman, J. Hatano et al., *Phys. Rev. Letters* **74**, 4309 (1995).
[54] A. L. Gruverman, J. Hatano, and H. Tokumoto, *Jpn. J. Appl. Phys.* **36**, 2207 (1997).
[55] L. M. Eng, M. Abplanalp, and P. Günter, *Appl. Phys. A* **66**, S679 (1998).
[56] L. M. Eng, M. Abplanalp, P. Günter et al., *J. Phys. IV France* **8**, 201 (1998).
[57] L. M. Eng, M. Bammerlin, Ch.Loppacher et al., *Ferroelectrics* **222**, 153 (1999).
[58] L. M. Eng, *Nanotechnology* **10**, 405 (1999).
[59] X. Li, A. Mamchik, and I.-W. Chen, *Appl. Phys. Letters* **79**, 809 (2001).
[60] M. Abplanalp, J. Fousek, and P. Günter, *Phys. Rev. Letters* **86**, 5799 (2001).
[61] J. Massanell, N. Garcia, and A. Zlatkin, *Optics Letters* **21**, 12 (1996).